

SCHOOL OF CIVIL ENGINEERING

JOINT HIGHWAY
RESEARCH PROJECT

JHRP-78-4

THE RELATION BETWEEN PERMEABILITY
AND PORE SIZE DISTRIBUTION OF
COMPACTED CLAYEY SILTS

Ignacio Garcia-Bengochea

i i i i i
i i i i i
i i i i i
CIVIL



PURDUE UNIVERSITY
INDIANA STATE HIGHWAY COMMISSION

Interim Report

THE RELATION BETWEEN PERMEABILITY AND
PORE SIZE DISTRIBUTION OF COMPACTED CLAYEY SILTS

To: J. F. McLaughlin, Director
Joint Highway Research Project

April 4, 1978
Project: C-36-5N

From: H. L. Michael, Associate Director
Joint Highway Research Project

File: 6-6-14

Attached is an Interim Report on the HPR-1(15) Part II Research Study entitled "The Relation Between Permeability and Pore Size Distribution of Compacted Clayey Silts". It has been authored by Mr. Ignacio Garcia-Bengochea, Graduate Instructor on our staff, under the direction of C. W. Lovell, L. E. Wood and A. G. Altschaeffl of our staff.

The results given in the attached study demonstrate the utility of pore size distribution to interpret changes in soil fabric and how these changes affect an engineering property. Conventional permeability predicting equations based on volumetric and grain size parameters have been found to be unsuitable for predicting the permeability of fine-grained soils. This study examines the relation between permeability and pore size distribution of compacted fine-grained soils. Empirical predictive equations based on two theoretical models for permeability were determined for each of the soil types tested.

The Report is submitted as partial fulfillment of the objectives of the Study. Copies of the report will also be submitted to ISHC and FHWA for their review, comment and similar acceptance.

Respectfully submitted,

Harold L. Michael
Harold L. Michael
Associate Director

HLM:jwb

cc: A. G. Altschaeffl	G. K. Hallock	C. F. Scholer
O. M. Bevilacqua	D. E. Hancher	M. B. Scott
W. L. Dolch	K. R. Hoover	K. C. Sinha
R. L. Eskew	R. F. Marsh	C. A. Venable
G. D. Gibson	R. D. Miles	L. E. Wood
W. H. Goetz	P. L. Owens	E. J. Yoder
M. J. Gutzwiller	G. T. Satterly	S. R. Yoder

Digitized by the Internet Archive
in 2011 with funding from

LYRASIS members and Sloan Foundation; Indiana Department of Transportation

Interim Report

THE RELATION BETWEEN PERMEABILITY AND
PORE SIZE DISTRIBUTION OF COMPACTED CLAYEY SILTS

by

Ignacio Garcia-Bengochea
Graduate Instructor in Research

Joint Highway Research Project

Project No.: C-36-5N

File No.: 6-6-14

Prepared as Part of an Investigation

Conducted by

Joint Highway Research Project
Engineering Experiment Station
Purdue University

in cooperation with the

Indiana State Highway Commission
and the
U.S. Department of Transportation
Federal Highway Administration

The contents of this report reflect the views of the author who is responsible for the facts and the accuracy of the data presented herein. The contents do not necessarily reflect the official views or policies of the Federal Highway Administration. This report does not constitute a standard, specification, or regulation.

Purdue University
West Lafayette, Indiana
April 4, 1978

1. Report No. JHRP-78-4	2. Government Accession No.	3. Recipient's Catalog No.
4. Title and Subtitle THE RELATION BETWEEN PERMEABILITY AND PORE SIZE DISTRIBUTION OF COMPACTED CLAYEY SILTS		5. Report Date April 1978
7. Author(s) Ignacio Garcia-Bengochea		6. Performing Organization Code
9. Performing Organization Name and Address Joint Highway Research Project Civil Engineering Building Purdue University W. Lafayette, Indiana 47907		8. Performing Organization Report No. JHRP-78-4
12. Sponsoring Agency Name and Address Indiana State Highway Commission State Office Building 100 North Senate Avenue Indianapolis, Indiana 46204		10. Work Unit No.
		11. Contract or Grant No. HPR-1(15) Part II
		13. Type of Report and Period Covered Interim Report
		14. Sponsoring Agency Code
15. Supplementary Notes Prepared in cooperation with the U. S. Department of Transportation, Federal Highway Administration. Part of the Study titled "The Effects of Pore Size Distribution on Permeability and Frost Susceptibility of Selected Sub-Grade Materials".		
16. Abstract This study examines 1) the relation between permeability and pore size distribution, and, 2) the influence of varying water content and compaction effort on the soil fabric of compacted fine-grained soils. Three blends of silt and kaolin were compacted at different energy levels and water contents. Falling head tests under back pressure were used to measure permeability. The mercury intrusion technique was used to measure pore size distribution. Freeze drying was used to minimize soil disturbance prior to mercury intrusion. A method of approximating the differential pore size distribution is described which simplifies the interpretation of pore size distributions. The soils tested were found to have a bimodal pore size distribution on a log diameter scale. Varying the compaction variables was at the expense of the large pore mode with little or no effect on the small pore mode. The permeability generally increased with increasing large pore mode. Empirical predictive equations for permeability based on pore size distribution parameters were determined for each of the soils tested. The pore size parameters used were based on theoretical models which relate permeability to pore size distribution.		
17. Key Words compacted soils, permeability, soil structure		18. Distribution Statement No restrictions. This document is available to the public through the National Technical Information Service, Springfield, Virginia 22161.
19. Security Classif. (of this report) Unclassified	20. Security Classif. (of this page) Unclassified	21. No. of Pages 179
22. Price		

ACKNOWLEDGEMENTS

The author would like to express his appreciation to his major professor, Dr. C. W. Lovell, for the constant support and understanding extended to him during the course of this investigation. A special thanks is extended to Dr. A. G. Altschaeffl and Dr. L. E. Wood for their valuable counseling and encouragement.

Thanks are extended to Dr. S. Diamond for his assistance and helpful discussions. Thanks also to Dr. M. E. Harr and Dr. W. L. Dolch for reviewing portions of the manuscript.

The laboratory assistance provided by Mrs. Janet Lovell and Dr. John Scully was extremely helpful. The secretarial and drafting work provided by Mrs. Janice Bollinger, Mrs. Edith Vanderwerp and Ms. Peggy McFarren was greatly appreciated.

The financial support for this research was provided by the Indiana State Highway Commission and the Federal Highway Administration. The research was administered through the Joint Highway Research Project, Purdue University, West Lafayette, Indiana.

The author had the good fortune of having Mr. Michael Reed as a research partner; his comradery and assistance during the course of this study will not be forgotten.

TABLE OF CONTENTS

	Page
LIST OF TABLES	vi
LIST OF FIGURES	vii
LIST OF ABBREVIATIONS AND SYMBOLS	xi
HIGHLIGHT SUMMARY.	xiv
INTRODUCTION	1
1 - LITERATURE REVIEW AND GENERAL DISCUSSION	3
1-1 Permeability and Fabric of Compacted Fine-Grained Soils	3
1-1.1 Permeability	4
1-1.2 Fabric	11
1-1.3 Permeability Models	15
1-2 Pore Size Distribution	23
1-2.1 Applications	25
1-2.2 Theory, Assumptions and Limitations	27
1-2.3 Presentation of Data	30
1-2.4 Differential Distribution and Calculation of Parameters	34
1-3 Soil Drying Methods	37
1-3.1 Air and Oven Drying	40
1-3.2 Freeze Drying	41
1-3.3 Critical Region Drying	42
1-3.4 Fluid Replacement	44
1-3.5 Method Used	45
2 - SOILS STUDIED	47
3 - APPARATUS AND EXPERIMENTAL PROCEDURE	51
3-1 Soil Mixing and Curing	51
3-2 Compaction	53

TABLE OF CONTENTS (Continued)

	Page
3-2.1 Apparatus	53
3-2.2 Procedure	55
3-3 Saturation and Permeation	58
3-3.1 Apparatus	58
3-3.2 Procedure	60
3-4 Freeze Drying	64
3-4.1 Apparatus	64
3-4.2 Procedure	67
3-5 Pore Size Distribution	68
3-5.1 Apparatus	69
3-5.2 Procedure	70
4 - RESULTS AND DISCUSSION OF RESULTS	72
4-1 Compaction	72
4-2 Saturation	75
4-3 Freeze Drying	79
4-4 Permeability	81
4-5 Pore Size Distribution	88
4-5.1 Replication	89
4-5.2 Contrasting Pore Size Distributions	91
4-6 Relation Between Permeability and Pore Size Distribution	110
5 - CONCLUSIONS AND RECOMMENDATIONS	122
5-1 Conclusions	122
5-2 Recommendations for Future Research	125
BIBLIOGRAPHY	127
APPENDICES	
APPENDIX A - Replicate Pore Size Distribution Curves	133
APPENDIX B - Permeability Tests	156
B-1 Calculations	157
B-2 Consolidation During Permeation	161
APPENDIX C - Critical Region Drying Problems	163
APPENDIX D - Pore Size Distribution Computer Programs	166
APPENDIX E - Purdue University Negative Numbers for Photographs	179

LIST OF TABLES

	Page
TABLE 1 -- SUMMARY OF PERMEABILITY MODELS USED	24
TABLE 2 - CLASSIFICATION OF SOILS STUDIED	50
TABLE 3 - SAMPLE CODE DESIGNATION	73
TABLE 4 - COMPACTION PARAMETERS OF SOILS TESTED	74
TABLE 5 - POROSITY MEASUREMENTS BEFORE AND AFTER FREEZE DRYING	80
TABLE 6 - PERMEABILITY AND EQUIVALENT PORE SIZE PARAMETERS	113
TABLE 7 - LINEAR REGRESSION EQUATIONS FOR PERMEABILITY AND PORE SIZE PARAMETERS (PSP)	119

LIST OF FIGURES

Figure	Page
1. Permeability of a Silty Clay at Three Compactive Efforts (from Mitchell et al. 1965)	5
2. Frequency Histogram of Pore Size Distribution	38
3. Grain Size Distributions for Soils Studied (after Reed, 1977)	49
4. Patterson-Kelley Blender	52
5. Kneading Compactor	54
6. Compaction Mold, Collar and Tamper	57
7. Permeameter Cells	59
8. Saturation Device (Right) and Permeameters (Left)	61
9. Sample Cage Suspended in Desiccator (from Reed, 1977) . . .	65
10. Freeze Drying Apparatus with Vacuum Pump, Condenser and Desiccator (from Reed, 1977)	66
11. Compaction Curves for 90% Silt and 10% Kaolin	76
12. Compaction Curves for 70% Silt and 30% Kaolin	77
13. Compaction Curves for 50% Silt and 50% Kaolin	78
14. Permeability vs Hydraulic Gradient for S9 Samples	82
15. Permeability vs Hydraulic Gradient for S7L Samples	83
16. Permeability vs Hydraulic Gradient for S7M and S7H Samples	84
17. Permeability vs Hydraulic Gradient for S5 Samples	85
18. Permeability and Net Volume Inflow vs Time for Sample S7LW	87

LIST OF FIGURES (Continued)

Figure	Page
19. Differential and Cumulative Pore Size Distribution Curves for 90% Silt-10% Kaolin Compacted at Medium Effort	93
20. Differential and Cumulative Pore Size Distribution Curves for 90% Silt-10% Kaolin Compacted at High Effort	94
21. Pore Size Distribution Curves for 90% Silt-10% Kaolin Compacted at Optimum and Dry of Optimum Water Contents for Two Efforts	95
22. Differential and Cumulative Pore Size Distribution Curves for 70% Silt-30% Kaolin Compacted at Low Effort	96
23. Differential and Cumulative Pore Size Distribution Curves for 70% Silt-30% Kaolin Compacted at Medium Effort	97
24. Differential and Cumulative Pore Size Distribution Curves for 70% Silt-30% Kaolin Compacted at High Effort	98
25. Pore Size Distribution Curves for 70% Silt-30% Kaolin Compacted at Optimum Water Content for Three Efforts	99
26. Pore Size Distribution Curves for 70% Silt-30% Kaolin Compacted Dry of Optimum for Three Efforts	100
27. Differential and Cumulative Pore Size Distribution Curves for 50% Silt-50% Kaolin Compacted at Low Effort	102
28. Differential and Cumulative Pore Size Distribution Curves for 50% Silt-50% Kaolin Compacted at Medium Effort	103
29. Pore Size Distribution Curves for 50% Silt-50% Kaolin Compacted at Optimum and Dry of Optimum Water Contents for Two Efforts	104
30. Particle Size Frequency Plot of the Soils Tested	106
31. Pore Size Distribution Curves for Three Soil Types Compacted at Medium Effort and Optimum Water Content	107
32. Pore Size Distribution Curves for Three Soil Types Compacted at Medium Effort and Dry of Optimum Water Content	108
33. Permeability vs Void Ratio	111
34. Permeability vs Capillary Model Equivalent Pore Size Parameter, $E(d^2) n$	115

LIST OF FIGURES (Continued)

Figure	Page
35. Permeability vs Marshall Equivalent Pore Size Parameter, d^2	116
36. Permeability vs Equivalent Hydraulic Radius Pore Size Parameter, R_H^2 n	117
37. Replicate Pore Size Distribution Curves for Sample S9MO	134
38. Replicate Pore Size Distribution Curves for Sample S9MO-D	135
39. Replicate Pore Size Distribution Curves for Sample S9MD	136
40. Replicate Pore Size Distribution Curves for Sample S9MW	137
41. Replicate Pore Size Distribution Curves for Sample S9HO	138
42. Replicate Pore Size Distribution Curves for Sample S9HD	139
43. Replicate Pore Size Distribution Curves for Sample S9HW	140
44. Replicate Pore Size Distribution Curves for Sample S7LO	141
45. Replicate Pore Size Distribution Curves for Sample S7LD	142
46. Replicate Pore Size Distribution Curves for Sample S7LW	143
47. Replicate Pore Size Distribution Curves for Sample S7MO	144
48. Replicate Pore Size Distribution Curves for Sample S7MD	145
49. Replicate Pore Size Distribution Curves for Sample S7MW	146
50. Replicate Pore Size Distribution Curves for Sample S7HO	147

LIST OF FIGURES (Continued)

Figure	Page
51. Replicate Pore Size Distribution Curves for Sample S7HD	148
52. Replicate Pore Size Distribution Curves for Sample S7HW	149
53. Replicate Pore Size Distribution Curves for Sample S5LO	150
54. Replicate Pore Size Distribution Curves for Sample S5LD	151
55. Replicate Pore Size Distribution Curves for Sample S5LW	152
56. Replicate Pore Size Distribution Curves for Sample S5MO	153
57. Replicate Pore Size Distribution Curves for Sample S5MD	154
58. Replicate Pore Size Distribution Curves for Sample S5MW	155
59. Closed System Falling Head Permeability Test	160
60. Changes in Effective Stress Caused by Flow Through Soils	160
61. X-ray Diffraction Patterns of Critical Region and Air Dried Soils	164

LIST OF ABBREVIATIONS AND SYMBOLS

AASHTO	- American Association of State Highway and Transportation Officials
A	- angstrom (10^{-10} m)
a	- area
ASCE	- American Society of Civil Engineers
ASTM	- American Society for Testing and Materials
b	- regression parameter
C	- Celsius
c	- logarithmic interval constant
cm	- centimeter (10^{-2} m)
C_s	- shape factor
°	- degree
d	- pore diameter
\hat{d}^2	- Marshall model pore size parameter
δ	- pore diameter corresponding to an intrusion pressure
Dept.	- Department
e	- void ratio
$E(d^2)$	- second moment about the origin of d
F	- Farenheit
$f(d_i)$	- volumetric frequency of d_i
ft^3	- cubic feet
γ	- unit weight

h	- total head
I.D.	- inside diameter
K	- specific or physical permeability, L^2
k	- permeability, L/t
L	- length
lbs	- pounds
\ln	- natural logarithm
log	- logarithm base 10
m	- meter
μ	- absolute viscosity
ml	- milliliter (1 cm^3)
mm	- millimeter (10^{-3} m)
μm	- micrometer (10^{-6} m)
n	- porosity
P	- intrusion pressure
%	- percent
psi	- pounds per square inch
PSP	- Pore Size Parameter
q	- volume flow rate
r	- pore radius
r^2	- coefficient of determination
R_H	- hydraulic radius
S	- hydraulic gradient
S.A.	- Surface Area, L^2
sec	- seconds
S_s	- Specific Surface Area (S.A./v)

σ'_z	- effective stress at z
T	- temperature
t	- time
θ	- contact angle
T_s	- surface tension
u	- water pressure
U.S.	- United States
V	- volume
v	- discharge velocity
ΔV	- net volume of inflow
v_s	- seepage velocity
V_v	- volume of voids

HIGHLIGHT SUMMARY

Information about the soil permeability is vital to the success of many geotechnical works. Various predictive equations based on volumetric and grain size parameters have been proposed to estimate the permeability. These predictive equations have had limited success for coarser soils, but have been completely unsatisfactory for fine-grained soils. Knowledge of the soil structure is essential to understanding and predicting the engineering behavior of fine-grained soils. The volumetric and grain size parameters are poor indicators of soil structure and cannot be expected to accurately reflect changes in permeability. This investigation utilizes pore size distribution measurements to examine the relationship between permeability and soil fabric of laboratory compacted clayey silts.

A method of approximating the differential pore size distribution is described which simplifies the interpretation of pore size distributions. The most frequent or modal pore diameters served as useful comparative parameters when contrasting pore size distribution curves for various soils.

Three blends of silt and kaolin were compacted by kneading compaction at two or three levels of effort. For each soil type and compactive effort, samples were prepared at three water contents:

optimum, dry of optimum, and wet of optimum. Closed system falling head permeability tests under back pressure were performed on each of the compacted samples. Freeze drying was successfully used to dehydrate specimens prior to pore size measurements. The mercury intrusion technique was used to determine the pore size distribution.

The pore size distributions of the soils tested were bimodal with a large pore mode occurring between 10 and 1 μm and a small pore mode occurring at 0.1 μm . Varying the compaction variables produced changes in the position and frequency of the large pore mode, but caused no change in the pore size distribution about the small pore mode for a given soil type. Permeability generally increased with increases in the frequency and position of the large pore mode.

Three theoretical permeability models which relate pore size distribution parameters to permeability were examined. Although the models were not completely successful in predicting permeability, the pore size parameters from two of the models did reflect, with several modifications, the influence of pore size distribution on permeability. These parameters were successfully used to determine empirical permeability prediction equations for the soils tested.

This study demonstrates the usefulness of pore size distribution measurements to interpret changes in soil fabric and to predict how these changes affect an engineering property.

INTRODUCTION

Permeability is one of the most important yet variable properties in Geotechnical Engineering. Conventionally, permeability is evaluated either by in situ or laboratory tests. In situ tests are costly and difficult to interpret because of the complex boundary conditions involved. Laboratory tests also present formidable problems, the most troublesome being obtaining representative samples. To circumvent the testing problems, methods of estimating permeability from grain size and volumetric characteristics have previously been attempted. These predictive equations have had limited success for coarser soils, and have proved to be completely unsatisfactory for fine-grained soils. The fundamental problem with these equations is that permeability is extremely sensitive to subtle changes in soil structure, a property which bulk volumetric parameters do not accurately reflect.

This investigation takes a more fundamental approach by examining the relationship between permeability and pore size distribution of compacted fine-grained soils. Three models of porous media, which utilize pore size distribution parameters to calculate permeability, are examined. Simple linear regression is used to determine permeability predicting equations from these pore size parameters and permeability measurements.

The fabric of compacted soils is also examined. The influence of varying water content and compaction effort on the pore size distribution of three soils is considered in light of existing models for the structure of compacted clay.

Pore size distributions were determined by the method of mercury intrusion. Dehydration of the soils prior to pore size measurements was accomplished by freeze drying. Both differential and cumulative pore size distributions are presented.

A closed system falling head test was used to measure the permeability of the compacted samples. Back pressure was applied to the samples during permeation to insure saturation, and the permeability tests were conducted at low hydraulic gradients.

1 - LITERATURE REVIEW AND GENERAL DISCUSSION

1-1 Permeability and Fabric of Compacted Fine-Grained Soils

Permeability is one of the most fundamental yet variable properties of soils in Geotechnical Engineering. Permeability must be considered in problems of seepage, drainage, dewatering, rate of settlement and rate of strength increase with pore pressure dissipation. Values of soil permeability may range across twelve orders of magnitude and are extremely sensitive to changes in soil composition and structure.

The measurement of soil permeability in the laboratory presents a formidable problem, but when these laboratory results are extrapolated to field permeability values for analysis purposes, enormous if not intolerable variability may result. The primary reason for this is that there exists no reliable way of determining the field soil structure and thus, no way to replicate it in the laboratory. The macrofabric of the in situ soil must also be considered (Rowe, 1972), but for compacted soils, these features, such as fissures, joints, and stratification, are not as prevalent.

The objectives of this study are to use pore size distribution measurements as an indicator of soil fabric:

- 1) to improve the understanding of the fabric of compacted fine-grained soils, and
- 2) to determine a relation between pore size distribution and permeability measurements for these same soils.

This section reviews the results of previous studies concerned with the permeability of compacted clays, discusses the importance of soil fabric of compacted clays, and examines several permeability prediction models which incorporate pore size distribution parameters.

1-1.1 Permeability

Lambe (1954) was one of the first investigators to examine the permeability of compacted fine-grained soils. He noted the pronounced affect that molding water content had on the permeability for a given soil compacted at a given effort. Lambe concluded that since these changes in permeability could not be accounted for by changes in dry density or void ratio, they must be caused by changes in the "arrangement of soil particles or 'structure'." Subsequent studies of the permeability of compacted clays and silts to water by Bjerrum and Huder (1957), and Mitchell, Hooper and Campanella (1965) found results similar to those obtained by Lambe. Figure 1, taken from Mitchell et al. (1965), shows the relationship between compaction water content and permeability of a silty clay prepared at three compaction efforts. The relation shown by this Figure may be considered typical for compacted fine-grained soils. Summarizing the results of the three investigations listed above (Lambe, L; Bjerrum et al., B; and Mitchell et al., M):

1. The permeability gradually decreases with increasing water content on the dry side of optimum for a given compaction effort (L, B, M); though, Mitchell et al. reported one soil for which this was not the case.

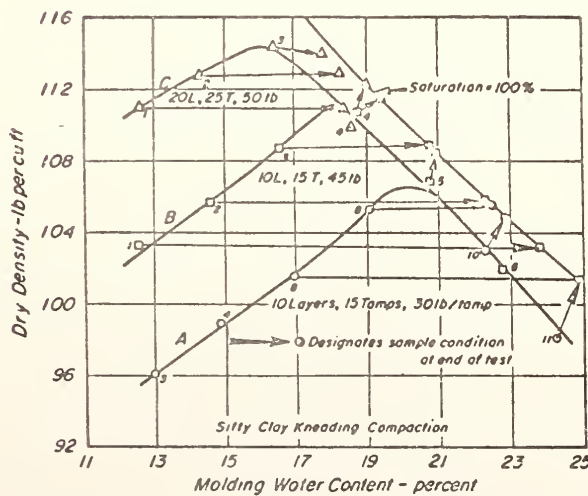
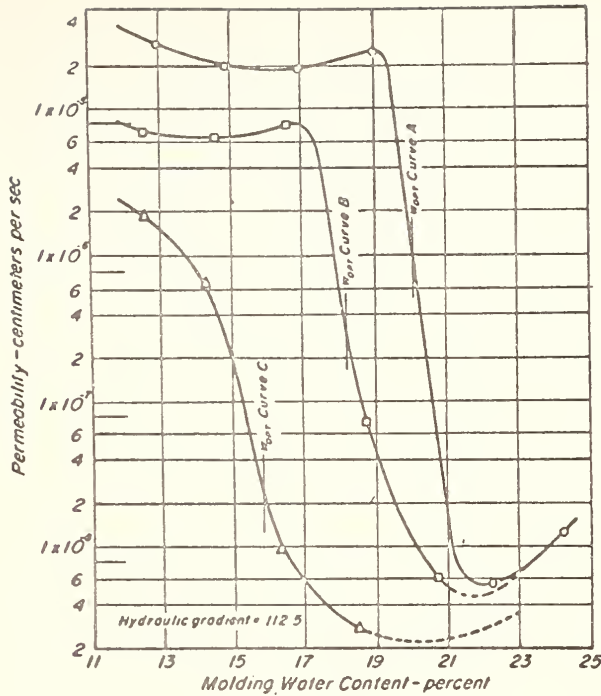


FIGURE 1 PERMEABILITY OF A SILTY CLAY AT THREE COMPACTIVE EFFORTS (FROM MITCHELL *et al* 1965)

2. Near optimum, the permeability undergoes a significant decrease of two to three orders of magnitude less than the dry side permeabilities with increasing water content for a given compaction effort (L, B, M).
3. Wet of optimum, the permeability may increase or decrease slightly with increasing water content for a given compaction effort, but generally it remains within the same order of magnitude as the permeability at optimum (L, B, M).
4. Increasing the degree of saturation by back-pressuring during permeation slightly increases the permeability, all other factors being constant (B, M). This effect is more pronounced on dry side samples (B). The permeability increases approximately with the cube of the degree of saturation, all other factors being constant (M).
5. Varying the compaction effort shifts the position of the permeability-molding water content curve, but the general trends (1 to 3 above) remain the same, as shown in Figure 1 (M).
6. For a given water content wet of optimum and a given dry density and soil type, static compaction produces a sample with a higher permeability than one compacted by kneading compaction (M).

Langfelder, Chen and Justice (1968) measured air permeabilities of compacted fine-grained soils and concurred with results 1 and 2 listed

above. They also determined that for water contents at or above optimum, the air permeability was essentially zero. For most of the soils which were tested at varying gradients, an "apparent threshold gradient" was obtained, whose magnitude increased as the air permeability decreased.

The Kozeny-Carman equation (Carman, 1956) has frequently been used to predict the permeability of other types of porous media and is given as:

$$k = \frac{\gamma}{\mu} \frac{1}{k_o k_T} \frac{e^3}{(1+e) s^2} \quad (1-1)$$

where k is the permeability (L/t)

γ is the unit weight of the permeant

μ is the absolute viscosity of the permeant

e is the void ratio

s is the internal surface area per volume of solids

k_o is the pore shape factor

k_T is the tortuosity

This expression has not been found to be suitable for predicting the permeability of fine-grained soils as shown by Lambe (1954), Michaels and Lin (1954), and Olsen (1962).

Michaels and Lin (1954) performed permeability tests on kaolin beds prepared and permeated with fluids of varying polarity and compressed to decreasing void ratios. They found that the rate of change of permeability was greater than that predicted by the Kozeny-Carman equation. Because these deviations were of the same order for the various fluids tested, they concluded that the effect was caused "...mainly by changes in aggregate size and particle orientation during mechanical compaction", rather than by interactions between the fluids and the particle surface. The permeability of kaolin decreased markedly with increasing

polarity of the fluid. They attributed this to the existence of a more dispersed structure resulting from an increase in the polarity of the fluid in which the clay beds were prepared. Finally, they concluded that interfacial effects such as adsorption and counter-electroosmosis are responsible for only minor changes in the permeability of kaolin.

Olsen (1962) conducted one dimensional consolidation-permeability tests on kaolinite, illite and Boston blue clay and also found discrepancies between the permeabilities calculated from the Kozeny-Carman equation and measured permeabilities as follows:

- 1) For void ratios greater than about 0.4 to 0.5 the permeability decreased more than predicted with decreasing void ratio.
- 2) For void ratios less than 0.4 the permeability decreased less than predicted with decreasing void ratio.
- 3) For rebounded samples the permeability increased at a rate less than predicted with increasing void ratio.

Olsen, after considering if the above discrepancies could be explained by non-Darcy flow, electrokinetic coupling, high viscosity, or tortuous flow path, concluded that only unequal pore sizes could account for the discrepancies. Olsen hypothesized a cluster or packet and domain model for the soil structure which would explain the unequal pore sizes. Recent investigations of fine grained soil fabric have confirmed Olsen's cluster hypothesis, as will be discussed below.

Several investigators including Hansbo (1960), Swartzendruber (1962), Miller and Low (1963), Olsen (1965) and (1966), Mitchell and Younger (1967), and Russell and Swartzendruber (1971) have investigated the validity of Darcy's law for fine-grained soils at low hydraulic gradients. Barring experimental errors, two explanations have been proposed to account for the non-linear relation between flow velocity and hydraulic gradient:

- 1) particle migration causing clogging and unclogging of the soil pores (Hansbo, 1960);
- 2) quasi-crystalline behavior of water near the clay surface (Miller and Low, 1963).

Some insight can be gained by examining hypothetical soil structures which might explain each of the above causes for non-Darcy flow.

For particle migration to be a factor, a small fraction of the smaller size soil particles (presumably non-clay) must exist in a loose state within the soil mass. These loosely held particles should be roughly the same size or slightly smaller than the larger pores which control the permeability of the porous medium. Mitchell and Younger (1967) found that for a compacted silty clay, particle migration caused changes in soil fabric during flow which led to non-Darcy effects; these effects were most significant for samples compacted at low water contents (significantly lower than optimum) and low densities. Such soils probably have a relatively high permeability, as discussed previously, and an unstable structure (susceptible to collapse or piping).

For quasi-crystalline water to be responsible for non-Darcy flow at low hydraulic gradients, the pores controlling the permeability

must be of size comparable to the thickness of the adsorbed water layer. This would mean a tightly packed soil fabric (with small pore size) containing a clay of high activity (Miller and Low, 1963). Such a soil would be expected to have a low permeability.

The factors affecting the permeability of soils and other porous media have been discussed by a number of authors, including Taylor (1948), Lambe (1954), Scheidegger (1957) and Leonards (1962). In general terms, three factors control the permeability of a soil:

- 1) the geometry of the porous network (i.e. the fabric);
- 2) the properties of the permeating fluid (viz., viscosity and density);
- 3) the surface interaction between the permeating fluid and the porous media.

From the various investigations just described, it is clear that the geometry of the porous network is by far the most important factor controlling the permeability of most fine-grained soils. The second factor above is of little consequence in geotechnical engineering since water is nearly always the pore fluid. The influence of the third factor on permeability should certainly be significant for soils of high plasticity (Schmid, 1957) or dispersive clays; however, this topic was not addressed in this investigation. Blends of silt and kaolin of low plasticity were used in an effort to minimize the influence of interactions between fluid and soil surface on the permeability.

Because of the importance of soil fabric on permeability, a brief review of some previous investigations dealing with the structure of compacted clays and silts is appropriate.

1-1.2 Fabric

Prior to commencing this discussion of soil fabric it is necessary to define the terms "fabric" and "structure" as used in this study.

According to Yong and Sheeran (1973):

"The structure of a soil has been defined as that property of soil which provides its integrity. An important component of structure is its fabric, i.e. the physical arrangement of soil particles including particle spacing and pore size distribution. When soil fabric is considered in conjunction with bonding forces and particle interaction mechanisms developed, the structure of soil is obtained ..."

The term "macrofabric", according to Mitchell (1976), will refer to "... those features that can be seen with the unaided eyes, or a hand lens ..." including "stratification, fissuring, voids, and large inhomogeneities ..." The importance of "macrofabric" in geotechnical engineering is discussed by Rowe (1972), and will not be considered in this study.

Lambe (1958) was one of the first investigators to hypothesize a model for the structure of compacted clay. He based his model on the principles of colloidal and crystal chemistry and the behavior of compacted clays. Lambe postulated that individual clay particles are the predominant units which influence the compaction characteristics and behavior of a soil mass. At low water contents a compacted soil is in an open and flocculated state because the suppressed double layer has reduced particle repulsion. As the molding water is increased toward optimum, the double layer expands which increases particle repulsion, but a more orderly particle arrangement is formed due to increased "lubrication". At water contents greater than optimum, the diffuse double layer continues to expand, increasing particle repulsion,

increasing the distance between particles, and resulting in a nearly parallel particle arrangement.

More recent investigations of soil structure employing scanning electron microscopy, X-ray diffraction, and pore size distribution measurements have resulted in modifications of Lambe's compacted soil model. As Yong and Sheeran (1973) stated:

"Examination of electron micrographs and soil performance shows that individual particles rarely act as single particle units, except for certain types of clays and under certain conditions,.... The different sizes and arrangements of particle groups observed in fabric viewing suggest that response behavior might be controlled by the kinds and arrangements of these particle groups."

Independent studies by Barden and Sides (1970) and Hodek (1972) have proposed a revision of Lambe's compacted clay model.

Barden and Sides (1970) combined microscopic fabric analysis with laboratory measurements to study: 1) the development and drainage of pore pressures and 2) the compression characteristics of compacted clays.

Hodek (1972) examined the strength and particle orientation characteristics of aggregations of kaolin formed by conventional mixing techniques prior to compaction. He then analyzed the influence of these kaolin aggregates at various water contents and of various sizes on the compaction characteristics and swelling pressure of compacted specimens.

Both investigations reached the conclusion that the behavior and characteristics of a compacted clay can be explained in terms of a deformable aggregate soil model. Prior to compaction, the soil particles are grouped in agglomerations or "peds" whose size and

strength characteristics are influenced by the molding water content. During compaction at low water contents (below optimum) these peds or aggregates have a high strength and are better able to resist the compaction pressures without much distortion. Thus, there exist two networks of pore space in the clay mass: a network of large inter-aggregate pores and a network of small intra-aggregate pores. As the molding water content increases (dry of optimum), the aggregates decrease in strength and suffer greater deformation during compaction. This results in a decrease in inter-aggregate pore space and an increase in dry density. Olson (1963), Langfelder et al. (1968), and Barden and Sides (1970) have all found that clays compacted near their optimum water contents have zero air permeability, which would indicate that the inter-aggregate pore network is no longer continuous. With increasing water content above optimum, the aggregates are easily distorted and fuse together making them indistinguishable. Individual particle reorientation and dispersion may occur at this stage.

Pore size distribution measurements of compacted clays by Diamond (1970) and (1971), Sridharan et al. (1971), Ahmed et al. (1974) and Bhasin (1975) have also provided strong evidence for a deformable aggregate soil model.

Diamond (1971) employed pore size distribution methods, scanning electron microscopy, and X-ray diffraction to study the fabric of impact compacted kaolinite and illite. Pore size distribution measurements indicated that clays compacted dry of optimum have a significant volume of pores between 1 and 10 μm in size while samples compacted at or above the optimum water content contained very little pore space greater than

0.1 μm in size. This conclusion was also reached by Ahmed et al. (1974) and Bhasin (1975) for other types of clayey soils and using improved soil drying techniques for pore size measurements. Scanning electron micrographs, presented by Diamond (1971), revealed individual aggregations of clay particles several microns in size and corresponding voids of the same size for samples compacted dry of optimum. Samples compacted at or above the optimum water content did not show these individual aggregations nor the large pore space. Using X-ray diffraction measurements of oriented compacted clay samples, Diamond found no evidence of increased particle orientation with increasing molding water content, as hypothesized by Lambe (1958).

Sridharan et al. (1971) performed pore size distribution measurements of statically compacted kaolin, illite, and Boston blue clay and artificially sedimented kaolin. Static compaction of a given soil at a given water content to decreasing void ratio values was found to be at the expense of the larger pores with little or no influence on pores about 0.1 μm in size. They reported that each type of clay had its own characteristically different pore size distribution when compacted at similar water contents. There appeared to be no obvious correlation between the pore size and grain size distributions. The shape of the pore size distribution curve was also found to be sensitive to the method of soil preparation. Artificially sedimented kaolinite had a pore size curve distinctly different from that for statically compacted kaolinite.

Ahmed et al. (1974) found no significant difference in the shapes of pore size distribution curves between clays prepared by impact and

by kneading compaction to a common water content and dry density.

Bhasin (1975) found that increasing the compactive effort on the dry side of optimum for a given soil decreases the total porosity and diminishes the fraction of large pores. Increasing the compaction effort on the wet side of optimum had little effect on either the total porosity or the distribution of pore sizes. He also concluded that:

"The gross differences in pore size distributions occurring at the same percentage compactations, for different soils and compaction efforts, emphasize the lack of control over the compacted product exercised by most end result compaction specifications."

To date, no pore size distribution measurements have been reported for field compacted fine-grained soils. Certainly, the sensitivity of soil fabric to slight changes in water content, compaction energy and method of compaction would warrant such an investigation.

1-1.3 Permeability Models

The aim of this section is to examine several of the relatively simple and conventional models used to describe flow through porous media in order to gain some insight into the relation between permeability and pore size distribution. The final objective will be to arrive at several pore size parameters, which can be calculated from a pore size distribution, and which may correlate with permeability measurements. Scheidegger (1974) and Bear (1972) both discuss the complex nature of a porous media and the limitations of conventional models for predicting permeability. They conclude that statistical modeling would be a more logical approach to predict permeability and present such models; however, owing to its complexity, statistical modeling of porous media was considered beyond the scope of this study.

Two classical models have been employed to describe the flow through porous media, viz., the equivalent capillary model and the equivalent hydraulic radius model. Both can be derived from the Hagen-Poiseuille equation as demonstrated by Leonards (1962).

The Hagen-Poiseuille equation for laminar flow through a cylindrical capillary is given as:

$$q = \frac{\pi \gamma S}{8\mu} R^4 \quad (1-2)$$

where q is the volume of flow per unit time
 R is the radius of the capillary
 S is the hydraulic gradient
 γ is the fluid unit weight
 μ is the absolute viscosity of the fluid.

Purcell (1949) employed a modified capillary model to calculate the permeability of sandstones from pore size distribution measurements. Purcell modeled the porous media as a set of parallel cylindrical capillaries of varying pore diameter extending from one end of the porous medium to the other. Each capillary is assumed to have a constant radius throughout its length. The frequency of occurrence of each capillary size is determined from the pore size distribution curve. Schiedegger (pp. 129-130, 1974) discusses a simplified method of calculating the permeability from this model and also discusses some of its limitations. Beginning with the Hagen-Poiseuille equation, the flow rate, q_i , through a capillary of radius r_i is given as:

$$q_i = \frac{\pi \gamma S}{8\mu} r_i^4 \quad (1-3)$$

Equation (1-3) can be rewritten as:

$$q_i = \frac{\gamma S}{8\mu} r_i^2 \pi r_i^2 \quad (1-4)$$

For more than one capillary of the radius r_i , let $\alpha(r_i)$ represent the number of pores of size r_i . Thus the flow rate through all capillaries of r_i becomes:

$$q_i = \frac{\gamma S}{8\mu} r_i^2 \alpha(r_i) \pi r_i^2 \quad (1-5)$$

The term " $\alpha(r_i) \pi r_i^2$ " is the "area-frequency" of the capillary radius r_i . It is evident that for any cross-section taken perpendicular to the direction of flow, the area-frequency of r_i will remain the same. Thus, multiplying the area-frequency by a unit length gives the volumetric frequency $f(r_i)$ of r_i (Harr, 1962 p. 4), which is the quantity measured by pore size distribution methods.

Considering a unit volume of pore space in the porous medium with a distribution of parallel capillaries traversing it, the volumetric-frequency distribution of the capillaries can be given as:

$$\sum_i f(r_i) = 1 \quad (1-6)$$

Combining equations (1-5) and (1-6), the total flow rate through all the capillaries through a unit volume of pore space is:

$$q = \frac{\gamma S}{8\mu} \sum_i f(r_i) r_i^2 \quad (1-7)$$

Dividing equation (1-7) by a unit area of pore space gives the average seepage velocity through the pores v_s :

$$v_s = \frac{\gamma S}{8\mu} \sum_i^1 f(r_i) r_i^2 \quad (1-8)$$

The discharge velocity v through a unit section of porous media is:

$$v = v_s n \quad (1-9)$$

$$v = \frac{\gamma S}{8\mu} n \sum_i^1 f(r_i) r_i^2 \quad (1-10)$$

where n is the porosity.

Applying Darcy's Law, " $v = k \cdot S$ ", to equation (1-10) gives:

$$k = \frac{\gamma}{8\mu} n \sum_i^1 f(r_i) r_i^2 \quad (1-11)$$

where k is the permeability.

The value " $\sum_i^1 f(r_i) r_i^2$ " is defined as the second moment about the origin of the pore size distribution and is usually represented as " $E(r^2)$ ".

If the pore diameter is considered rather than the pore radius, equation (1-11) becomes:

$$k = \frac{\gamma}{32\mu} E(d^2) n \quad (1-12)$$

Replacing the permeability k by the "specific or physical permeability, K " and using $k = K \gamma / \mu$, equation (1-12) becomes:

$$K = C_s E(d^2) n \quad (1-13)$$

where C_s is a shape factor which is equal to 1/32 for cylindrical pores.

There are several shortcomings of this equation, as pointed out by Scheidegger; (1974):

- 1) All pores are assumed to go in one direction.
- 2) Tortuosity is not considered.
- 3) The shape factor is considered constant for all pore sizes.
- 4) The value of $E(d^2)$ is extremely sensitive to the frequency of the larger pores.
- 5) The model is an oversimplification of the porous media.

Considering equation (1-13) as an empirical equation and solving for C_s from actual pore size and permeability measurements, Purcell found that changes in " $E(d^2) n$ " (or its equivalent) accurately reflected changes in permeability. However, the value of C_s (or its equivalent) varied for the different materials tested, and for a given material at varying porosities, C_s increased with increasing permeability.

Childs and Collis-George (1950) and Marshall (1958) employed another form of the capillary model using the pore size distribution to calculate permeability. They considered two unit cross-sections of a porous medium placed together such that the pores from one surface are randomly connected to those of the other surface. Each of the cross-sections contain cylindrical pores of varying radius. The pore size distributions for each of the two cross-sections are assumed to be identical and represented as:

$$\sum_i f(r_i) = n \quad (1-14)$$

where $f(r_i)$ is again the volumetric frequency of occurrence of pore r_i and n is the porosity. Note that a unit volume of porous medium and

not a unit volume of pore space is being considered; therefore, the sum of the volumetric frequency is equal to the porosity.

The probability that a pore r_i from the i^{th} cross-section is joined with a pore r_j from the j^{th} cross-section, according to probability theory, can be represented as:

$$r_i \rightarrow r_j = f(r_i) f(r_j) \quad (1-15)$$

or the product of the two probabilities as each is independent of the other. The flow rate through the capillary connecting r_i and r_j from equation (1-4) above can be represented as:

$$q_{r_i \rightarrow r_j} = \frac{\gamma S}{8\mu} \tilde{r}^2 f(r_i) f(r_j) \quad (1-16)$$

where \tilde{r} is assumed to be the smaller of the two pore sizes r_i and r_j . It follows that the total quantity of flow through a unit volume of porous medium is:

$$q = \frac{\gamma S}{8\mu} \sum_i^n \sum_j^n \tilde{r}^2 f(r_i) f(r_j) \quad (1-17)$$

The discharge velocity v is:

$$v = \frac{\gamma S}{8\mu} \sum_i^n \sum_j^n \tilde{r}^2 f(r_i) f(r_j) \quad (1-18)$$

and using Darcy's law to solve for the permeability, k , yields:

$$k = \frac{\gamma}{8\mu} \sum_i^n \sum_j^n \tilde{r}^2 f(r_i) f(r_j) \quad (1-19)$$

Rewriting equation (1-19) in terms of pore diameter and specific permeability:

$$K = \frac{1}{32} \sum_i^n \sum_j^n \hat{d}^2 f(d_i) f(d_j) \quad (1-20)$$

or

$$K = C_s \hat{d}^2 \quad (1-21)$$

where

$$\hat{d}^2 = \sum_i^n \sum_j^n \tilde{d}^2 f(d_i) f(d_j) \quad (1-22)$$

n is the porosity, and
 C_s is the shape factor.

The value of \hat{d} will be referred to as the Marshall model pore size parameter.

The third model examined was the Kozeny hydraulic radius model. Scheidegger (1957) and Leonards (1962) discuss its derivation, and Scheidegger (Chapter 6, 1957) presents a critique of the model. From the Hagen-Poiseuille equation, the seepage velocity v_s through the pore space is assumed to be:

$$\frac{Q}{a} = v_s = C_s \frac{\gamma_s}{\mu} R_H^2 \quad (1-23)$$

where a is the cross-sectional area of flow and
 R_H is the hydraulic radius.

The discharge velocity v is:

$$v = C_s \frac{\gamma_s}{\mu} R_H^2 n \quad (1-24)$$

Applying Darcy's law, the permeability is equal to:

$$k = C_s \frac{\gamma}{\mu} R_H^2 n \quad (1-25)$$

The specific permeability is then equal to:

$$K = C_s R_H^2 n \quad (1-26)$$

The hydraulic radius R_H can be expressed as (Leonards, 1962):

$$R_H = \frac{n}{S_s} \quad (1-27)$$

where S_s is the surface area per unit volume or the specific surface.

Section 1-2.3 will describe a method of calculating the specific surface S_s from the pore size distribution (Rootare and Prenzlow, 1967) as follows:

$$S_s = 4 n \sum_i \frac{f(d_i)}{d_i} \quad (1-28)$$

where $\sum_i f(d_i) = 1$.

The hydraulic radius R_H may then be expressed as a pore size parameter as follows:

$$R_H = \frac{1}{4 \sum_i \frac{f(d_i)}{d_i}} \quad (1-29)$$

and the specific permeability as:

$$K = C_s n \frac{\frac{1}{4} \sum_{i=1}^4 \frac{f(d_i)}{d_i}}{\sum_{i=1}^4 f(d_i)}^2 \quad (1-30)$$

Summarizing, three different models have been described which involve the calculation of permeability from pore size distribution. The pore size parameters from each of the models will be correlated with actual permeability measurements for the soils tested to gain some insight into the relationship between the permeability and pore size distribution of fine-grained soils. Table 1 presents a summary of the models.

1-2 Pore Size Distribution

The measurement of pore size distribution is one technique of inferring the relative arrangement of particles and pores (i.e., the fabric) of a soil. Frequently, knowledge of the gross soil properties is insufficient information to understand or predict the behavior of a soil when it is subjected to changed conditions. Information about the pore size distribution and changes in distribution with changed conditions can be useful in interpreting soil behavior. Pore size information may also be helpful in obtaining information about the depositional history of a soil, the movement of fluids and solids through a soil, and the chemical reactivity of a soil. Compression, sample disturbance or remolding, structural collapse and swelling can all be detected by determining changes in pore size distribution.

This writer believes that the measurement of pore size distribution has been refined to such a stage that it may become a routine

TABLE 1 SUMMARY OF PERMEABILITY MODELS USED

1) VARIABLE DIAMETER CAPILLARY MODEL

$$\text{Equation} \quad K = C_s E(d^2) n$$

$$\text{Pore Size Distribution Parameter} \quad E(d^2) = \sum_i^1 f(d_i) d_i^2$$

$$\text{where } \sum_i f(d_i) = 1$$

2) MARSHALL MODEL

$$\text{Equation} \quad K = C_s \hat{d}^2$$

$$\text{Pore Size Distribution Parameter} \quad \hat{d}^2 = \sum_i^n \sum_j^n \tilde{d}^2 f(d_i) f(d_j)$$

$$\text{where } \tilde{d} = d_i \text{ if } d_i < d_j$$

$$\text{or } \tilde{d} = d_j \text{ if } d_i \geq d_j$$

$$\text{and } \sum_i f(d_i) = \sum_j f(d_j) = n$$

3) HYDRAULIC RADIUS MODEL

$$\text{Equation} \quad K = C_s R_H^2 n$$

$$\text{Pore Size Distribution Parameter} \quad R_H = \frac{1}{4 \sum_i^1 \frac{f(d_i)}{d_i}}$$

$$\text{where } \sum_i f(d_i) = 1$$

K = specific permeability, L^2

n = porosity

C_s = shape factor

d_i = pore diameter, L

$f(d_i)$ = volumetric frequency of d_i

test for research studies as well as for special practical projects where knowledge of the soil fabric is required.

1-2.1 Applications

Pore size distribution studies have found application in several fields including chemical engineering, petroleum engineering, materials engineering, soil science and geotechnical engineering. Ahmed (1971) presents a thorough review of the application of pore size distribution measurements primarily in the geotechnical field. Several of the pore size distribution studies not discussed by Ahmed (1971) will be mentioned here.

Silveira (1965) combined pore size distribution calculations with probabilistic modeling to study the problem of fine particles passing through protective sand filters. The pore size distribution is calculated from the grain size distribution by finding the probability of the various particle sizes occurring in assemblages of three spherical particles tangent to each other. From the assemblages, equivalent pore diameters are calculated and a pore size distribution curve is generated. With the pore size distribution calculated for the filter material, the absorbing Markov chain process is used to calculate the mean distances which a given soil particle will travel through the filter. This ingenious approach can be used to determine the suitability of a filter material and the thickness of filter required to prevent clogging.

Sridharan (1968) successfully applied pore size distribution studies to calculate the negative pore pressures in partly saturated clays. By measuring the surface area of a soil and its pore size

distribution, Sridharan was able to estimate the negative pore water pressures resulting from adsorption and capillary retention of water for compacted and artificially sedimented soils. The objective of his research was to gain a better understanding of the shear strength of partly saturated soils by examining the soil structure.

Badger and Lohnes (1973) used mercury intrusion pore size distribution measurements to study the fabric of natural and compacted loess. Samples of loess compacted in the laboratory to void ratios equal to that of natural loess were found to have fewer large pores than the undisturbed loess. They also identified several types of loess soil structure by comparing the grain size and pore size distributions.

Lohnes, Tuncer and Demirel (1976) studied the affect of precipitation on the structure of tropically weathered basaltic soils. Pore size distribution measurements with mercury intrusion revealed that increased precipitation resulted in a finer pore fabric for the residual soils tested. Void ratio measurements did not correlate with these changes in pore size distribution.

Reed (1977) demonstrated the relation between frost heave and pore size distribution of compacted silty soils. Conventionally, the frost susceptibility of a soil is predicted from the grain size distribution and soil texture, and no consideration is given to soil fabric. Reed's work demonstrated that samples compacted dry of optimum display significantly greater frost heave than those compacted at optimum or wet of optimum. He also determined an empirical equation to predict frost heave from pore size distribution parameters of the soils tested.

Bhasin (1975) presented a critical review of the various techniques available to measure pore size distribution of silty-clayey soils. He concluded that only the mercury intrusion method is capable of measuring the entire range of pore sizes, up to five orders of magnitude, of fine grained soils.

1-2.2 Theory, Assumptions and Limitations

Pore size distribution determinations for this study were performed with mercury intrusion. The mercury intrusion equipment employed has a pressuring capacity of 15,000 psi and is capable of intruding pores from 600 μm to 0.016 μm in size. New commercial equipment currently available has extended the lower pore size limit to 0.004 μm by increasing the pressure generating capacity to 60,000 psi.

The mercury intrusion technique is based on the principle that the surface tension of a non-wetting liquid (one which has a contact angle greater than 90° with a given solid) will oppose the entry of the liquid into a small pore of a solid. Washburn (1921) determined that this opposition could be overcome by external pressure, and that the external pressure required was inversely proportional to the pore diameter. Assuming a cylindrical pore, Washburn calculated the relation to be:

$$P = \frac{4 T_s \cos \theta}{d} \quad (2-1)$$

where P is the absolute pressure required

T_s is the surface tension of the intruding liquid

θ is the contact angle between the solid and the liquid

d is the pore diameter.

Mercury was used as the intruding fluid because, according to Winslow and Diamond (1970), "... its practical advantages include low vapor pressure, relative inertness in terms of chemical reactivity, and the fact that it is normally non-wetting for most kinds of surfaces." The surface tension of mercury used for this study was that determined by Kemball (1946) and recommended by Diamond (1970), of 484 dynes/cm at 25° C.

Diamond (1970) demonstrated that the contact angle between mercury and clay minerals is dependent on the mineral present. He measured, by the sessile drop method, the contact angle for mercury on kaolinite or illite which was within one degree of 147°; and mercury on montmorillonite which was within one degree of 139°. A contact angle of 147° was used for this study since kaolinite was the principal clay mineral present in the soils tested.

Briefly, pore size distribution is determined in the following manner. The sample is initially evacuated and surrounded by mercury, the pressure is raised in small increments and the volume of mercury entering the sample after each increment is recorded. Each pressure increment forces mercury into the accessible soil pores of a diameter larger than or equal to that calculated by the Washburn equation for the given pressure. In this manner, the volume of pore space between pressure increments, and thus diameter decrements, is recorded, generating a pore size distribution.

The assumptions and sources of error of the mercury intrusion technique are discussed in detail by Ritter and Drake (1945), Rootare (1968), Winslow (1969), and Diamond (1970), but it is worth reviewing

the more important aspects. The most important consideration is that the pore diameter measured at a given pressure is the diameter of the opening of the pore. "If there exist in the material pores which are considerably larger than the largest entrances to them, these pores will be measured as the size of the largest opening" (Ritter and Drake, 1945). For this reason, the pore diameters measured are referred to as limiting pore diameters; the "true" pore size distribution curve could contain more pore volume in the larger diameters than the pore size distribution measured.

Other assumptions or factors to be considered for mercury intrusion are:

- 1) Only pores accessible from the outside of the sample are penetrated.
- 2) The minimum pore size measured is dependent on the pressure capacity of the porosimeter.
- 3) The soil is considered to be incompressible during pressurization and does not break down.
- 4) The contact angle and surface tension values are assumed constant during pressurization.
- 5) The mercury will not react with the soil during intrusion.
- 6) Cylindrical pore shapes are assumed to calculate pore diameter.

In Geotechnical Engineering, the anisotropy of the fabric is frequently of interest. Unfortunately, the mercury intrusion technique is of little value in this respect because the intrusion process occurs in all directions which have large enough pore openings for the mercury to enter.

As Winslow (1969), Diamond (1970), and Bhasin (1975) all pointed out, the proper determination and calculation of pore size distributions is dependent on several precautions and corrections which must be considered:

- 1) During the intrusion procedure, enough time must be allowed for the mercury to reach an equilibrium intrusion for each pressure increment, prior to measuring the incremental volume of intrusion.
- 2) After the initial filling of the sample container with mercury, there remains a small volume of air trapped outside the sample. For pressures less than one atmosphere, a Boyle's law correction must be made to account for the decreasing volume of air as the pressure increases.
- 3) Another volume correction must be included for the compression of mercury and the expansion of the sample container (the glass penetrometer). This volume correction is only significant for pressures higher than 100 psi, and should be determined experimentally by a mercury intrusion run without a sample.

1-2.3 Presentation of Data

Two methods have been used to graphically present pore size distributions: the differential distribution curve and the cumulative distribution curve. Both are useful for interpreting the shape and changes in shape of pore size distributions. The differential distribution shows:

- 1) the type of distribution,
- 2) the most frequent or modal pore sizes,
- 3) the symmetry of the distribution,
- 4) any gaps or irregularities in the data, and
- 5) permits comparison of various curves.

The cumulative distribution displays the fraction of pore space greater or smaller than a given size, and the fraction of pore space between any two unmeasured pore sizes can be quickly evaluated. Ideally, to fully illustrate the pore size distribution of a material, both the differential and the cumulative pore size curves should be presented.

The differential distribution curve consists of some differential pore volume function plotted against its corresponding pore diameter. Drake and Ritter (1945) were the first to present such curves. The method they proposed has been found to be suitable when the range of pore sizes extend over one or two orders of magnitude. For fine-grained soils, however, the range of pore sizes may extend across three to five orders of magnitude. As Winslow and Diamond (1971) stated,

"...the differential presentation is severely distorted if the range of diameters covers several orders of magnitude; it vastly overemphasizes the apparent importance of the finest pore sizes at the expense of the coarser sizes."

An alternate method of determining the differential distribution which may be free of the distortion problems is presented in Section 1-2.4.

The cumulative distribution curve consists of a plot of a cumulative void volume parameter versus its corresponding pore diameter. The cumulative void volume parameter commonly used is the volume of voids per dry weight of solid. For this study, however, the cumulative volume of voids per volume of sample, or cumulative

porosity, was used because of its familiarity to geotechnical engineers. With this exception, the cumulative pore size distribution curves presented in this study are presented in the same fashion as those shown by Diamond (1970), Sridharan et al. (1971), Ahmed et al. (1974) and Bhasin (1975).

If pore size distribution measurements are to be correlated with soil properties either to understand or predict soil behavior, it is desirable to express the pore size distribution in mathematical terms. Drake and Ritter (1945) have used curve fitting techniques to quantify relatively simple pore size distributions, but for most soils the distributions are generally very complex and frequently multimodal, which makes curve fitting a very arduous and impractical task. An alternative is to determine descriptive measures of the pore size distribution which reflect the shape of the entire distribution and which accurately reflect changes in soil behavioral properties. Section 1-1.3 examined three models for predicting permeability which employ pore size distribution parameters, as shown on Table 1.

The hydraulic radius permeability model requires knowledge of the surface area of the porous medium. Conveniently, Rootare and Prenzlow (1967) presented a method of calculating surface area from pore size distribution measurements. The formula is given as:

$$S.A. = - \frac{\int_0^V p \, dv}{\frac{T}{s} \cos \theta} \quad (2-2)$$

where S.A. is surface area

P is the pressure applied

T is the surface tension of the intruding liquid

θ^s is the contact angle between the intruding liquid and solid

dV is the differential volume of pores intruded

V_v is the total volume of pores.

Substituting the Washburn equation (2-1) into equation (2-2) for P yields:

$$S.A. = 2 \int_0^V v \frac{dv}{r} \quad (2-3)$$

where dv is the differential volume of pores intruded between r and dr .

The specific surface area S_s , by definition, is equal to the surface area S.A. divided by the total volume V , therefore:

$$S_s = \frac{2}{V} \int_0^V v \frac{dv}{r} \quad (2-4)$$

Factoring the volume of voids out of the integral results in:

$$S_s = \frac{2}{V} \int_0^1 \frac{dv}{r} \quad (2-5)$$

$$S_s = 2n \int_0^1 \frac{dv}{r} \quad (2-5)$$

where n is the porosity.

Expressing equation (2-5) in a discrete form and substituting $f(r_i)$, the volumetric frequency, for dv yields:

$$S_s = 2n \sum_i^1 \frac{f(r_i)}{r_i} \quad (2-6)$$

Rewriting equation (2-6) in terms of pore diameter d yields:

$$S_s = 4n \sum_i \frac{f(d_i)}{d_i} \quad (2-7)$$

Theoretically, this method of determining the specific surface area is valid only if there are no "ink-bottle pores" and if the pressure applied is sufficient to intrude all of the accessible pore volume. Neither of these assumptions were fully satisfied in this study. As mentioned previously, the mercury intrusion technique measures "limiting pore diameters"; consequently, ink bottle pores are measured as pores of the neck diameter in size. Also, the intrusion pressure capacity of the equipment used was only able to penetrate about 95% of the pore volume. These two limitations may result in some disparity if the specific surface area, as calculated by equation (2-7), is compared to surface area measurements determined by other means. This does not, however, preclude the use of the equation as a descriptive parameter of the pore size distribution.

1-2.4 Differential Distribution and Calculation of Parameters

Soils are, basically, an agglomeration of various size particles with a pore network present where particles are not. The pore system, is extremely complex in geometry; therefore, to speak of a pore network in terms of pore sizes and diameters is a rather abstract concept.

Scheiddeger (1957), in an effort to clarify the nebulous nature of a pore diameter and its distribution, has considered a probabilistic approach to define a pore system. He defines a pore diameter at any

one point within the pore space as "...the diameter of the largest sphere which contains this point and remains wholly within the pore space." In this way, a pore "diameter" can be assigned to each point in the pore space, and a pore size distribution can be defined by determining what fraction f of the pore space has a pore diameter between δ and $\delta + d\delta$ (δ denotes pore diameter). Scheiddeger, in effect, considers the pore diameter δ to be a continuous random variable with some probability distribution of occurrence given by:

$$\int_0^{\infty} f(\delta) d\delta = 1 \quad (2-8)$$

Although, Scheiddeger's definition of a pore diameter is more precise than that measured by mercury intrusion, the concept of a pore diameter being a continuous random variable is very useful for analysis purposes. Statistical methods and probability theory may be used to analyze pore size distributions.

The usual procedure for determining the density function $f(x)$ of a continuous random variable "x" is to estimate it from limited statistical data. The procedure involves grouping the data into classes (or intervals) of x and forming a frequency distribution, by determining the proportion of measurements in each of the classes. The probability distribution of x is, thus, approximated by a discrete frequency distribution across intervals of x . Details of the procedure are presented in Walpole and Myers (1972, pp. 41 to 45) and Harr (1977).

The same procedure may be applied to pore size distribution measurements by mercury intrusion. Each pressure increment corresponds

to a decrease in pore diameter from δ_{i-1} to δ_i which represents a class or interval of the pore diameter. Associated with each of these intervals is the fraction of porosity $f(d_i)$ measured between δ_i and δ_{i-1} , where d_i is the midpoint between δ_i and δ_{i-1} .

To approximate the differential distribution a frequency histogram is plotted. The histogram is conventionally drawn with equal class widths in order to prevent distortions in the data. Since pore size distributions extend across several orders of magnitude, plotting a histogram with classes of constant width is not practical. The frequency of the smaller pores is overemphasized, as previously discussed in Section 1-2.3.

To overcome these distortions in a pore size frequency histogram, the class widths may be set at logarithmically equal intervals such that:

$$\log \delta_{i-1} - \log \delta_i = c \quad (2-9)$$

$$\frac{\delta_{i-1}}{\delta_i} = 10^c \quad (2-10)$$

where δ is the pore diameter corresponding to an intrusion pressure and c is the logarithmic interval constant.

From equation (2-1), it is evident that the intrusion pressure is inversely proportional to the pore diameter. For each pressure increment to correspond to a logarithmically equal class width, the pressure P must be raised as follows:

$$\frac{P_i}{P_{i-1}} = 10^c \quad (2-11)$$

By increasing the pressure of intrusion according to equation (2-11) and maintaining c constant the pore size data can be presented in a histogram as shown by Figure 2.

The differential pore size distribution is approximated from the frequency histogram by connecting the values of d_i , $f(d_i)$ as shown in Figure 2, where d_i , the midpoint of each class, is calculated as follows:

$$d_i = \left(\delta_i + \delta_{i-1} \right)^{\frac{1}{2}} \quad (2-12)$$

and $f(d_i)$ is fraction of porosity intruded between δ_{i-1} and δ_i . Such a curve is referred to as a frequency polygon (Harr, 1977 pp. 6 and 7). All the differential distributions presented in this study were determined directly from the frequency polygon of the pore size measurements as shown in Figure 2.

The pore size parameters used in the permeability predicting models, shown on Table 1, were also calculated from d_i and $f(d_i)$. No graphical integration was necessary. The parameters were calculated directly from the mercury intrusion data by computer.

1-3 Soil Drying Methods

The measurement of pore size distribution by mercury intrusion requires dry samples. The dehydration of soil samples without changing the fabric presents a serious problem. Several methods have been developed to remove the water from soils. Various means have also been used to check for fabric changes caused by dehydration.

Before discussing the drying techniques, it would be fruitful to mention how fabric changes may be detected. The first requirement is

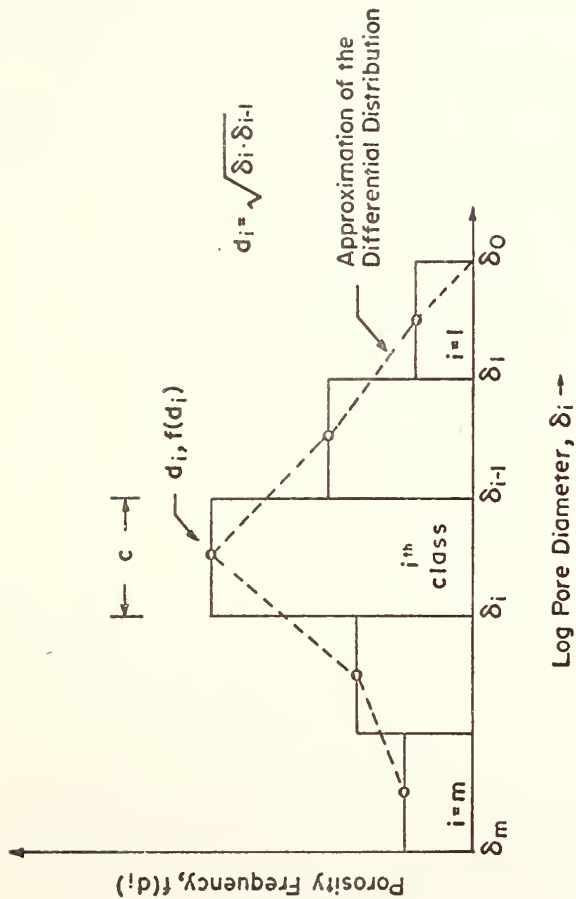


FIGURE 2 FREQUENCY HISTOGRAM OF PORE SIZE DISTRIBUTION

to have an idea of the kind of fabric change which may take place as a result of a particular drying technique. The dehydration process may cause shrinkage, expansion, cracking, fabric reorientation or even mineralogical changes. Knowing what to expect will dictate what to monitor before and after water removal.

Volume changes usually accompany fabric changes, and since volume change is relatively easy to measure, it is commonly monitored. Diamond (1970), Sridharan, Altschaeffl and Diamond (1971), Ahmed (1971), Bhasin (1975), Zimmie and Almaleh (1976) and Reed (1977) all measured a volumetric characteristic such as total volume, porosity or void ratio before and after dehydration. This should be a requirement for all mercury porosimetry studies. In this way, any large shrinkage or expansion of dehydrated samples can be detected and the efficacy of the drying procedure can be judged.

Another technique for monitoring fabric changes during dehydration may be used to contrast separate dehydration methods. This method involves comparing the pore size distribution curves of soils prepared in identical fashion but dried by different techniques. Diamond (1970), Sridharan et al. (1971) and Ahmed, Lovell and Diamond (1974) present such comparisons. These types of comparisons are useful because they show both the total volumetric difference and in what pore size range these differences are taking place.

If mineralogical change is suspect as a result of a dehydration process, more sophisticated soil fabric and composition analysis may be required. Differential thermal analysis, X-ray diffraction and scanning electron microscopy techniques are useful in determining what

mineralogical changes are being caused by the dehydration technique. The applications and suitability of these methods is discussed in greater detail by Mitchell (1976) and Yong and Warkentin (1975). These methods have seldom been used in pore size distribution studies; although, Bhasin (1975) made extensive use of them to check the reliability of critical-region drying.

The three most frequently used methods of drying soils are air or oven drying, freeze drying, and critical region drying. The proper technique is dependent on the soil to be tested and the time and costs one is willing to expend.

1-3.1 Air and Oven Drying

Simple air or oven drying has been used by Diamond (1970) and Sridharan et al. (1971). The success of this drying technique is largely dependent on the degree of saturation, strength, and compressibility characteristics of the soil. Air or oven drying results in the evaporation of water from the soil through the air-water menisci. As the water exits, meniscus radii become smaller, increasing the surface tension, which results in increasing compressive forces on the soil fabric. If these compressive forces exceed the soil structural "strength", shrinkage will result. Some clays may crack and increase in volume because of the shrinkage forces. Yong and Warkentin (1975, pp. 197-206) discuss the shrinkage process in greater detail.

Sridharan et al. (1971) and Ahmed et al. (1974) concluded that clays compacted at low initial degrees of saturation suffered only minor shrinkage with oven drying. This was not the case for compacted clays near or above their optimum water content, however. Their explanation

for this behavior was that the drier soil had a greater strength because of the large negative pore pressures. In general, air or oven drying is not an effective drying method for saturated clayey soils because of the large shrinkage that occurs with drying. Evidence gathered by Zimmie et al. (1976), Diamond (1970) and Bhasin (1975) confirm this.

1-3.2 Freeze Drying

Freeze drying is another method of removing the water from soils. The method consists of quickly freezing a small soil specimen to cryogenic temperatures, followed by vacuum drying the frozen sample to remove the water by sublimation. This process eliminates the air-water menisci-shrinkage effect replacing it with an air-solid system. Ahmed (1971) and Zimmie et al. (1976) describe the theory and process in detail. However, the more salient aspects of the process, and how the soil fabric can be disturbed during dehydration are worth reviewing.

Quick freezing to very low temperatures is done primarily for two reasons. The rapid freezing process minimizes ice crystal nucleation and water migration, thus preventing frost heaving and swelling. There is also some evidence that freezing water to cryogenic temperatures reduces the degree of ice crystallization (Ahmed, 1971). By reducing the degree of ice crystallization, the 10% volume expansion which normally results from freezing liquid water to ice, just below 0°C, can be reduced. If the freezing technique is not effective, significant swelling of the soil sample can take place.

The vacuum drying process is also critical to the success of the freeze drying technique. When the soil sample is withdrawn from the

freezing media, it is quickly placed in a vacuum chamber and allowed to heat up. The pressure and temperature in the chamber must be maintained below the triple point of water to prevent liquid water from forming in the sample. If liquid water should form, the same mechanism which causes shrinkage of air dried specimens will result in shrinkage of the freeze dried specimens.

In effect, deficiencies in the freeze drying method may result in either sample swelling or shrinkage, depending on whether the freezing process or the drying process is ineffective. It is conceivable that both swelling and shrinkage may occur in a freeze dry run. If such were the case and the net volume change was small, any significant fabric changes taking place would go undetected by volume monitoring the drying procedure.

Freeze drying of soils, according to Diamond (1970), Tovey and Yan (1973), Ahmed et al. (1974) and Zimmie et al. (1976), if properly conducted, is far superior to air or oven drying for most clayey soils. Though some volume changes may take place as a result of freeze drying, they will generally be less than 5%.

1-3.3 Critical Region Drying

Critical region drying is the third and most complex procedure of dehydrating soils. The method consists of elevating the temperature and pressure of a saturated soil specimen in a controlled manner, to the critical region of water. In the critical region both the gas phase and the liquid phase have the same specific volume and thus exist in a single phase. Once the critical region is reached, the pressure and temperature of the sample are slowly reduced in a way that the

water in the sample remains in the gas phase. When atmospheric conditions are reached, the sample has been "dried" without imposing the air-water menisci-shrinkage forces on the soil fabric. Bhasin (1975) presents a more detailed explanation of the process.

Several problems may arise when using the critical region dehydration technique. The temperature and pressure regulation schedule must be gradual enough so that water in the sample is not subject to large gradients. Flow into or out of the sample as a result of too rapid a pressure-temperature change can cause either compression or swelling, depending on whether flow is out of or into the sample.

To reach the critical region of water, the pressure must be raised to 3800 psi and the temperature to 380°C. The alteration of the soil composition at such extreme conditions must be considered. Bhasin (1975), after careful mineralogical analysis of various natural and artificial soils, found that no mineralogic change took place as a result of critical region drying. Bhasin's conclusion that critical region drying does not alter the mineralogic composition of soils was valid for the soils he tested. However, to extrapolate this conclusion for all soils would not be correct.

This study was originally designed to use critical region drying for dehydrating the soil specimens. However, during preliminary critical region runs, void ratio increases of 35 to 40% were measured after drying. Mineralogical analysis of the soil before and after critical region drying revealed that the soil contained large fractions of kaolin and dolomite. During the drying process the kaolin and dolomite reacted to form a plagioclase feldspar; Appendix C contains further details of this reaction.

Critical region drying is a complicated and arduous procedure in its present state of development, but if oven drying and freeze drying are not suitable for a particular soil, it may be the only alternative available. Based on the experiences of this study, critical region drying should always be monitored with both volume measurements and mineralogical analysis to check the efficacy of the drying.

1-3.4 Fluid Replacement

Tovey and Yan (1973) discuss fluid replacement as a possible drying technique. The method involves impregnating a sample with an organic liquid to replace the pore fluid. After replacement, the sample is air or oven dried or critical region dried. For air drying, the replacement fluid is usually a liquid of low surface tension such as methanol or acetone. This will reduce the shrinkage forces on the soil during drying. For critical region drying, two fluid replacements are necessary. The sample must initially be impregnated with acetone, then placed in a high pressure cell and impregnated again with carbon dioxide. Liquid carbon dioxide is a more suitable fluid for critical region drying than water because of its lower critical state (31.1°C and 1050 psi). The lower temperatures and pressures reduce the possibility of mineral alterations.

Fluid replacement is not without its problems, however. Tovey (1970) and Smart (1966) (as reported by Tovey and Yan, 1973) both found that swelling frequently accompanies fluid replacement. Therefore, volume monitoring would be necessary prior to replacement, after replacement, and after drying. Tovey and Yan (1973) conclude that fluid replacement and air or oven drying does reduce the amount of

shrinkage if compared to air or oven drying alone, but the method does not eliminate shrinkage completely. Fluid replacement and critical region drying may prove to be fruitful if a suitable replacement technique is used.

Of the various dehydration methods available, only freeze drying and critical region drying are suitable for most clayey soils, if fabric disturbance is to be minimized. Soil drying should always be monitored with at least volumetric measurements. Finally, regardless of the drying method used, the need for precise and careful laboratory technique cannot be overemphasized. Sample trimming, volumetric measurements and insufficient drying times can be significant sources of errors.

1-3.5 Method Used

The drying technique used for this study was the freeze drying method recommended by Zimmie and Almaleh (1976). Liquid nitrogen was used as the freezing agent, and vacuum drying was performed at room temperature without a refrigerant. Zimmie et al (1976) measured negligible volume expansion of kaolinitic soils after freezing in liquid nitrogen and felt that no intermediate cooling fluids would be necessary if the samples were kept small (less than 8 mm on a side). This recommendation was followed in this study.

Vacuum drying at room temperature was used because as Zimmie et al stated: (1) "...sublimation is an evaporative process accompanied by cooling, so, although the specimen container is exposed to room temperature, the sample temperature will remain below freezing;" and (2) the rate of sublimation is a function of sample temperature, thus

the lower the temperature, the lower the rate of sublimation. By vacuum drying at room temperature without using a refrigerant, the drying technique was simplified and accelerated. Zimmie et al. determined that 5 to 6 hours of vacuum drying would be sufficient for kaolinitic soils and 9 to 10 hours would be sufficient for montmorillonitic soils. To be conservative, 8 to 10 hours of vacuum drying was felt to be sufficient for this study. After freeze drying, the samples were stored in a dessicator containing anhydrous magnesium perchlorate to prevent the samples from adsorbing moisture.

The success of the freeze-drying technique used in this study was strongly influenced by the size of the samples. Too large a sample resulted in cracking and large volume changes after freeze drying. The method was not 100 percent successful. A small but significant percentage of the samples which were freeze dried had to be discarded because they cracked or crumbled apart, as was also reported by Zimmie et al. For the successful runs, however, the maximum volume changes experienced as a result of freeze drying was about 3%, which agrees with what Reed (1977) determined.

2 - SOILS STUDIED

The soils were selected based on certain desirable characteristics and within the limitations imposed by mercury intrusion testing. The soils are intended to be representative of natural silty clays which are frequently employed in earthwork construction. It was hoped that the method of compaction and the types of soils used would give a wide range of permeabilities. However, since the affect of chemical changes in the pore water on soil permeability was beyond the scope of this study, it was necessary to use clays of low activity. This limited the minimum permeability measured to about 10^{-8} cm/sec. The pore size distribution measurements, because of the small samples necessary, limited the maximum particle size to a fine sand and required as homogeneous a soil as practicable. For these reasons, the soils tested were blends of natural silt and commercial kaolin clay, artificially prepared in controlled proportions.

The silt was taken from a natural loess deposit, near the Wabash River, in southwestern Indiana. The soil was excavated from the second bench level on the east side of U. S. Highway 41, about 1 mile south of Patoka, Indiana. After air drying, the loessial blocks were passed through a No. 40 U. S. standard sieve to remove any large particles and to break down the initial soil structure. X-ray diffraction analysis revealed that the silt was composed primarily of quartz and dolomite with small amounts of calcite and feldspar also present. Although the

loessial soil contained only about 1 to 3% clay size particles, a separate X-ray diffraction analysis was also performed on the clay fraction. The preparation technique developed by Kinter and Diamond (1956) was used for this analysis. Illite, kaolinite and montmorillonite were found to be present, with a possible trace of vermiculite. As shown on Figure 3, the silt has a very uniform gradation with approximately 85% of the particles between 0.07 and 0.01 mm in size. The silt is non-plastic, as shown in Table 2.

Edgar plastic kaolin was blended with the silt to prepare the soil combinations to be tested. The kaolin is commercially processed to remove material coarser than 40 μm in size, dried in a tunnel dryer to 300° to 450°F, and then pulverized. The manufacturer claims that 99.5% of the clay mineral composition is kaolin with the remainder being quartz or mica. The classification properties of the kaolin, as determined by Bhasin (1975), are: specific gravity of solids = 2.65, liquid limit = 59%, plasticity index = 22%, and the clay fraction (% less than 2 μm) = 76%.

The three artificial blends of silt and kaolin were tested:

90% silt - 10% kaolin

70% silt - 30% kaolin

50% silt - 50% kaolin

Grain size distribution curves and soil classification properties for each of the mixes are shown on Figure 3 and Table 2, respectively.

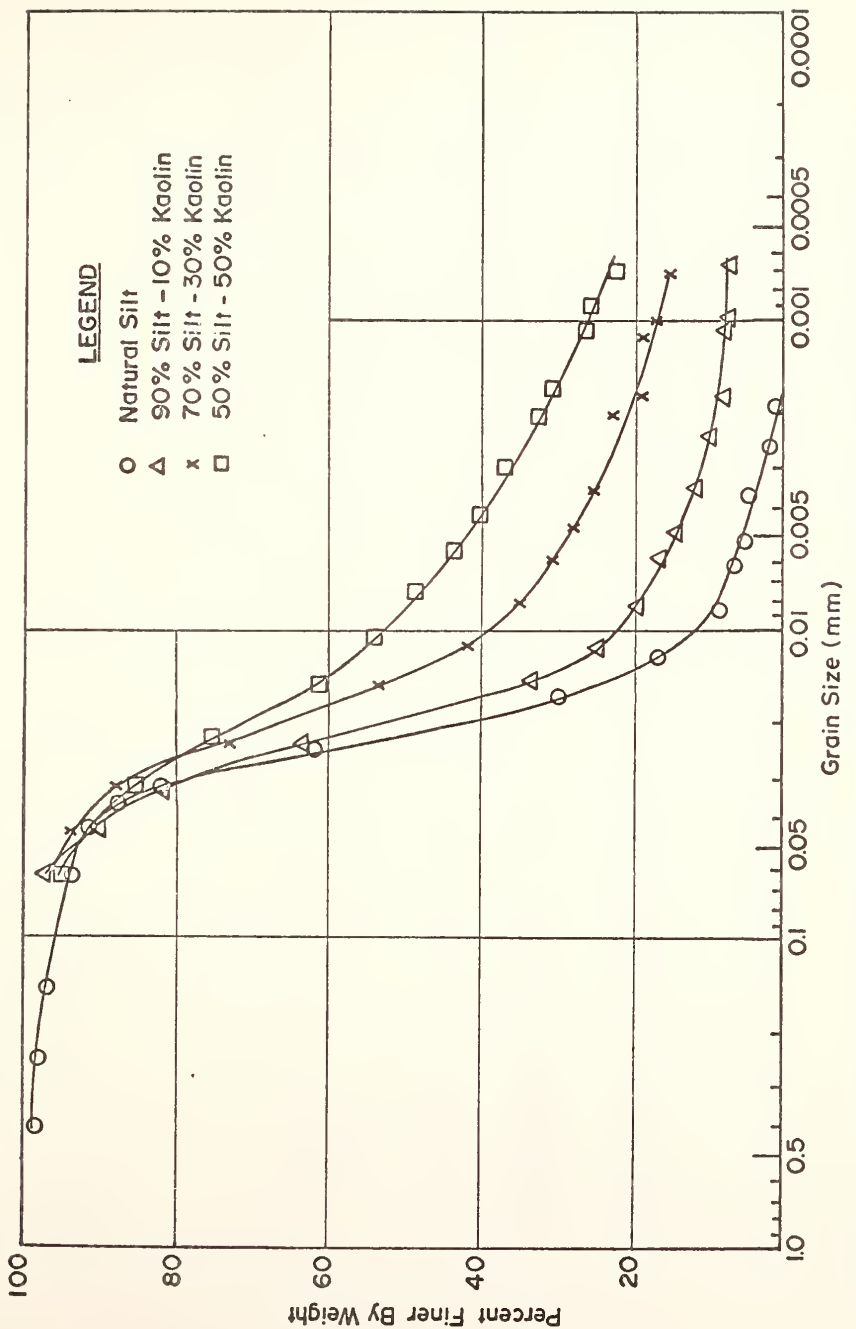


FIGURE 3 GRAIN SIZE DISTRIBUTIONS FOR SOILS STUDIED (AFTER REED, 1977)

TABLE 2 CLASSIFICATION OF SOILS STUDIED

	Specific Gravity Gs	Liquid Limit (%)	Plasticity Index (%)	Clay Size Fraction (% < 2 μ m)	Soil Classification	
					AASHTO ASTM D3282-73	Unified ASTM D2487-69
Natural Silt	2.73	—	NP	2	A-4 (O)	ML
90% Silt and 10% Kaolin	2.72	—	NP	9	A-4 (O)	ML
70% Silt and 30% Kaolin	2.71	25.3	7.0	21	A-4 (5)	CL-ML
50% Silt and 50% Kaolin	2.69	36.7	9.7	33	A-4 (II)	ML

3 - APPARATUS AND EXPERIMENTAL PROCEDURE

3-1 Soil Mixing and Curing

All soil mixing for this study was done with a Patterson-Kelley liquid solid mechanical blender. The blender, shown in Figure 4, consists of a slowly rotating V shell housing a high speed rotating bar. The rotating bar contains several dispersion blades and two sprayers. Connected to the rotating bar is a graduated cylinder which serves as the reservcir for the deionized water. A stopcock at the base of the cylinder regulates the quantity and rate of flow into the shell.

The mixing procedure was begun by placing the desired proportions of air dried silt and kaolin into the blender. It was found that 2 kg of soil was a sufficient amount of soil to prepare one sample. The soil was dry mixed for approximately 10 minutes. Deionized water was then added at a rate of 50 to 75 ml per minute while the soil was being mixed. Once the desired quantity of water was added, the end caps of the blender were removed, and the soil was scraped off the inside walls of the shell. After the scraping, mixing was resumed for about 7 minutes, followed again by scraping and another 7 minutes mixing period. Following the final mixing, the soil was removed from the shell and sealed inside two polyethylene bags. The bagged samples were placed in a high humidity barrel and cured for two days.

Experimentation revealed that in order to achieve the desired water contents it was necessary to add 0.5% less water to the air-dry

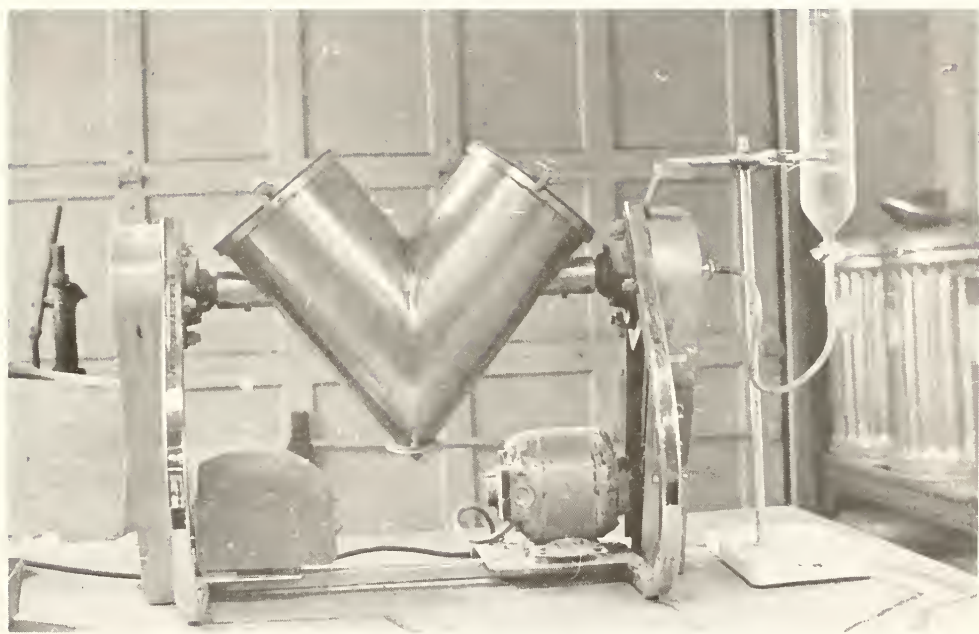


FIGURE 4 PATTERTON-KELLEY BLENDER

soils than calculated. This procedure gave total water contents within 0.25% of the desired water contents. Less than the calculated amount of water was added because the silt and kaolin were at some small initial water content in the air dried state.

3-2 Compaction

3-2.1 Apparatus

Kneading compaction and special sample preparation procedures were used in order to obtain a high degree of homogeneity in the prepared samples. An electrically driven, semi-automatic kneading compactor, manufactured by the August Company, was used to prepare the samples. The kneading compactor is shown on Figure 5. The compactor foot pressure is controlled by a pneumatic-hydraulic system with a standard air regulator and pressure gage. The triangular shaped foot rotates 60 degrees between each tamp providing uniform coverage of the sample surface. Two minor problems were encountered with the kneading compactor during the course of this study. First, the foot pressure imparted on the soil is not directly determinable. It is controlled by an air regulator, and a pressure gage measures the hydraulic-pneumatic pressure in the compaction system. Gaudette (1960) and Reed (1977) have determined calibration curves for converting gage pressure to the actual foot pressure being applied to the soil; however, these curves are not unique. Seasonal changes of temperature and humidity can cause a significant change in foot pressure for a given gage pressure, particularly at the lower pressures. In an effort to overcome this problem, the groups of samples of a given soil type to be compacted at the same energy level, were usually prepared within the same two week

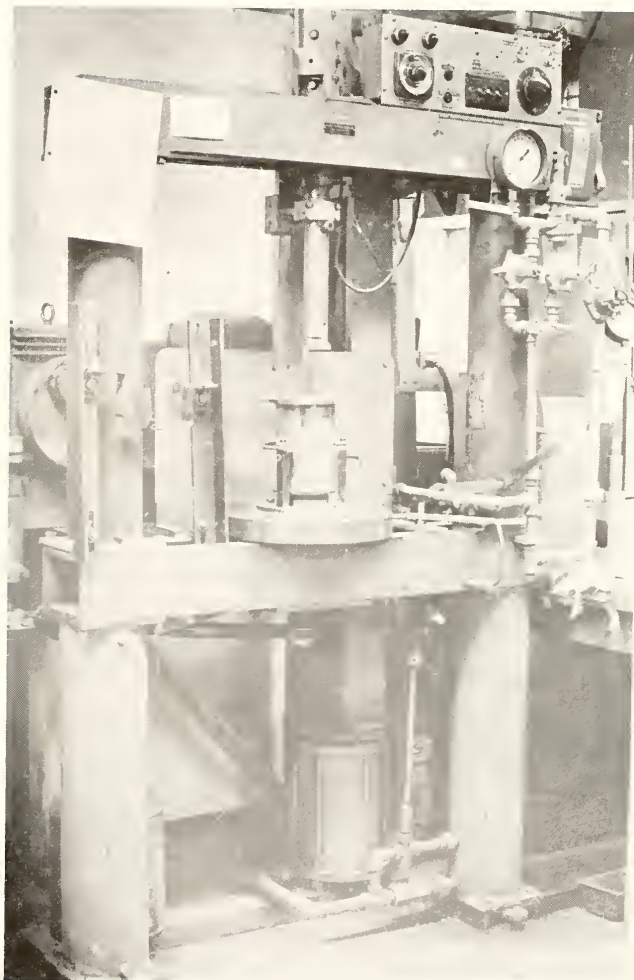


FIGURE 5 KNEADING COMPACTOR

period. Thus a group of samples was compacted at approximately the same energy level and gage pressure, though the peak foot pressure during compaction was unknown. It is suggested that before future research using the kneading compactor is undertaken, a simple and accurate method of calibrating gage pressure to foot pressure be devised, which can be repeated on a periodic basis. One other problem was encountered when using the kneading compactor. If the foot was not at the bottom of its stroke when a series of tamps was begun, the first few tamps gave exceedingly high foot pressures. Bailey (1976), Gaudette (1960) and Aughenbaugh et al. (1963), present further details about the operation of the kneading compactor.

3-2.2 Procedure

All samples were compacted using the same procedure with the exception of the varying energy levels. Following the two day curing period, the samples were compacted in a cylindrical lucite mold 4.0 inches in diameter and 4.89 inches in length which was coated with silicon oil. A circular base plate extended 0.31 inches into the bottom of the mold, thus making the compacted sample 4.58 inches long. These dimensions are identical to those specified by AASHTO T 99-70 (i.e., $1/30 \text{ ft}^3$ in volume). A circular strip of filter paper 4 inches in diameter was placed on the base plate prior to placing the soil in the mold. The filter paper served two purposes: 1) to prevent the soil from adhering to the base plate, and 2) to prevent the soil from plugging the porous stones during permeation. The soil was placed in the mold and compacted in five layers of approximately equal thickness. Thirty tamps of the compaction foot were applied per layer. Prior to

the mechanical compaction of each layer, the layer below was scarified, fresh soil was added and manually tamped three times with a piston tamper. The scarification of each layer prevented cracking at the contact between the layers. The initial manual tamping was necessary to densify the fresh soil just enough to prevent the mechanical foot from punching through the layer. Once the compaction procedure was completed, the collar was removed and the soil sample was trimmed flush with the top of the lucite mold. The weight of the sample and mold was then taken, and the remaining soil trimmings were used for water content determinations. After placing another circular strip of filter paper 4 inches in diameter on the top of the sample, the mold and sample were ready to be placed in the permeameter cell.

Several difficulties were encountered during the preliminary compaction runs. Soils with water contents 3 to 4 percent greater than the optimum water content could not be compacted with the kneading compactor. The soil would stick to the compaction foot during the upward stroke thus preventing effective compaction. Soils with a water content slightly greater than the optimum water content presented another problem. During the downward stroke of the compaction foot, the soil adjacent to the foot would heave upward. This heaving created sufficient forces to unseat the mold from the base plate. This problem was overcome by building a collar which could be fastened to the base plate assembly. Figure 6 shows the mold, collar and tamper.

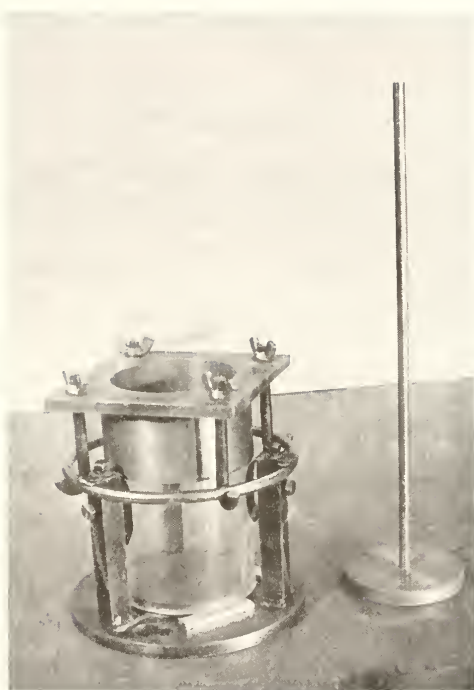


FIGURE 6 COMPACTION MOLD, COLLAR AND TAMPER

3-3 Saturation and Permeation

3-3.1 Apparatus

As was discussed in Section 1-1.1, the permeability of a soil is a function of the degree of saturation. To maximize the permeability and minimize the effect of the degree of saturation, samples were brought as close to full saturation as practicable prior to permeation.

The permeameter cells used to house the soil samples during saturation and permeation are shown on Figure 7. The cells consist of a lucite tube and two lucite end caps containing brass porous stones. The transparent lucite parts allow one to view the soil during permeation. This was very advantageous because changes in sample volume, cracking, and washing out of soil particles could be detected. The top end cap is inset with a porous stone and rests flat on the sample top. The base cap has a 1/8 inch slot for the mold to rest in, and the porous stone is inset in the bottom of the lucite tube. The drainage lines in both caps are 1/4 inch in diameter. Four grooves radiate outward from the center of the caps. The grooves reduce the constriction of flow between the end cap and the porous stone and prevent air bubbles from blocking the drainage line. Quicklock fittings connect the drainage lines to the permeameter or saturation devices. The end caps and mold are fastened together by four bolts and wing nuts. "O" rings, inset in the caps, are compressed against the edges of the cylindrical mold, providing a pressure tight seal.

The soil was compacted directly in the lucite mold to reduce seepage along the walls. The permeameter cell was designed so the mold fit directly into the two caps without compressing or shifting the

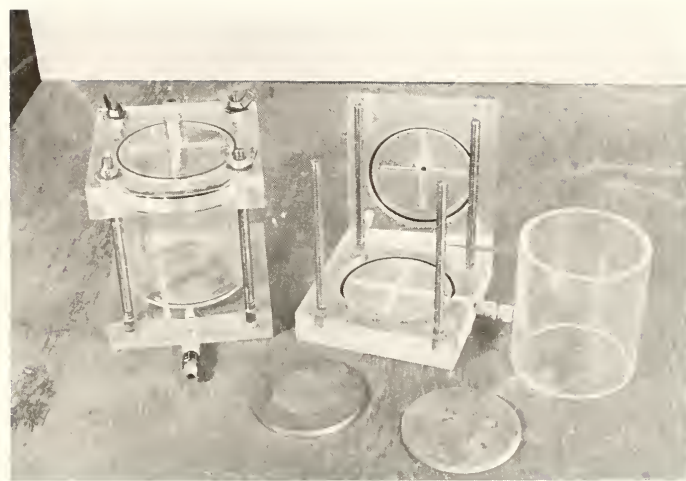


FIGURE 7 PERMEAMETER CELLS

sample within the lucite tube. Once the sample was placed in the permeameter cell, it was confined to prevent an increase in volume.

The saturation device, built by Reed (1977), consists of two reservoirs, two air pressure regulators and one air pressure gage. The reservoirs could be pressurized independently or together, and a vacuum system could be connected to the outflow reservoir.

The permeameters used are closed system, falling head permeameters with provisions for back pressuring. Because of the wide range of permeabilities to be measured, two permeameters were built. The two permeameters are nearly identical except for the inside diameters of the standpipes. The permeameter used for measuring the more permeable soils has 1/2 inch I.D. standpipes, while the other has 1/4 inch I.D. standpipes. The standpipe reservoirs could be pressurized simultaneously from one regulator or independently from two regulators. A vacuum could be applied to one or both reservoirs. Meter sticks were used to measure the water elevation heads. Connected to both permeameters was one common reservoir containing deionized, distilled water. The permeameters were designed to be used for both saturation and permeation, but in order to accelerate the testing program, the saturation device, described above, was used for saturation. Figure 8 shows the saturation device and permeameters used.

3-3.2 Procedure

Following compaction, the lucite tube holding the sample was connected to the two end caps. The bottom cap was filled with distilled water and held a saturated porous stone. The top cap and porous stone were attached dry. The assembled permeameter cell was then connected

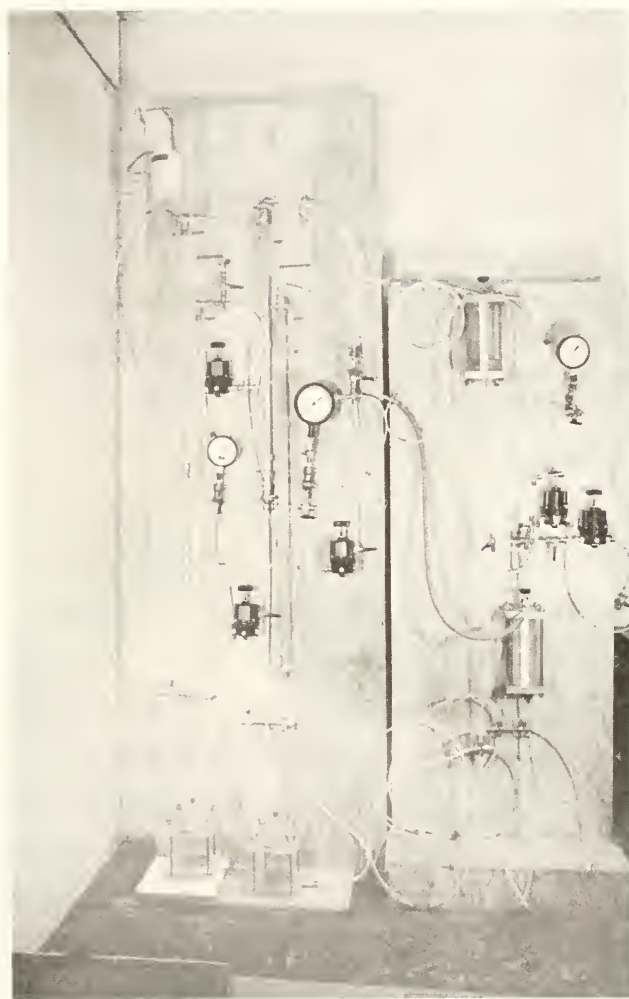


FIGURE 8 SATURATION DEVICE (RIGHT) AND PERMEAMETERS (LEFT)

to the saturation apparatus. A vacuum of about 5 psi absolute pressure was placed on the top of the sample while the bottom end was under approximately 18 inches of water head. This condition was maintained for about 8 hours permitting deionized, deaired water to flow upward through the sample and allowing air bubbles to escape. Vacuum saturation of samples was found to be very effective for samples compacted on the dry side of optimum. Simply passing water through dry side samples under a low head difference seldom gave degrees of saturation greater than 88%; although vacuum saturation consistently resulted in saturation levels greater than 95%.

After vacuum saturation, back pressuring was begun. The pressures on the two ends of the sample were raised in 5 psi increments with the pressure at the base of the sample 3 to 5 psi greater than the pressure at the top. This was done with the hope that, as the back pressuring increased, a fraction of the air remaining in the sample would go into solution and flow out the top of the sample. Fifteen to 30 minutes were allowed to pass between the application of pressure increments. When the bottom end pressure reached 50 psi, both ends of the sample were connected to a common air regulator maintaining a 50 psi back pressure overnight.

Preliminary testing to establish a reliable saturation technique revealed that it was important not to exceed a 5 psi pressure differential across the sample. In preliminary tests, a 10 to 20 psi pressure differential was used, and the sample could be seen consolidating in the permeameter cell. A gap of about 1/4 inch was visible across the base of the sample. When the pressure differential

was eliminated, the gap would fill in, but large horizontal cracks extending completely across the sample would appear. Such samples were obviously unsatisfactory for permeability testing but would not have been detected if the samples were not visible. Appendix B provides further details concerning seepage forces and consolidation.

With the samples at 50 psi back pressure and the saturation process complete, the permeability tests were then conducted. The quicklock connections on the permeameter cell permitted the easy transfer of the cell from the saturation apparatus to the permeameter while maintaining the high pressure in the cell. A one meter head difference in the water columns was established between the two standpipes, and a 50 psi back pressure was placed on both of the columns. The cell was then connected to the permeameter and permeation was begun. The direction of flow as from top to bottom across the sample. Figure 59 in Appendix B shows a sketch of the permeability test. Periodic readings of the elevation heads in the columns, the time of the readings, and the air temperature were taken. The frequency of the readings depended on the rate of flow. It was assumed that the air temperature was equal to the water temperature to normalize the permeability readings to 20⁰C. The permeability tests varied in duration from one to six days, depending on the permeability of the soil. At least ten to twelve readings were taken for each sample. Some samples were repermeated to check the reproducibility of the test. This was done by disconnecting the permeameter cell from the permeameter apparatus, reestablishing the one meter head difference between the standpipes, and reconnecting the cell to the permeameter.

Following permeation, the samples were dissected to check for uniformity, and trimmed for freeze drying and pores size distribution measurements. Because of this, it was important to prevent sample disturbance and volume changes when removing the permeated soil from the lucite mold. At the completion of permeation, the sample was gradually depressurized from 50 psi in 5 psi decrements per 15 (or more) minutes. When atmospheric pressure was reached, the sample was kept in the mold (at constant volume) for at least 2 hours. If the back pressure on the sample was released too rapidly, the sample would swell noticeably when the end caps of the permeameter were removed.

3-4 Freeze Drying

Freeze drying was used to dehydrate samples prior to mercury intrusion. The procedure used by Zimmie et al. (1976) and Reed (1977) was used for this study. The effectiveness of the drying procedure was checked by the volumetric method discussed in Section 1-3.

3-4.1 Apparatus

The apparatus used in this study was assembled by Reed (1977) and this description is taken directly from his work (p. 44).

Figures 9 and 10 show the basic components of the freeze drying equipment which include:

- "1) Wire cage to hold the samples during freezing and sublimation.
- 2) Large Dewar flask containing liquid nitrogen into which the sample and cage are dipped.



FIGURE 9 SAMPLE CAGE SUSPENDED IN DESICCATOR (FROM REED, 1977)

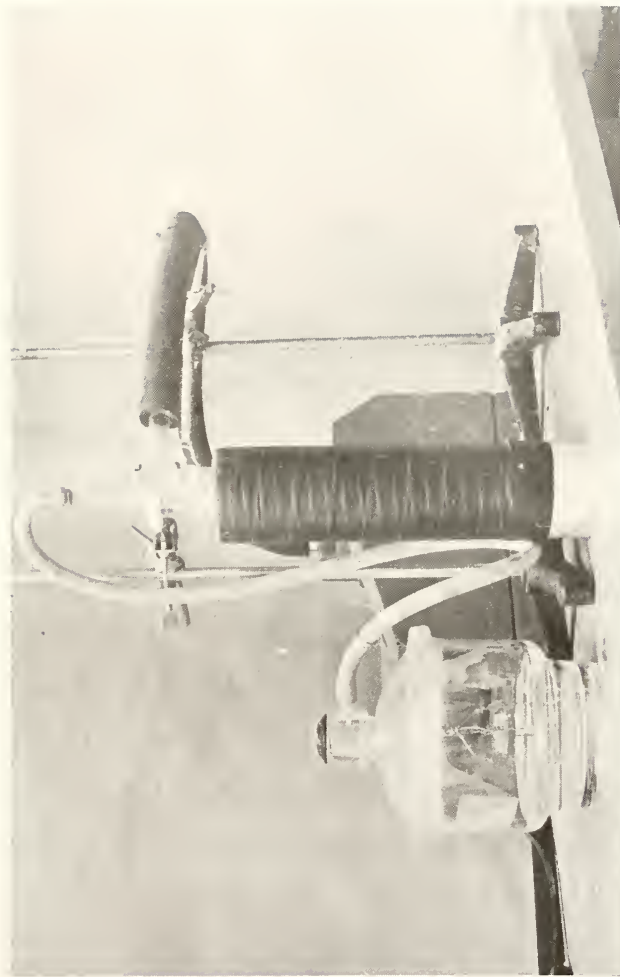


FIGURE 10 FREEZE DRYING APPARATUS WITH VACUUM PUMP, CONDENSER AND DESICCATOR (FROM REED, 1977)

- 3) Dessicator with inside wire support from which sample cage is suspended during sublimation.
- 4) Vacuum pump, capable of evacuating to less than 0.01 mm of mercury.
- 5) Condenser, which is hooked between the dessicator and vacuum pump in order to prevent vapor from the soil entering the pump. Liquid nitrogen contained in a Dewar flask was used to cool the condenser."

3-4.2 Procedure

After depressurizing the permeated soil, the samples were ready for dissection and freeze drying. The permeameter cell was disassembled, and the mold and soil were weighed to determine the final degree of saturation. The soil was then extruded by an hydraulic extruder. Quickly and carefully, small cubes were trimmed from the compacted sample for freeze drying. The small specimens were trimmed with a razor blade and were approximately 8 mm long on each side. Four or five samples were trimmed. Two or three were taken from about 1 inch below the top of the sample, and the remaining ones were taken from 1 inch above the sample bottom. The trimmed samples were placed in the cage and lowered into liquid nitrogen. They remained in liquid nitrogen for approximately ten minutes. While the samples were immersed in the liquid nitrogen, bubbles would form and adhere to the sides of the soil cubes. Although it was not done in this study, it would have been beneficial to vibrate the specimens while they were immersed to prevent insulation from the cold source.

While the small specimens were being frozen, the remaining soil was utilized to determine the water content and porosity within the

compacted sample. Samples from the top, middle and bottom of the remaining soil were trimmed into cubes 3 to 4 cm on a side. Wax displacement, as described in U. S. Dept. of the Army, EM 1110-2-1906 (1970), was used to measure the porosity. The results of these measurements were averaged and compared to both the gross sample porosity after compaction, and the porosity measured after freeze drying. The post freeze dry porosity was measured by mercury displacement in the porosimetry run. Thus, three different porosity measurements were made to check the effectiveness of freeze drying; one of the gross compacted sample, another of the dissected sample after permeation, and one of the freeze dried sample.

After the small samples had been in the liquid nitrogen the proper length of time, they were quickly transferred, in the wire cage, to the dessicator for vacuum drying. The samples were vacuum dried for eight to ten hours then stored in a dessicator containing anhydrous magnesium perchlorate to remove any remaining moisture. The samples remained in the desiccator, which was kept under a slight vacuum, until they were used for pore size determinations.

Reed (1977) explains the importance of the more salient procedural details. The most important detail was to trim the freeze dry samples no larger than specified above because the larger samples often cracked and experienced large volume changes.

3-5 Pore Size Distribution

The apparatus and procedure used in this study to measure pore size distribution by mercury intrusion is basically the same as that employed by Ahmed (1971), Bhasin (1975) and Reed (1977). For this reason the

descriptions and details which follow are kept brief. The references listed above should be consulted if further details are desired.

3-5.1 Apparatus

Three primary components are required to measure pore size distribution by mercury intrusion: a penetrometer, a filling device and a porosimeter. The penetrometer is a glass capillary stem with a bulb on one end which is used to house the sample. The capillary stem is calibrated in 0.002 ml increments and has a capacity of 0.20 ml. A steel cap and teflon fastener fit over the bulb which, when greased and sealed, maintains a pressure tight seal. The filling device is a two chambered glass tube which holds the penetrometer during filling and low pressure intrusion. The filling device is connected to a pressure control board which, in turn, is connected to a vacuum pump, McLeod gauge, mercury manometer and bleeder valve. The vacuum pump is for pumping down the pressure in the filling device to the required vacuum prior to mercury filling. The McLeod gauge is for measuring pressures less than 1 mm of mercury, while the manometer is used to measure pressures greater than 1 mm of mercury but less than atmospheric pressure.

Pressures greater than atmospheric are applied by an Aminco-Winslow Porosimeter. The porosimeter has a pressure capacity of 15,000 psi and an electrical-mechanical sensing device which measures volumetric increments of 0.0001 ml in the penetrometer stem. Intrusion pressures are measured by two Bourdon pressure gauges on the porosimeter: one which has a capacity of 1,000 psi and the other a capacity 15,000 psi.

3-5.2 Procedure

Following freeze drying, the samples to be intruded were trimmed with a hammer and chisel along several faces then blown clean with a dry air stream. The trimming method was intended to cause a tensile break in the soil to prevent surface pores from being smeared shut. The sample was weighed, then sealed in the penetrometer and weighed again. The penetrometer and sample were placed in the filling chamber and evacuated to 0.010 to 0.015 mm of mercury. Evacuation generally required about 30 minutes of pumping to reach the required pressure. At this point, the penetrometer was filled with mercury.

Filling the penetrometer with mercury was accomplished by rotating the filling device so that the level in the mercury reservoir would just cover the opening in the penetrometer stem. The vacuum pump was turned off, and air was bled into the assembly to a pressure of 20 mm of mercury. Raising the pressure in the filling device forced mercury into the penetrometer, enveloping the soil specimen. In some cases an air bubble would remain trapped between the top of the sample and the glass surface of the penetrometer. When this occurs, Bhasin (1975) recommended that the pressure be increased to 40 mm or 80 mm of mercury to surround the soil completely with mercury. A small air bubble was always present after filling due to the volume of air in the bulb prior to filling. If the bubble appeared to be trapped above the sample and if it was rather large, the filling pressure was raised, but if the bubble was small, the filling pressure was left at 20 mm of mercury.

After filling the penetrometer, the filling device was rotated back to its original position breaking off the mercury column at the penetrometer stem. The stem reading and the filling pressure were

recorded. The pressure was then raised in increments, noting the position of the stem reading after each increment. This process is referred to as the low pressure intrusion and was continued to atmospheric pressure.

When atmospheric pressure was reached, the penetrometer was removed from the filling device, weighed and placed in the porosimeter. Because the penetrometer fit into the porosimeter in a "stem down" position, the specimen, located at the top of the penetrometer bulb, was under tension induced by the suspended column of mercury below it. To bring the sample at atmospheric pressure, the porosimeter pressure was raised to 4 psi. The probe reading was recorded at 4 psi, and the pressure was increased incrementally to about 14,000 psi. Probe readings were taken after each increment of pressure when the incremental intrusion was complete.

4 - RESULTS AND DISCUSSION OF RESULTS

4-1 Compaction

The three blends of clayey silt used were prepared by three levels of kneading compaction effort. The medium effort was selected such that the optimum dry density of the 90% silt-10% kaolin mix was nearly equal to the optimum dry density of the same soil compacted by the AASHTO T99-70 procedure (i.e. standard Proctor). The high compaction effort was intended to produce an optimum dry density about 8 to 10% higher than the medium effort, thus approximating the modified Proctor compaction effort. A low compaction effort was also used.

After generating preliminary compaction curves for the soils and efforts to be used, the samples which would be used for permeability and pore size measurements were prepared at selected water contents. Three molding water contents were generally used to represent a compaction effort: one sample was prepared near the optimum water content, one was prepared about 1.5 to 3% dry of optimum and one was prepared about 1.5 to 3% wet of optimum water content.

Table 3 summarizes the code designation used to identify the soils tested in this study. The code designation gives the soil type, compaction effort, and relative water content with respect to its optimum. Table 4 presents the compaction parameters (dry density, water content and degree of saturation) measured after compaction and again after permeation for the twenty-two samples tested. Permeability

TABLE 3 SAMPLE CODE DESIGNATION**Soil Type**

- S9 - 90% Silt and 10% Kaolin
- S7 - 70% Silt and 30% Kaolin
- S5 - 50% Silt and 50% Kaolin

Compaction Effort (Hydraulic System Pressure)

- L - Low Compaction Effort; 4.0 psi
- M - Medium Compaction Effort; 8.5 psi
- H - High Compaction Effort; 40. psi

Moisture Condition

- O - Near Optimum Water Content
- O-D - Slightly Dry of Optimum Water Content
- D - Dry of Optimum Water Content
- W - Wet of Optimum Water Content

Example S9HO: 90% Silt and 10% Kaolin compacted at 40 psi gauge pressure near the optimum water content

TABLE 4 COMPACTION PARAMETERS OF SOILS TESTED

SAMPLE CODE	Dry Density	Water Content After Compaction	Saturation After Compaction	Water Content After Permeation	Saturation After Permeation
	pcf	%	%	%	%
S9MO S9MO-D S9MD S9MW	109.7	16.2	81	18.6	93
	109.2	14.4	70	20.4	100
	106.7	11.7	54	21.4	99
	108	17.1	81	18.3	87
S9HO S9HD S9HW	120.4	11.9	79	13.7	91
	117.4	7.5	46	17.3	105
	115.4	13.8	80	15.9	92
S7LO S7LD S7LW	107.8	19.0	91	19.9	95
	103.3	16.9	72	23.6	101
	106.4	20.3	94	20.8	96
S7MO S7MD S7MW	113.9	14.6	82	17.4	98
	108.1	13.5	65	21.4	103
	111.4	16.9	89	18.0	94
S7HO S7HD S7HW	120.1	12.7	85	14.9	99
	118.0	10.5	66	16.3	103
	116.3	14.8	88	16.3	98
S5LO S5LD S5LW	105.6	19.8	90	21.3	97
	99.3	18.3	71.3	26.1	102
	103.9	21.2	92.6	22.1	97
S5MO S5MD S5MW	108.4	18.1	89	19.9	98
	99.5	16.6	65	26.4	103
	106.8	19.9	93	20.3	96

and pore size distribution measurements were made for each of the samples. Figures 11, 12 and 13 present the compaction curves, the location of each of the sample points, and the permeability measured for each of the samples.

4-2 Saturation

As mentioned previously, it was necessary to saturate samples prior to permeation; three successive steps were followed for the saturation process. Water was first passed through the sample under a vacuum pressure differential of about 10 psi. Water was then passed through the soil, while applying back pressure, under a pressure differential of 3 to 5 psi. Finally, the permeability tests were conducted at a 50 psi back pressure. The vacuum saturation technique was very effective in increasing the degree of saturation of the dry side samples. Table 4 shows that all samples compacted dry of optimum had a final saturation of about 100%. However, the vacuum saturation may have caused a slight consolidation in some of the samples because of the high pressure differential across the sample. As shown in Appendix B, seepage forces cause increases in effective stress which can equal the water pressure differential across a sample. In retrospect, the saturation procedure could have been improved by limiting the pressure differential during vacuum saturation to 5 psi and increasing the back pressure to 75 to 100 psi.

Table 4 shows the saturation of each of the samples after permeation as measured from the gross sample. It is important to note that these values were measured after the 50 psi back pressure was removed; thus, the saturation during permeation was not known. From

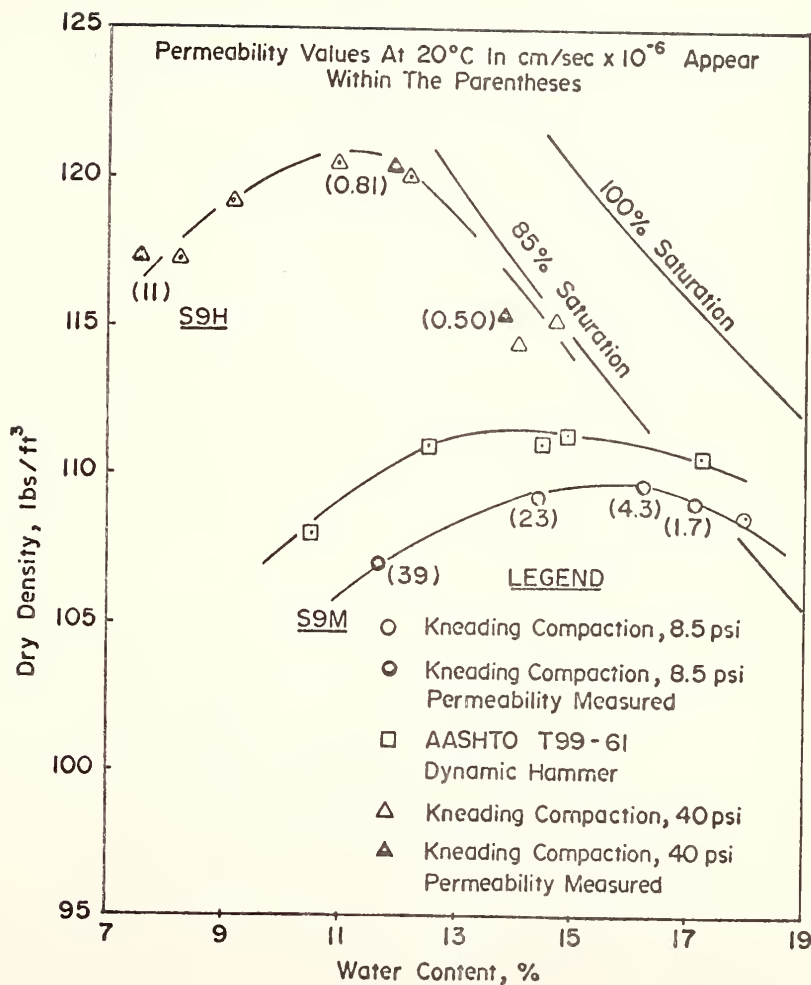


FIGURE 11 COMPACTION CURVES FOR 90% SILT AND 10% KAOLIN

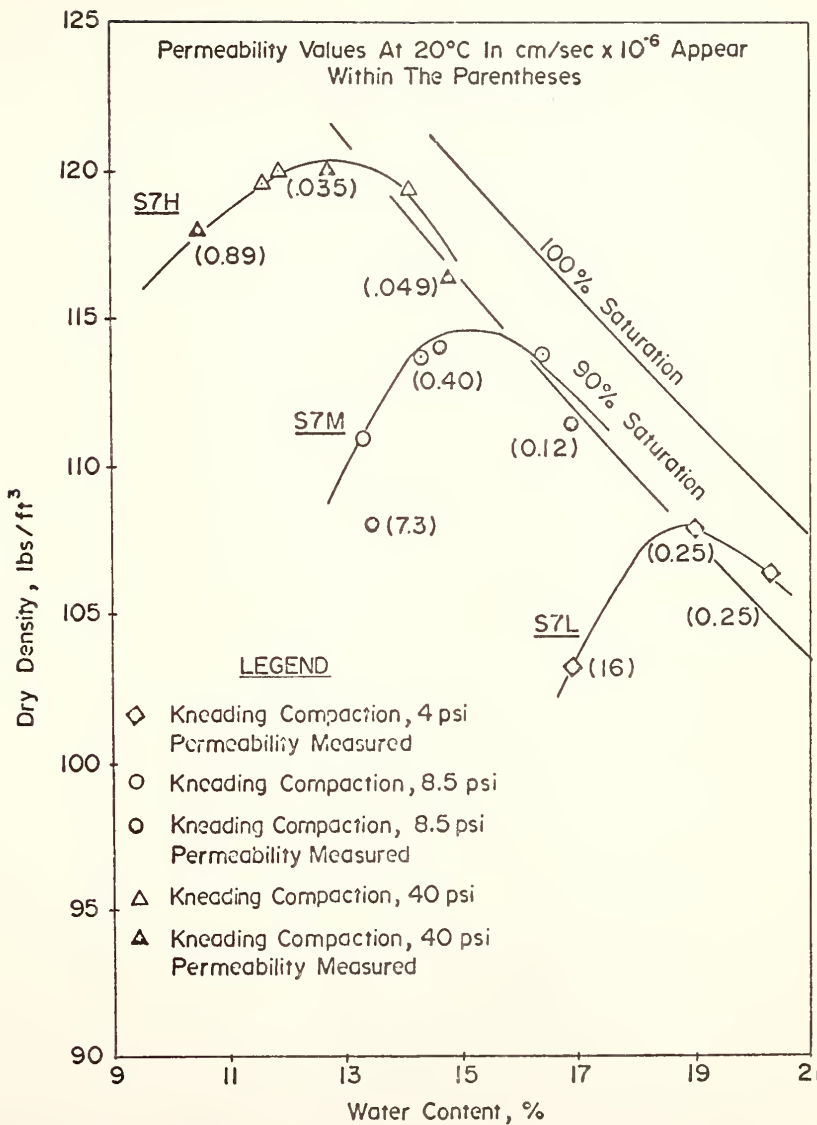


FIGURE 12 COMPACTION CURVES FOR 70% SILT AND 30% KAOLIN

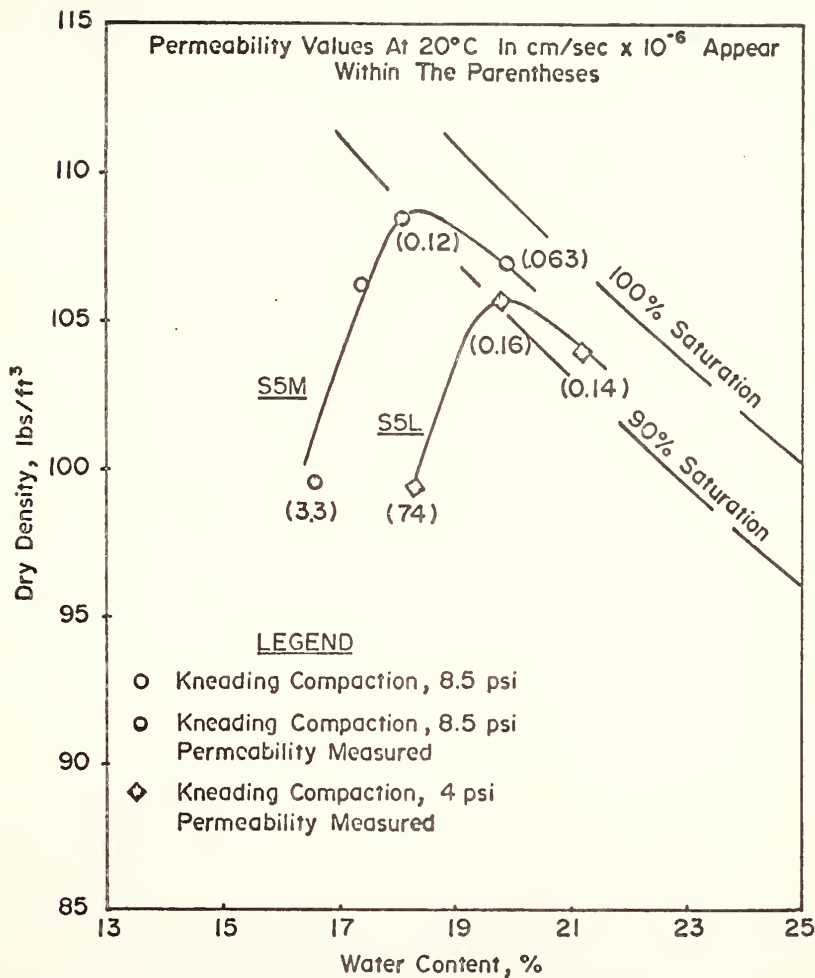


FIGURE 13 COMPACTION CURVES FOR 50% SILT AND 50% KAOLIN

the theoretical relationship between degree of saturation and back pressure presented by Lowe and Johnson (1960), the degree of saturation during permeation can be estimated. At 50 psi back pressure, an initial degree of saturation of $S_i = 93\%$ is necessary to bring a sample to full (100%) saturation, and $S_i = 91\%$ is required to bring a sample to 99% saturation (for back pressuring at constant volume). If this criterion is used, all but one of the samples were 99% saturated and all but three of the samples were 100% saturated during permeation.

4-3 Freeze Drying

It was critical to monitor changes in volume during the different phases of the investigation to detect sample disturbance. Table 5 presents porosity measurements made after compaction, after permeation, and after freeze drying. As shown, some of the samples experienced a 1 to 3% change in volume between the time of compaction and the measurement of pore size distribution. Several sources of error are likely to have caused the volume changes. Contrasting columns 1 and 2 of Table 5, it is apparent that some samples experienced a 1 to 2% increase in volume after permeation. This probably occurred when the samples were extruded; a slight swelling may have resulted when the confining mold was removed. Contrasting columns 2 and 3 of Table 5 indicates that freeze drying may have also resulted in slight volume changes (both shrinkage and expansion) of 1 to 3% for some of the samples. Reasons for the volume changes due to freeze drying were discussed previously in Section 1-3. Random scatter of the porosity measurements and sample fabric may also explain some of the volume changes.

TABLE 5 POROSITY MEASUREMENTS BEFORE AND AFTER FREEZE DRYING

SAMPLE CODE	1 Porosity After Compaction (Gross)	2 Porosity * After Permeation (Avg)	3 Porosity After Freeze Drying (Avg)	Porosity Change (3-1)
S9MO	.35	.36	.36	0.01
	.36	.36	.38	0.02
	.37	.37	.38	0.01
	.36	—	.36	0.00
S9HO	.29	.31	.31	0.02
	.31	.32	.33	0.02
	.32	.33	.34	0.02
S7LO	.36	.36	.36	0.00
	.39	.39	.39	0.00
	.37	.37	.37	0.00
S7MO	.33	.34	.35	0.02
	.36	—	.38	0.02
	.34	.35	.35	0.01
S7HO	.29	.29	.29	0.00
	.30	—	.33	0.03
	.31	.31	.30	- 0.01
S5LO	.37	.38	.37	0.00
	.41	—	.40	- 0.01
	.38	.38	.37	- 0.01
S5MO	.35	.37	.36	0.01
	.41	.42	.41	0.00
	.36	.36	.36	0.00

* Measured by wax displacement. Values missing were too soft to trim or were not measured.

The final column of Table 5, however, indicates that the maximum volume change from compaction to pore size measurement was 3%. This was felt to be a tolerable amount.

4-4 Permeability

The permeability was measured by a closed system, falling head apparatus under a back pressure of 50 psi. The hydraulic gradient during the tests varied from 10 to 1. The range of permeability tested extended from 10^{-4} to 10^{-8} cm/sec. Appendix B discusses the permeability test and calculation procedures used.

Since the temperature was not controlled during the permeability tests, it was monitored with each water level reading. The permeability readings were normalized to a 20°C temperature as suggested by Lambe and Whitman (1969) as follows:

$$k_{20^{\circ}\text{C}} = \frac{\mu_T}{\mu_{20^{\circ}\text{C}}} k_T \quad (4-1)$$

where $k_{20^{\circ}\text{C}}$ is the permeability at 20°C
 k_T is the permeability at temperature T
 $\mu_{20^{\circ}}$ is the absolute viscosity of water at 20°C
 μ_T is the absolute viscosity of water at $T^{\circ}\text{C}$
 T is the average temperature between two water level readings in $^{\circ}\text{C}$.

Shown on Figures 14 through 17 are the permeability measurements plotted versus mean hydraulic gradient for each of the samples. It is apparent that some of the samples did not perform in accordance with Darcy's law, which requires that the permeability remain constant with changes in hydraulic gradient. Some of the samples, such as S7LW, S7LO, S7MW etc., initially showed a decrease in permeability with decreasing

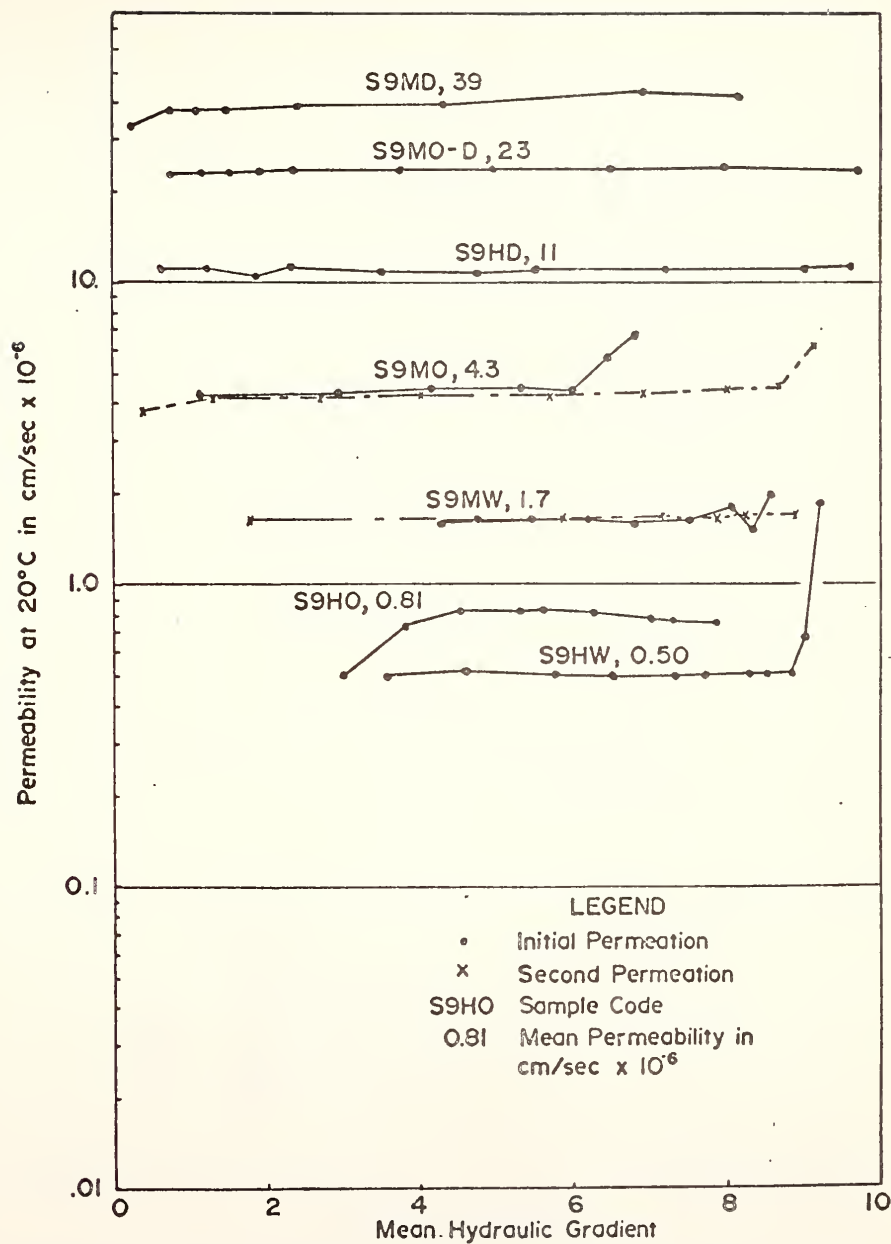


FIGURE 14 PERMEABILITY VS HYDRAULIC GRADIENT FOR S9 SAMPLES

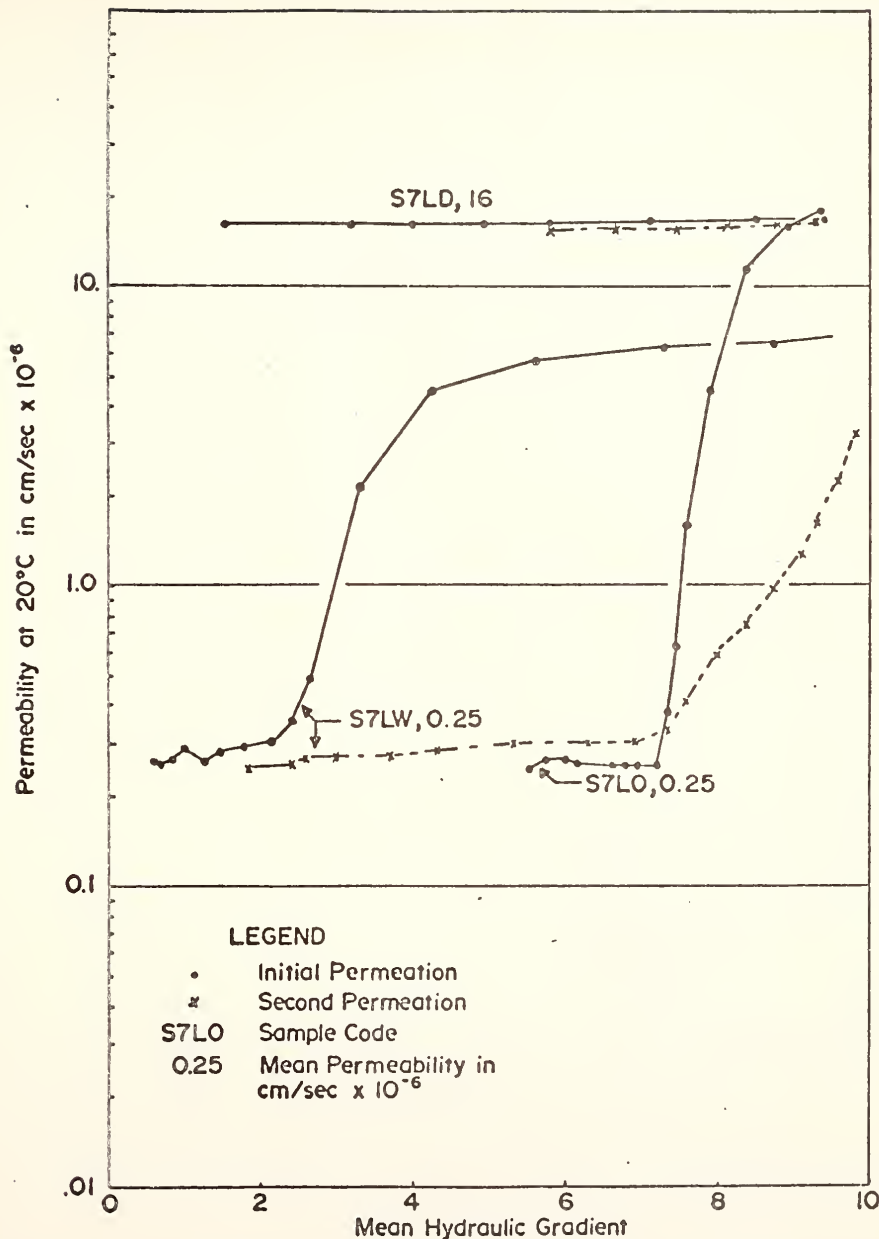


FIGURE 15 PERMEABILITY VS HYDRAULIC GRADIENT FOR S7L SAMPLES

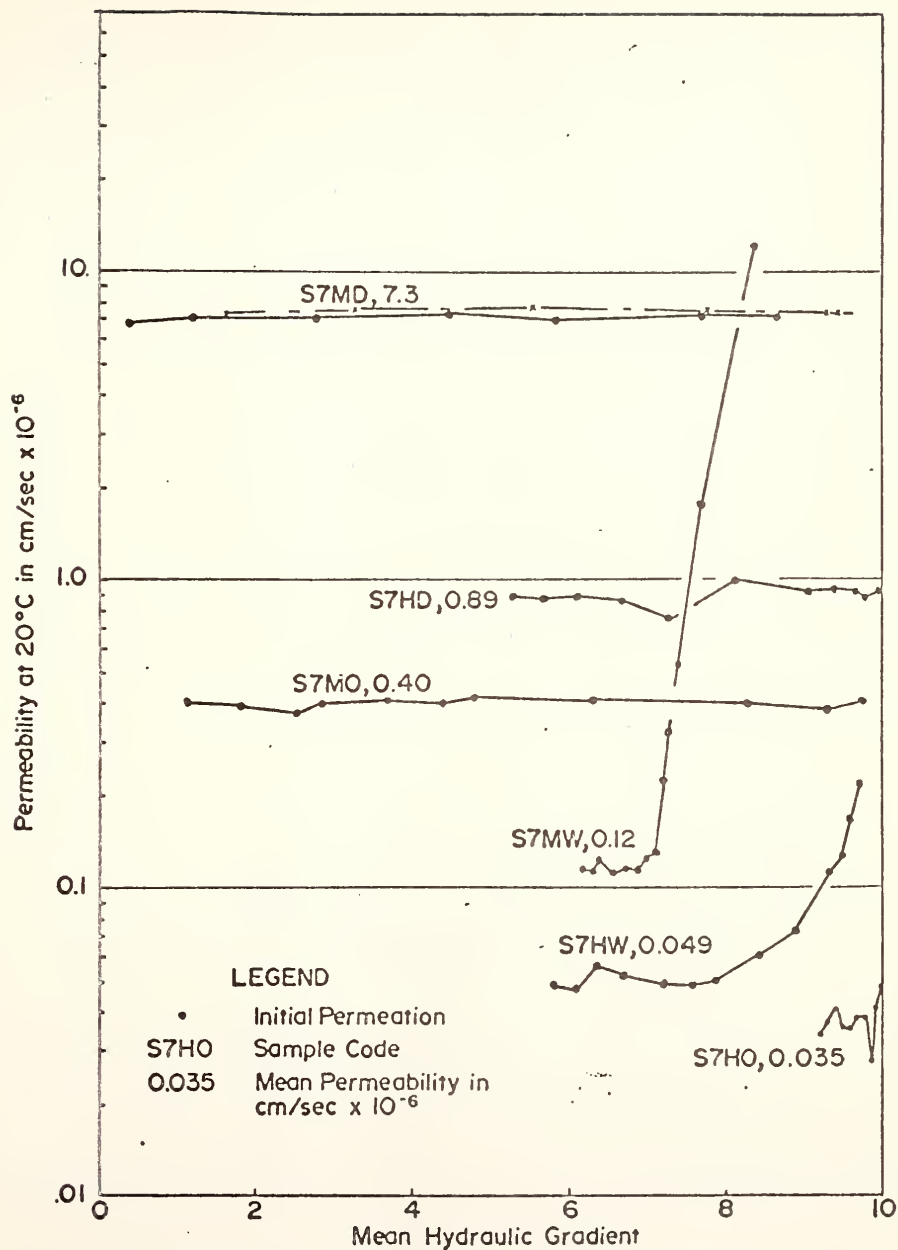


FIGURE 16 PERMEABILITY VS HYDRAULIC GRADIENT FOR S7M AND S7H SAMPLES

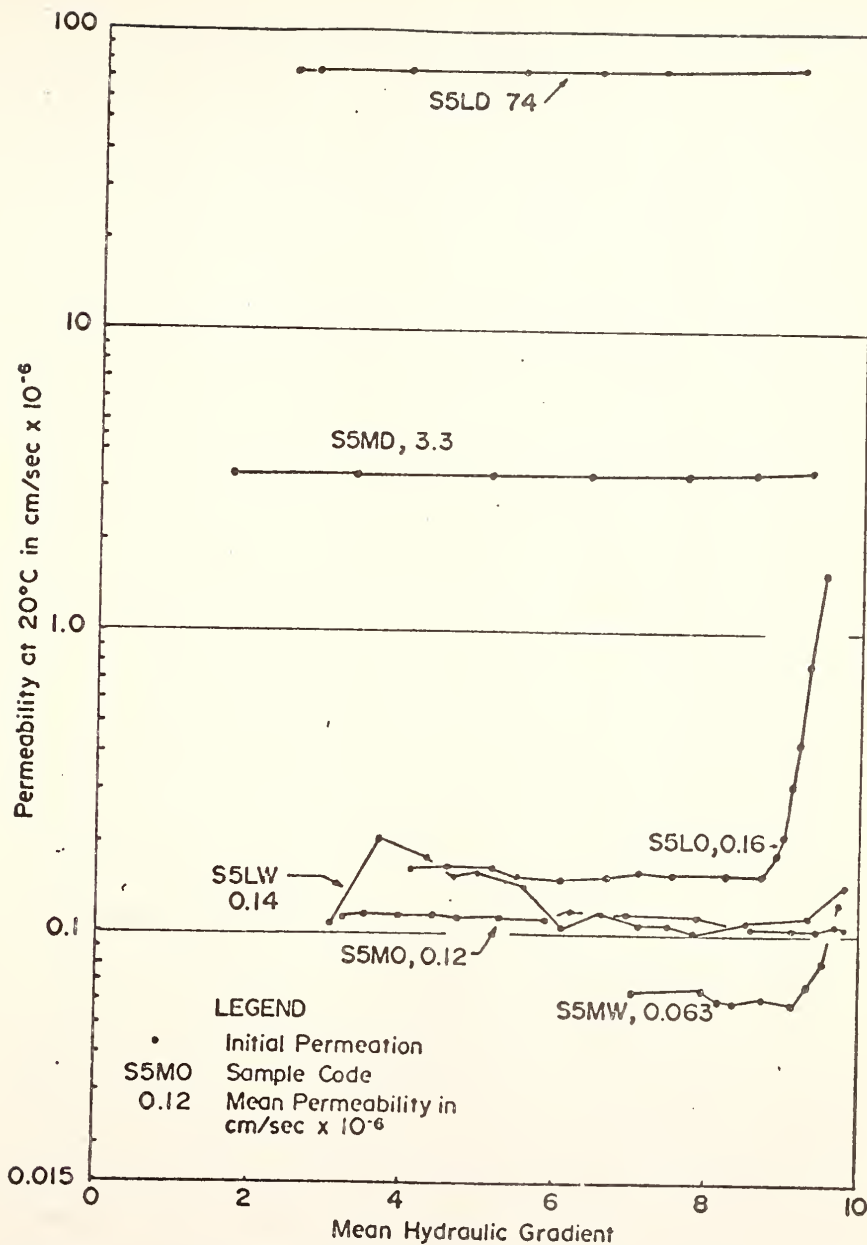


FIGURE 17 PERMEABILITY VS HYDRAULIC GRADIENT FOR S5 SAMPLES

hydraulic gradient then tended to level out to a constant permeability value. This type of behavior was initially thought to be caused by non-Darcy type flow discussed previously (Miller and Low, 1963 or Hansbo, 1960); however, a closer examination of the data revealed that this was not so. Sample S7LW will be used as an example. This sample was permeated twice, and as shown in Figure 15, the permeability-hydraulic gradient relation was different for each of the runs. Figure 18 shows the relation between permeability and net cumulative volume of inflow plotted versus time for sample S7LW. The net cumulative volume of inflow was determined as described in Appendix B. The Figure clearly indicates that initially, steady-state flow did not exist in the sample, thus rendering the permeability calculations inaccurate. A probable cause for the initial net inflow of water into the sample was that the sample may have lost part of its 50 psi back pressure when it was transferred from the saturation device to the permeameter. When permeation began, several hours were required to equilibrate the flow in the sample. As shown in Figure 18, once steady-state flow conditions were approached, the permeability measurements tended to stabilize, agreeing with Darcy's law.

The permeability values assigned to each of the samples were calculated from an average of six to eight measurements from the stabilized portion of the permeability-hydraulic gradient curves. The scatter in the permeability values was partially due to the accuracy of the water level readings and temperature fluctuations between readings. Only one sample, S5LW, shown on Figure 17, exhibited some peculiar permeability fluctuations which could not be explained.

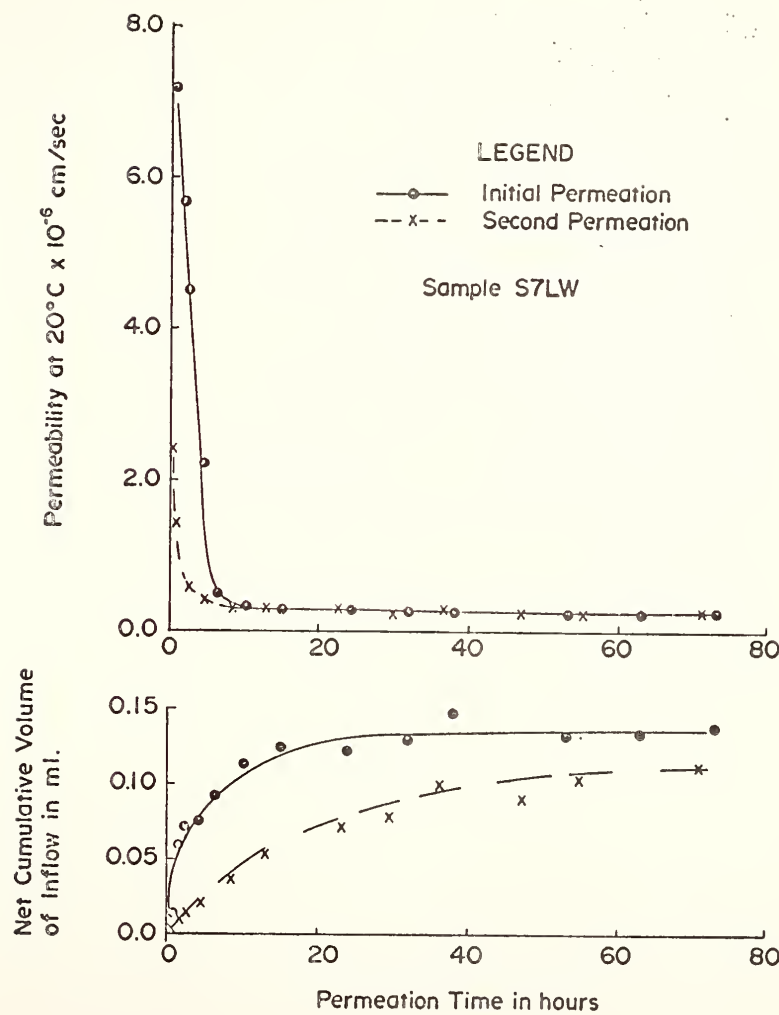


FIGURE 18 PERMEABILITY AND NET VOLUME INFLOW VS TIME FOR SAMPLE S7LW

The relation between the compaction curves and the permeability values are shown on Figures 11, 12 and 13. The results generally agree with trends found by Lambe (1954), Bjerrum and Huder (1957), and Mitchell et al. (1965), which were previously discussed. The dry side samples generally had permeabilities one to three orders of magnitude greater than the optimum and wet side samples. There was little difference between the permeabilities of the optimum and wet side samples for a given compaction effort and soil type.

4-5 Pore Size Distribution

Pore size distribution curves are shown on Figures 19 through 32 and in Appendix A on Figures 37 through 58. Each of the figures consist of a differential and cumulative graph of the porosity (volume of voids intruded divided by the total volume) versus the logarithm of the pore diameter. Also shown on the Figures are the compacted water contents and the permeabilities of each of the samples. The differential plots were determined as described in Section 1-2.4. The large data points along the ordinate axis of the cumulative plots represent the porosity of the pore size specimen as measured by mercury displacement. Several general observations are evident from the pore size distribution figures.

The differential plots provide a useful complement to the cumulative plots for representing pore size distributions. The most volumetrically frequent or "modal" pore sizes are clearly depicted as peaks on the differential plots. When contrasting separate pore size distribution curves, the location and size (both height and width) of these peaks serve as useful comparative descriptive parameters.

Hereafter, the most frequent pore diameters will be referred to by their proper statistical name, modes.

The pore size distribution measurements of the samples tested in this study displayed two modes (bimodal) when considered on a log diameter scale. The relative position and size of these modes gave clear indications of the nature of the soil fabric. One of the modes was between 10 and 1.0 μm and will be referred to as the large pore mode. The other mode occurred consistently at 0.1 μm and will be referred to as the small pore mode.

All of the pore size distribution curves showed little or no volume of pores larger than 10 μm .

4-5.1 Replication

The reliability and reproducibility of pore size distribution measurements was one of the topics addressed in this study. As mentioned previously, several precautions were taken to insure homogeneous compacted samples. A minimum of two pore size distributions were measured from each sample. The plots of these pore size measurements are presented in Appendix A, Figures 37 through 58. Overall the replication of the pore size distribution measurements was felt to be quite good. Only one sample, S7MO (shown on Figure 47), produced significant scatter between pore size measurements.

The most obvious reason for scatter in replicate pore size distribution curves is natural variability of the soil fabric. Some of the specimens may have suffered more compression or disturbance than others. Such differences in fabric may be detected by comparing the location and size of the large pore modes and comparing the porosities

of each of the specimens. Examples of these discrepancies are shown by S9HO (Figure 41), S9HW (Figure 43), S7HO (Figure 50) S7HW (Figure 52), and S5LD (Figure 54).

Measurement errors may also account for scatter in replicate pore size distribution curves. Significant differences in the cumulative pore size curves may result because of a high initial intrusion in some of the specimens. This intrusion at the larger diameters is probably caused by cracks in the specimen due to poor drying techniques or by a trapped air pocket on the surface of the specimen when it was initially surrounded with mercury. Such specimens will give erroneous porosity measurement which are too high. The cumulative plots of these samples will not coincide, but the differential plots should be nearly identical. Examples are S9HD (Figure 42) and S5LW (Figure 55).

Measurement errors may occur when the pore volume of a specimen exceeds the intrusion capacity of the porosimeter (the probe limit). Such specimens yield a negative intrusion at the higher pressures (smaller pore diameters) as shown by samples S7LD (Figure 45) and S5LD (Figure 54). The apparent negative intrusions result from the corrections for the compression of mercury.

If differential pore size curves are plotted, it is imperative that the pressure increments be taken at logarithmically equal intervals; otherwise, serious distortions of the differential curves will result, as discussed in Section 1-2.4. This fact was not fully appreciated in this study until after the pore size distribution measurements were made. As mentioned previously, a proper pressure increment schedule for mercury intrusion should be:

$$\frac{P_i}{P_{i-1}} = 10^c$$

where P is the intrusion pressure and "c" is the logarithmic interval constant. The value of c generally varied between 0.16 and 0.23 with an average of 0.2 for pores smaller than 50 μm in size. In retrospect, c should have been kept constant during all the pore size measurements. Samples S7L0 (Figure 44) and S7LW (Figure 46) exhibit examples of the distortions which can occur. Both figures show slight discrepancies of the small pore mode because of poor pressure spacings in the small pore diameter range.

Several of the samples, including S9MO (Figure 37), S9MO-D (Figure 38), S9MD (Figure 39) and S5MO (Figure 56), show excellent replication of pore size distribution measurements.

The specimen with the porosity closest to the gross compacted sample porosity was chosen to represent a given sample, if no major measurement errors were evident in its pore size distribution curves. The first specimen which appears in the legend of the pore size figures in Appendix A was the one selected to represent each of the samples.

4-5.2 Contrasting Pore Size Distributions

This section discusses:

- 1) changes in pore size distribution produced by varying compactive water content and compactive effort for a given soil, and,
- 2) pore size distributions of different soils prepared at similar compactive effort and moisture conditions relative to their optimum water contents.

The 90% silt - 10% kaolin is the first soil examined. Its compaction curves are presented on Figure 11, and its pore size distribution curves are shown on Figures 19, 20 and 21. From the pore size figures it is evident that the pore size distributions are bimodal with differences in the large pore mode accounting for the changes in soil fabric, while the small pore modes remain nearly constant. Figures 19 and 20 show the large pore mode decreasing with increasing water content on the dry side of optimum. Only minor differences in the large pore mode are present between optimum and wet side samples for a given compactive effort. The permeability values of each of the samples increase with increasing large pore mode. Figure 21 shows that as the compactive effort is increased, the large pore mode decreases for both dry side and optimum samples. The permeability, again, decreases with decreasing large pore mode. This same Figure also indicates that the small pore mode is not affected by changes in compactive effort or moisture condition; its frequency and location remain fixed.

Figure 12 shows the compaction curves of the 70% silt-30% kaolin soil and Figures 22 through 26 show its pore size distribution curves. For each of the three compaction efforts the dry side samples have a significantly greater large pore mode than the optimum and wet side samples, as shown by Figures 22, 23 and 24. The wet side and optimum samples have nearly identical differential distributions for the high and medium compactive efforts; however, for the low compactive effort, the wet side sample has a slightly higher large pore mode than its optimum counterpart. The permeabilities of the optimum and wet side

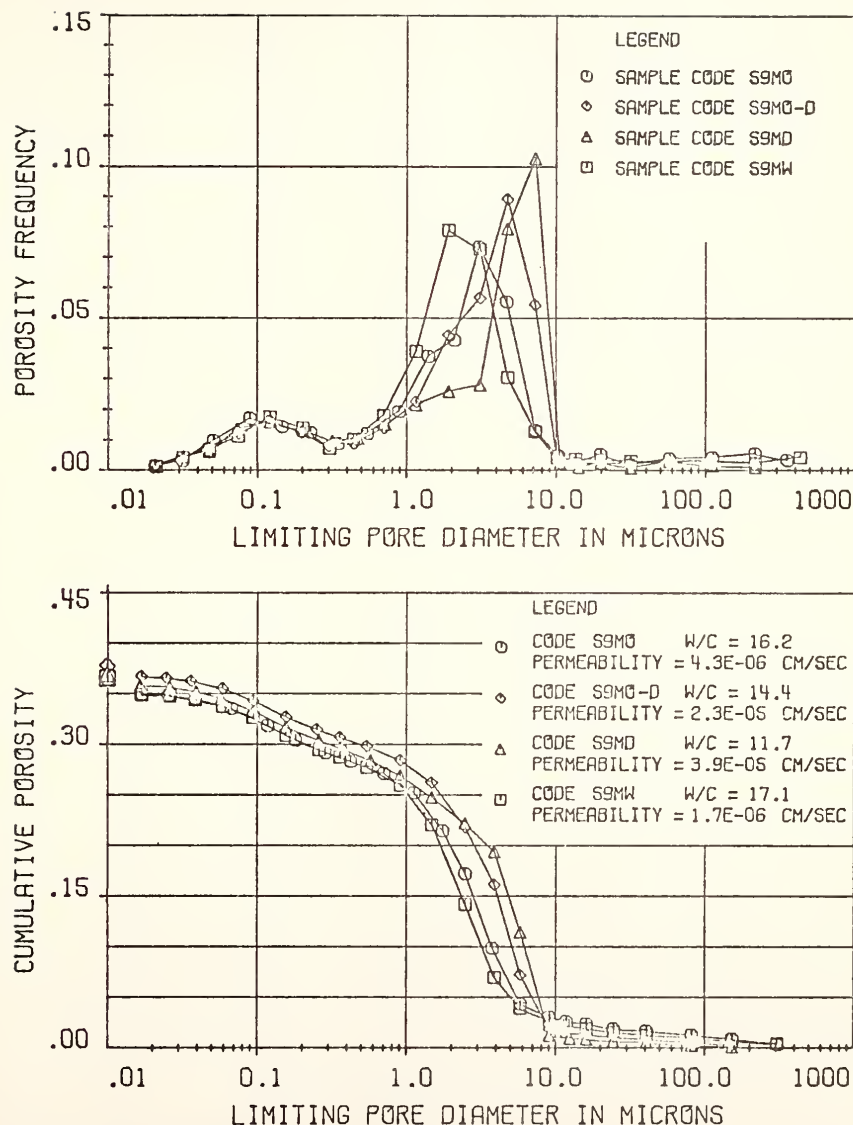


FIGURE 19 DIFFERENTIAL AND CUMULATIVE PORE SIZE DISTRIBUTION CURVES FOR 90% SILT-10% KAOLIN COMPAKTED AT MEDIUM EFFORT

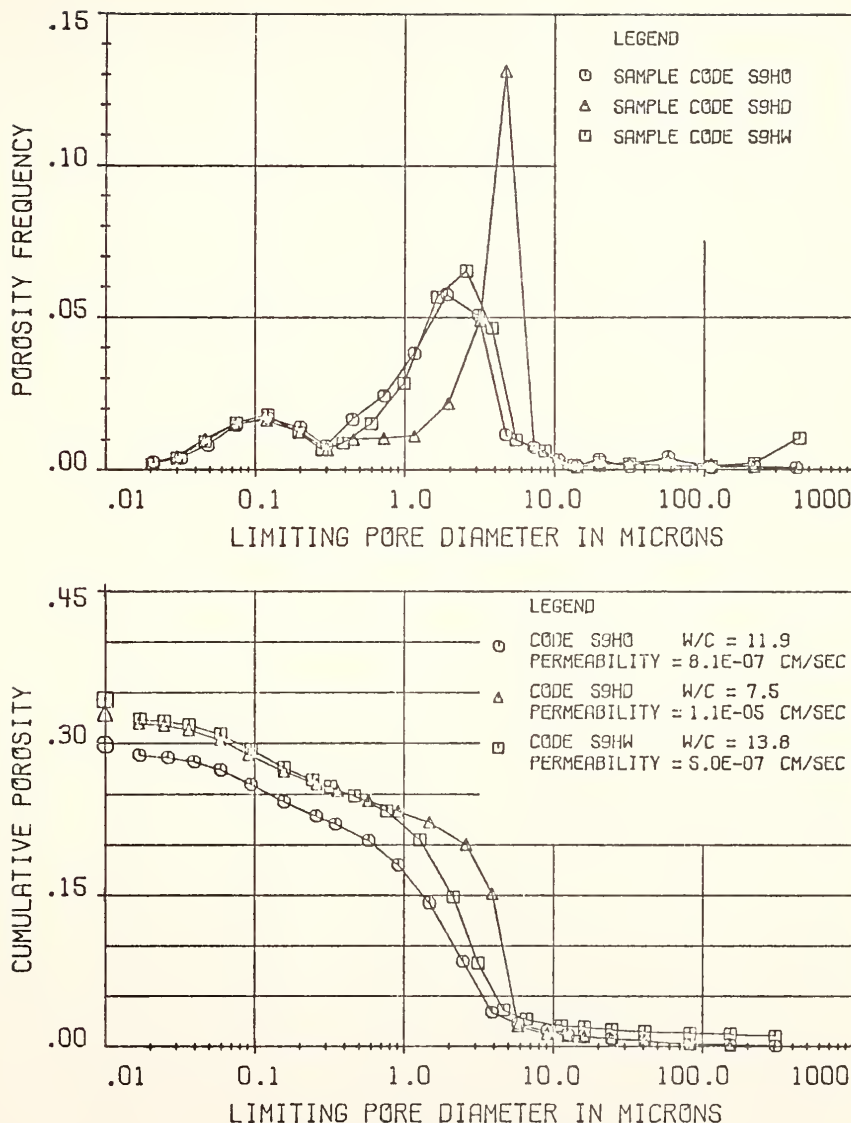


FIGURE 20 DIFFERENTIAL AND CUMULATIVE PORE SIZE DISTRIBUTION CURVES FOR 90% SILT-10% KAOLIN COMPAKTED AT HIGH EFFORT

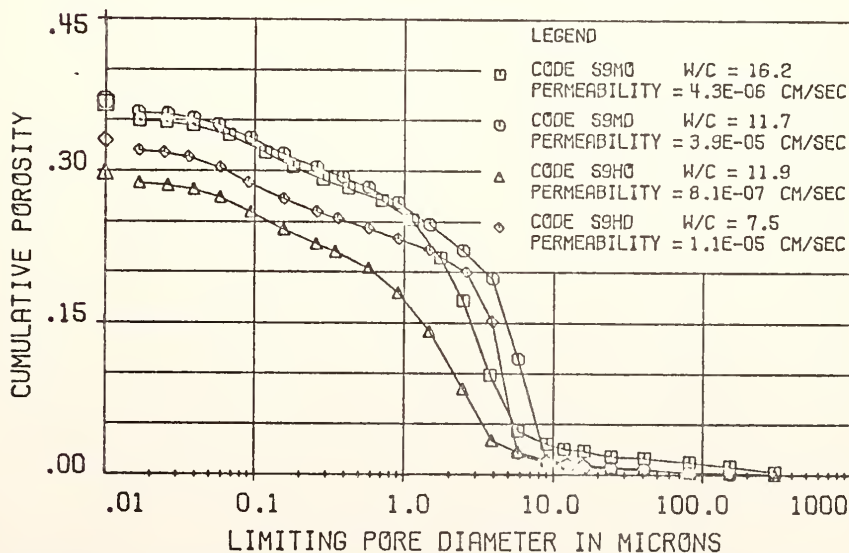
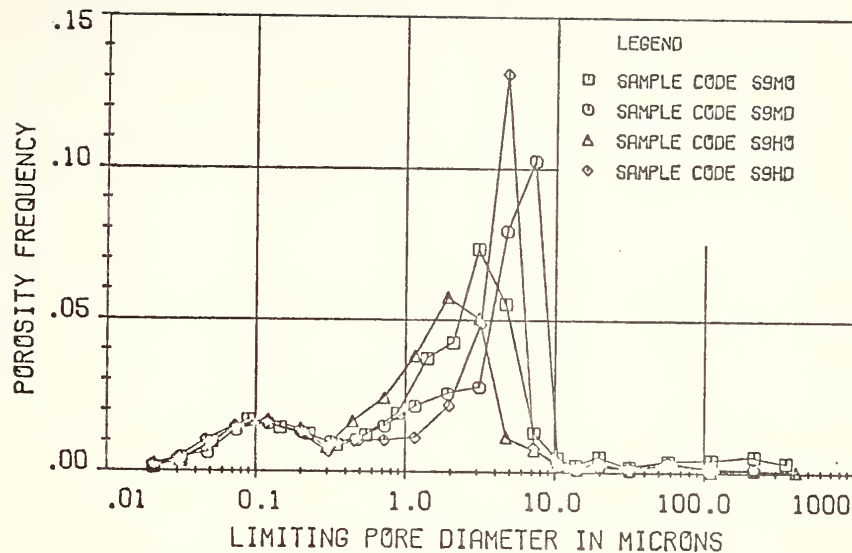


FIGURE 21 PORE SIZE DISTRIBUTION CURVES FOR 90% SILT- 10% KAOLIN COMPACTED AT OPTIMUM AND DRY OF OPTIMUM WATER CONTENTS FOR TWO EFFORTS

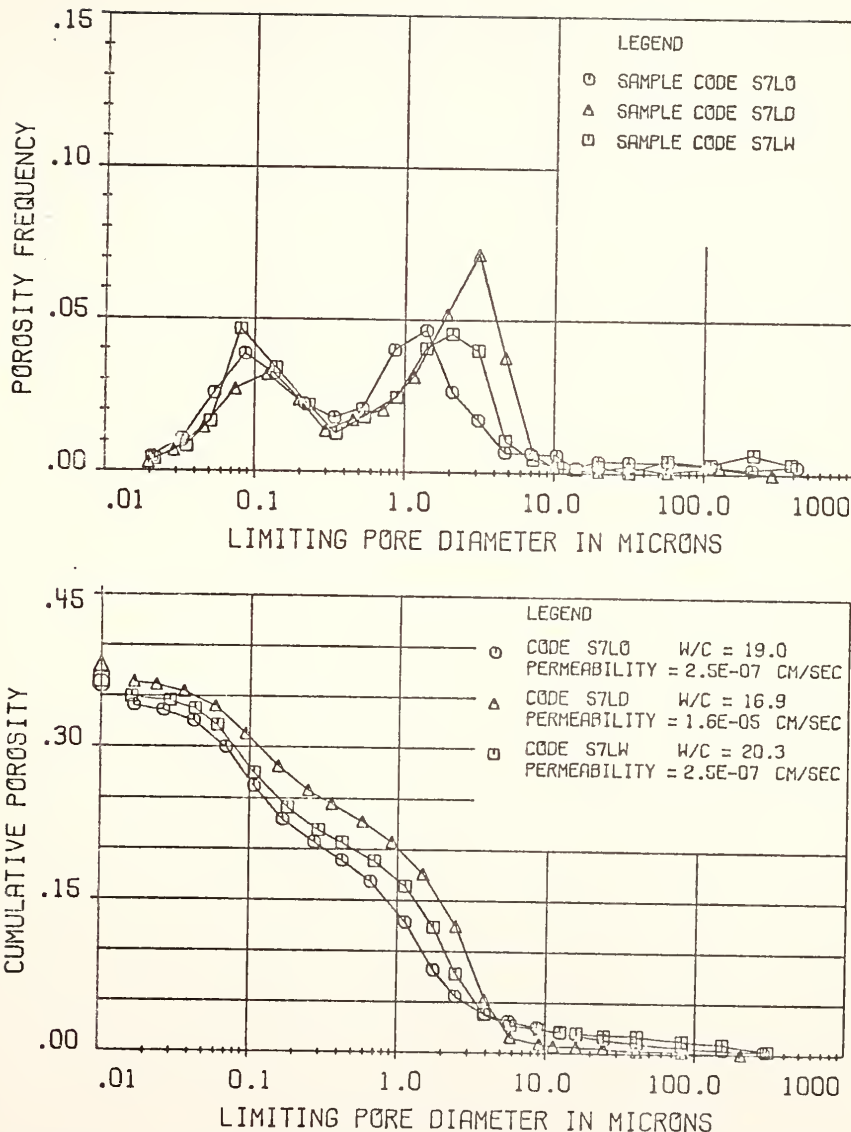


FIGURE 22 DIFFERENTIAL AND CUMULATIVE PORE SIZE DISTRIBUTION CURVES FOR 70% SILT - 30% KAOLIN COMPACTED AT LOW EFFORT

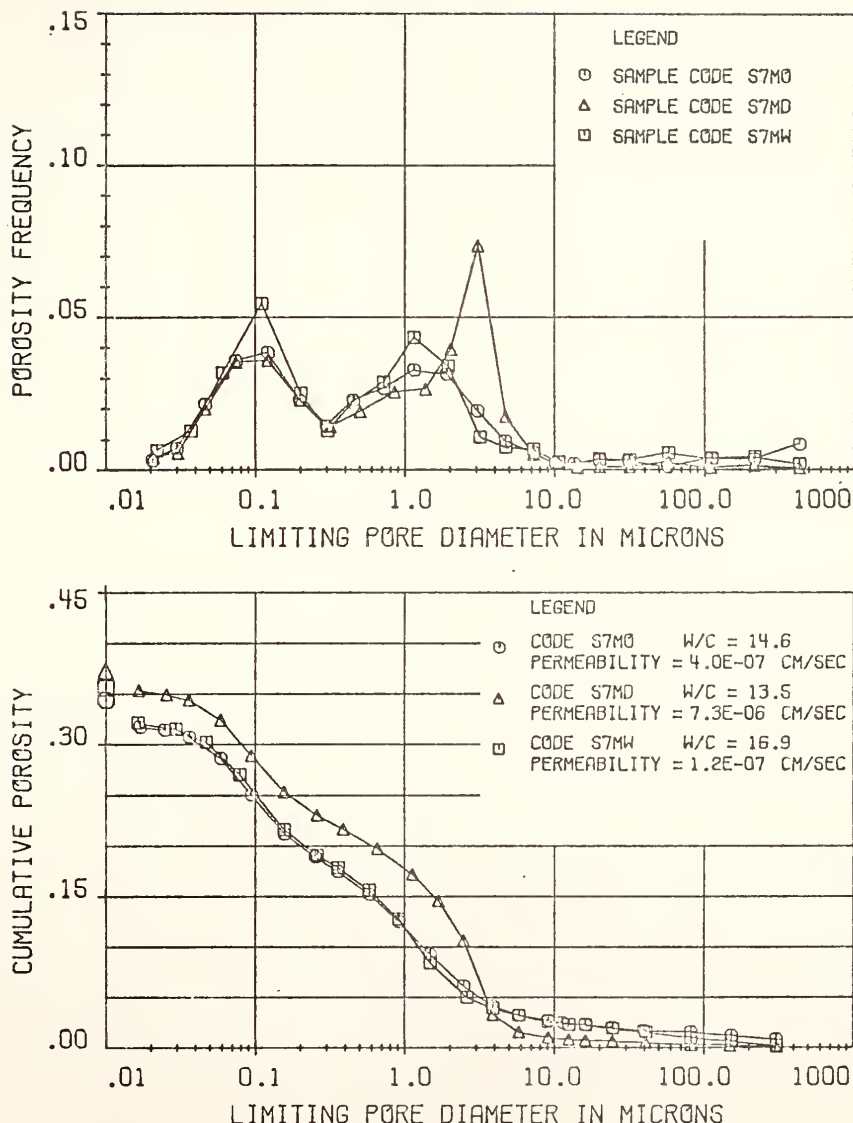


FIGURE 23 DIFFERENTIAL AND CUMULATIVE PORE SIZE DISTRIBUTION CURVES FOR 70% SILT - 30% KAOLIN COMPACTED AT MEDIUM EFFORT

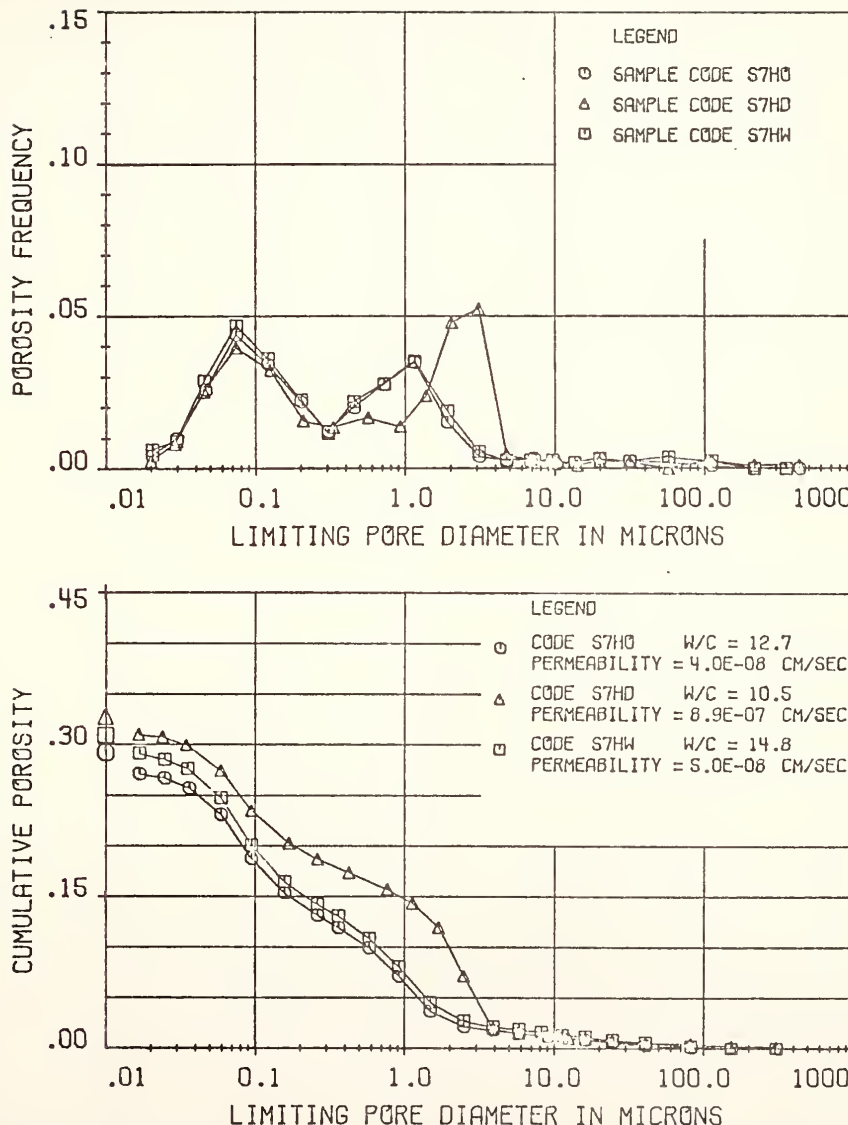


FIGURE 24 DIFFERENTIAL AND CUMULATIVE PORE SIZE DISTRIBUTION CURVES FOR 70% SILT-30% KAOLIN COMPACTED AT HIGH EFFORT

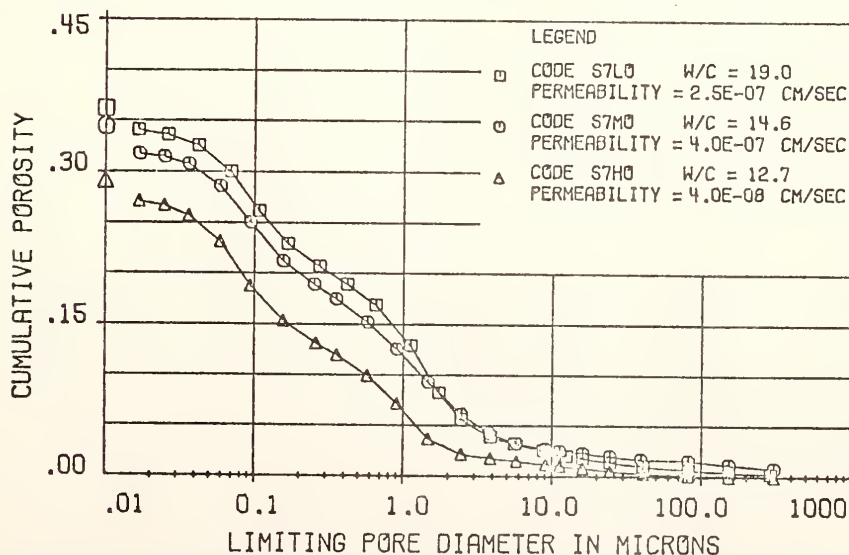
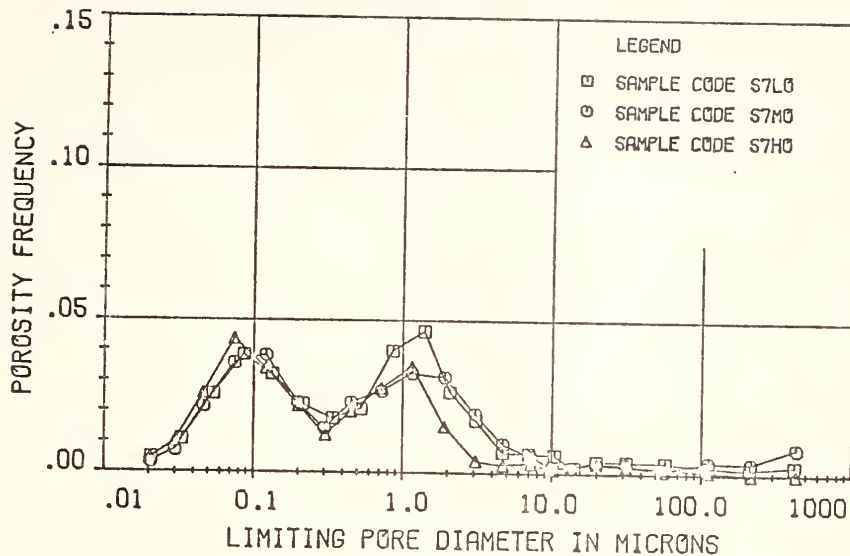


FIGURE 25 PORE SIZE DISTRIBUTION CURVES FOR 70% SILT-30% KAOLIN COMPACTED AT OPTIMUM WATER CONTENT FOR THREE EFFORTS

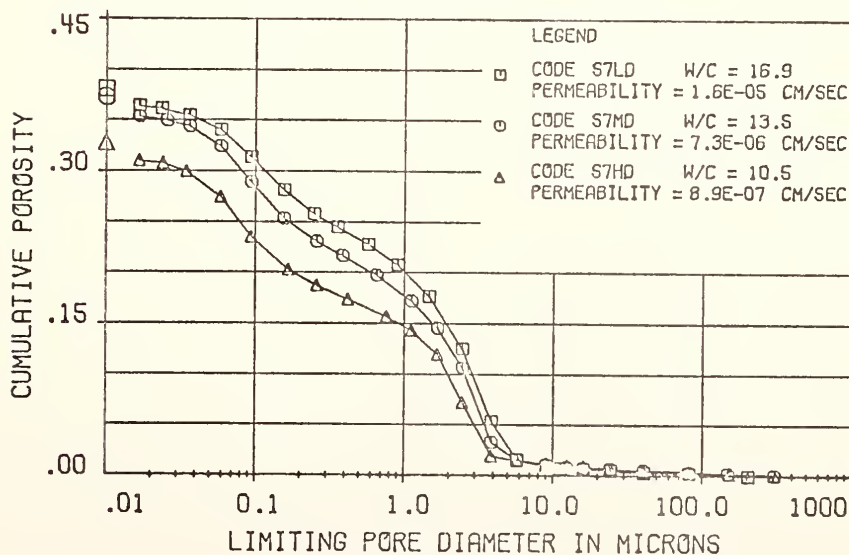
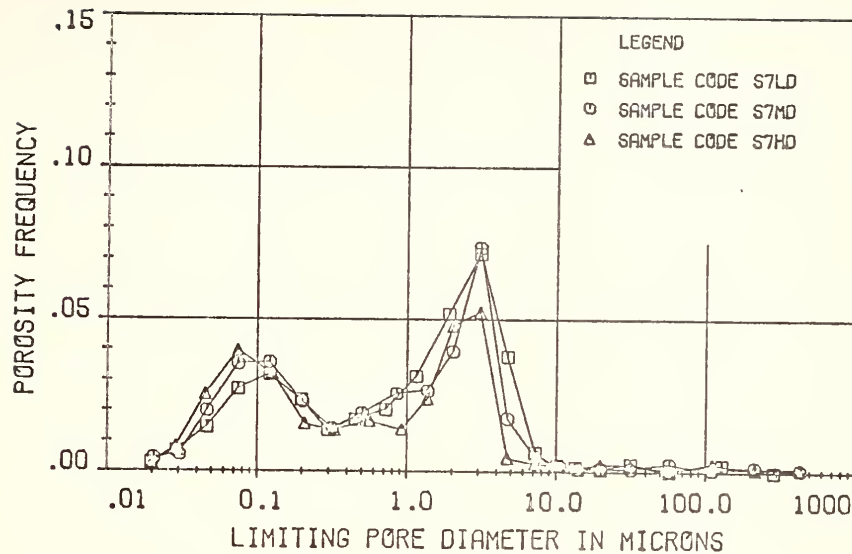


FIGURE 26 PORE SIZE DISTRIBUTION CURVES FOR 70% SILT-30% KAOLIN COMPACTED DRY OF OPTIMUM FOR THREE EFFORTS

samples are nearly equal at each of the three compactive efforts. The effect of increasing compactive effort on optimum and dry side samples is evident on Figures 25 and 26, respectively. The magnitude of the large pore mode remains unchanged for the optimum sample; however, the frequency (or height) of the mode decreases with increasing compactive effort. The same is true of the dry side samples; increasing the compactive effort decreases the frequency of the large pore mode but does not change its value. A small discrepancy is shown in Figure 25 between the permeability and pore size distribution of samples S7LO and S7MO. From the differential distribution curves, sample S7LO would be expected to have a slightly higher permeability than S7MO, but the opposite is true. The small pore mode of the 70% silt - 30% kaolin soil, unlike the 90% silt - 10% kaolin soil, does seem to undergo a very slight decrease with increased compactive effort, as shown in Figures 25 and 26.

The 50% silt - 50% kaolin soil exhibits a distinctly different fabric pattern than the other two soil types tested. Figure 13 shows the compaction curves, and Figures 27, 28 and 29 display the pore size curves. The pore size distributions indicate that samples compacted at optimum or wet of optimum water content have little or no large pore mode, while dry side samples exhibit quite a distinct large pore mode. This explains why the 50% - 50% soil was the most sensitive to changes in permeability between dry side and wet side samples. Figure 29 is inconclusive about the affect of increased compaction effort on the small and large pore mode. It would appear that the increased effort did little to alter the dry side and optimum sample pore size distributions, respectively.

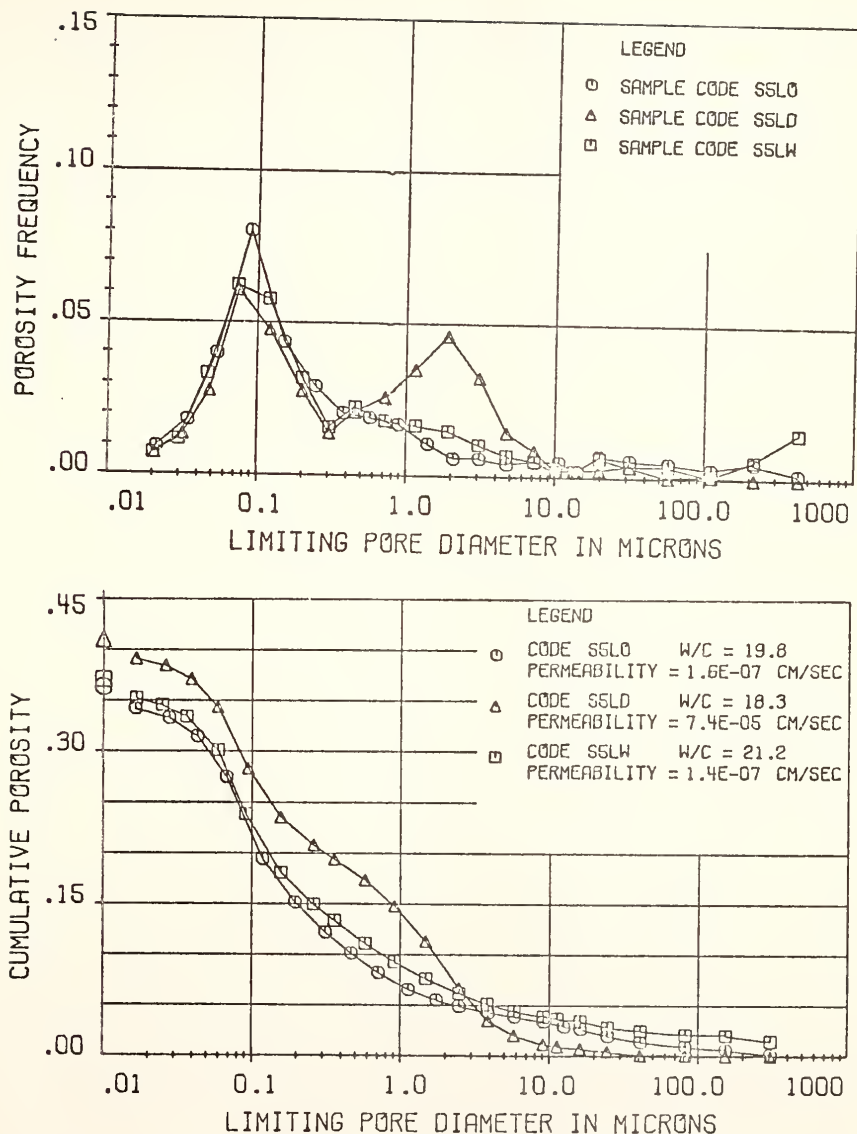


FIGURE 27 DIFFERENTIAL AND CUMULATIVE PORE SIZE DISTRIBUTION CURVES FOR 50% SILT-50% KAOLIN COMPACTED AT LOW EFFORT

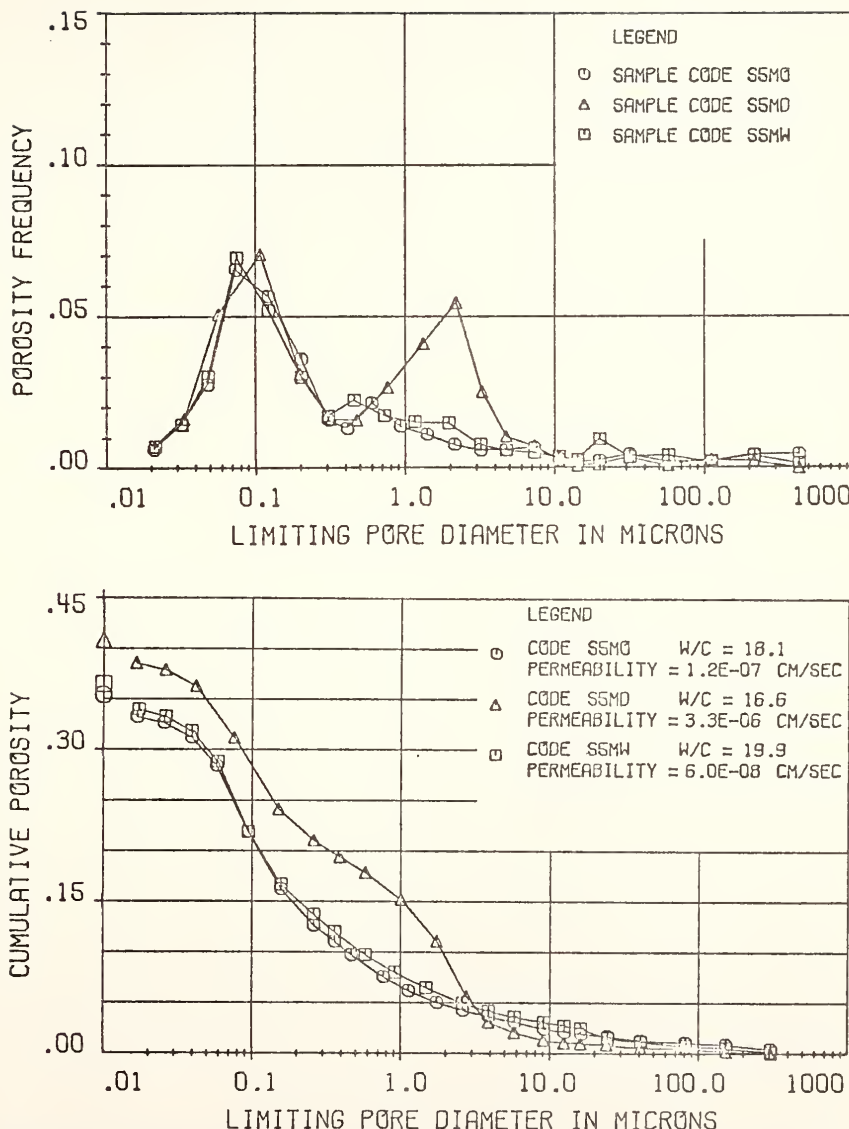


FIGURE 28 DIFFERENTIAL AND CUMULATIVE PORE SIZE DISTRIBUTION CURVES FOR 50% SILT-50% KAOLIN COMPACTED AT MEDIUM EFFORT

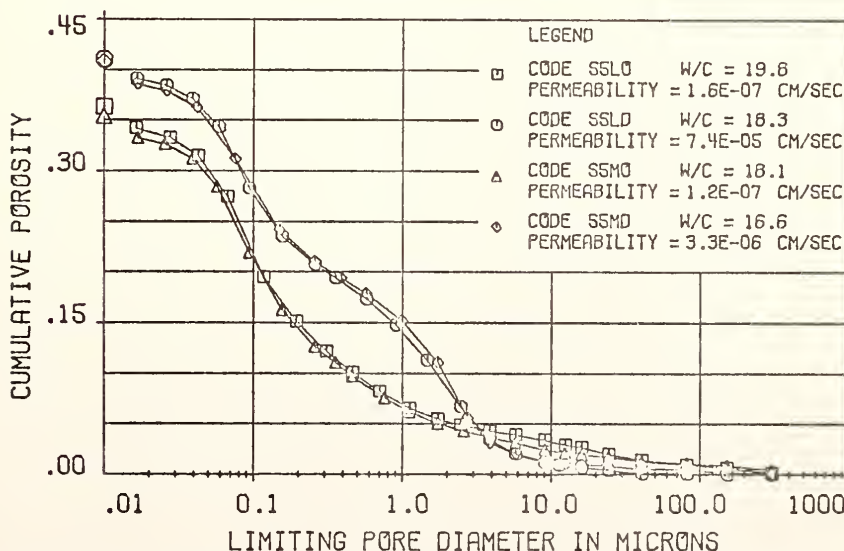
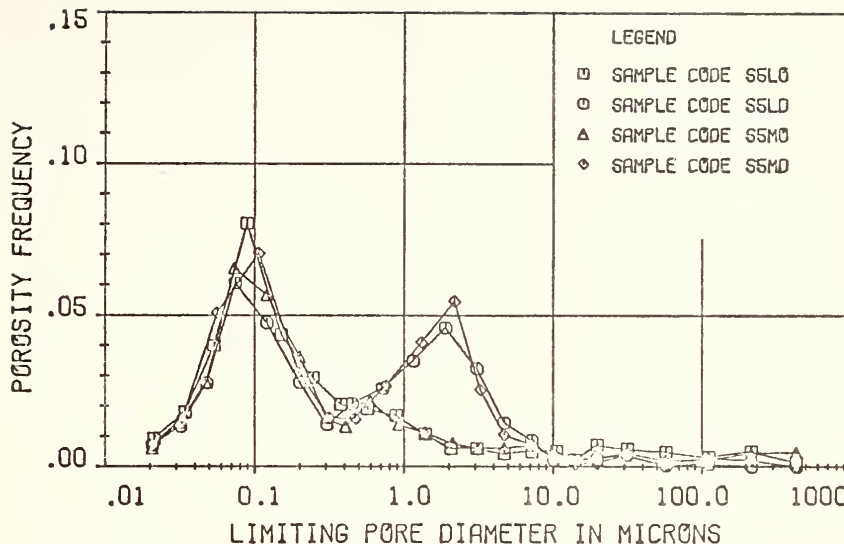


FIGURE 29 PORE SIZE DISTRIBUTION CURVES FOR 50% SILT - 50% KAOLIN COMPACTED AT OPTIMUM AND DRY OF OPTIMUM WATER CONTENTS FOR TWO EFFORTS

A contradiction between the permeabilities and pore size distributions of the two dry side samples, S5LD and S5MD, is shown on Figure 29. The two samples appear to have nearly identical pore size distributions; however, the permeability of S5LD is an order of magnitude greater than that of S5MD. The cause of the discrepancy is unknown. However, sample S5LD was the only sample which was too fragile to trim for wax displacement measurements; it literally crumbled apart when it was extruded from the permeameter mold. The low compactive effort and low initial degree of saturation resulted in a sample with an extremely small soaked strength. This made the task of trimming pore size specimens rather difficult. Because of these factors, it is believed that the true pore size distribution of sample S5LD was underestimated.

Figure 30 is a particle size frequency plot of the three soil types. The frequency was determined by the same methods used to calculate the differential pore size curves. Logarithmically equal particle size intervals were taken from the cumulative grain size distributions (Figure 3). The specific gravity of solids was assumed to be constant, which introduced a slight error in the relative frequencies of the clay and silt fractions. However, the error was not felt to be significant.

Figures 31 and 32 contrast the pore size distributions of the three soil types all compacted at medium effort and optimum and dry of optimum water contents, respectively. Comparing the particle size and pore size volumetric frequency plots it is evident that both are bimodal; although, the complete distribution of the clay size

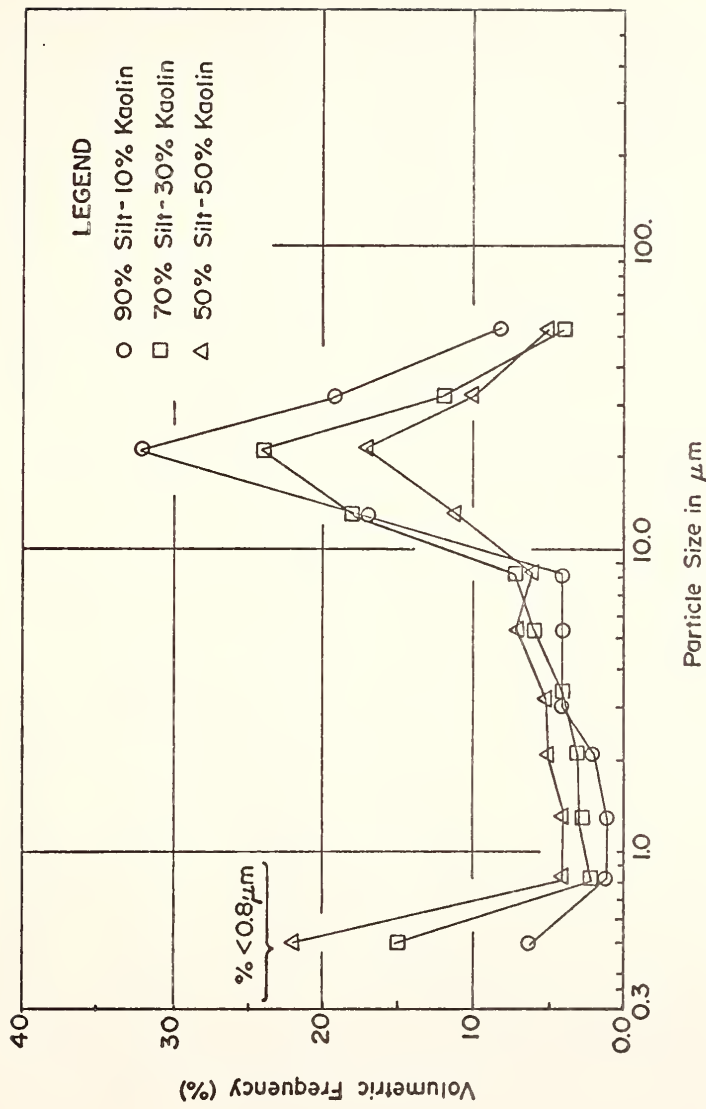


FIGURE 30 PARTICLE SIZE FREQUENCY PLOT OF THE SOILS TESTED

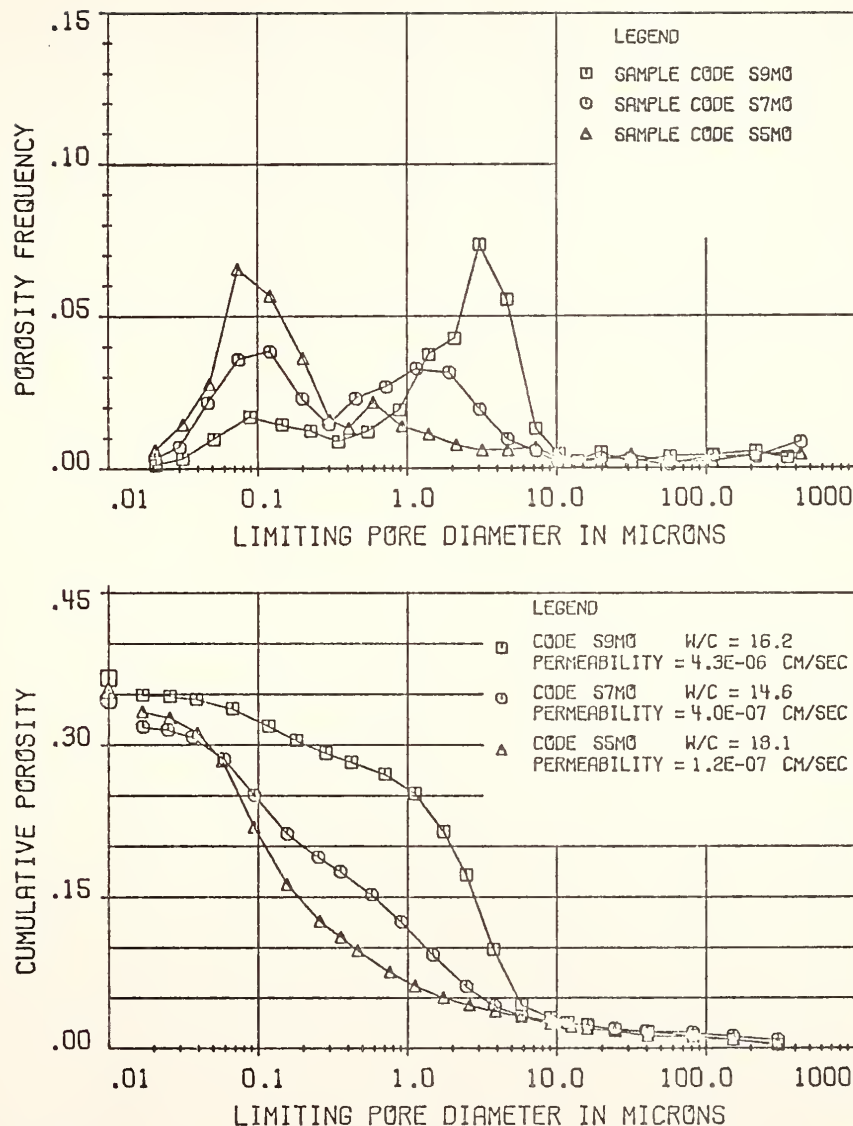


FIGURE 31 PORE SIZE DISTRIBUTION CURVES FOR THREE SOIL TYPES
COMPACTED AT MEDIUM EFFORT AND OPTIMUM WATER
CONTENT

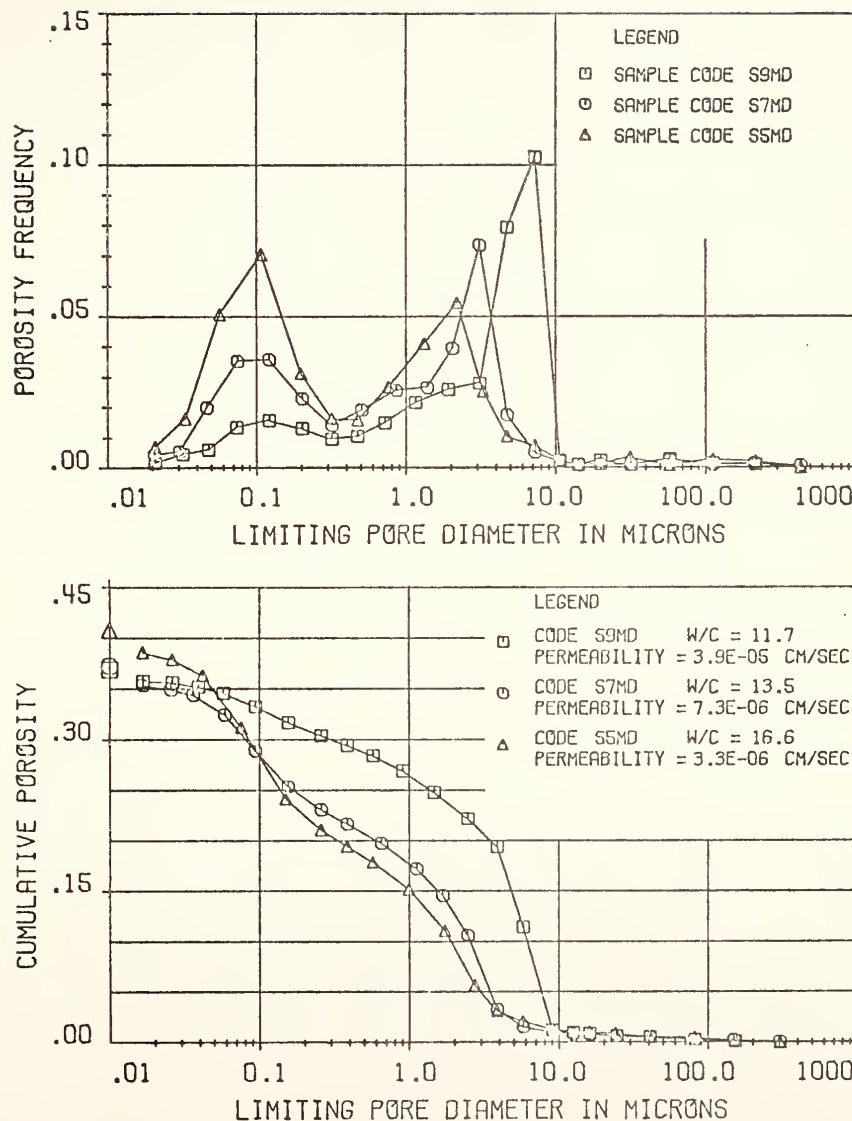


FIGURE 32 PORE SIZE DISTRIBUTION CURVES FOR THREE SOIL TYPES COMPACTED AT MEDIUM EFFORT AND DRY OF OPTIMUM WATER CONTENT

fraction was not obtained. The large pore mode of the soils increases with increasing silt content, while the small pore mode remains at 0.1 μm , but increases in frequency with increasing clay content. The larger pores are probably inter-silt and inter-aggregate pores, and the smaller pores are intra-aggregate pores.

Comparing the permeability values and pore size distributions of the three soils shown on Figures 31 and 32, the permeability decreases with a decrease in the large pore mode.

For the soils tested the position and frequency of the large pore mode appears to be the best indicator of changes in soil fabric caused by varying water content and compactive effort for a given soil type. The distribution of the smaller pores remained relatively fixed for each of the soil types.

Of the three soil types, only the 50% silt - 50% kaolin behaved in accordance with the deformable aggregate model of clay fabric proposed by Barden and Sides (1970) and Hodek (1972). For water contents at or greater than optimum very few large pores remained and no significant large pore mode was evident.

The other two soil types were strongly influenced by the large fraction of silt present. A significant volume of large pores always remained, regardless of the compactive effort or water contents used.

Based on the rather limited number of soils used in this study it is hypothesized that the shape of the differential pore size distribution in the small pore region ($< 0.02 \mu\text{m}$) may serve as an identification or "signature" of a given soil type. The value of the small pore mode is no doubt related to the size of clay particles present,

while the frequency is related to the amount of clay in the soil.

Factors such as plasticity, swelling potential and clay mineral content are probably related to the characteristics of the small pore mode.

Further research would be required to test this hypothesis.

4-6 Relation Between Permeability and Pore Size Distribution

From the qualitative observations discussed in the previous section it is evident that the permeability is related to the distribution of pores about the large pore mode. The objective of this section is to quantify this relationship.

Previous investigators including Taylor (1948) and Lambe and Whitman (1969) have shown that the log of permeability is linearly related to the void ratio of some soils. From Figure 33 it is apparent that the relationship is not valid for compacted fine-grained soils. This agrees with the fact that the void ratio had little or no relationship to the large pore mode and its frequency. This Figure clearly shows that gross volumetric parameters cannot account for changes in permeability of compacted soils; consequently, any permeability predicting equations based on these volumetric parameters is not suitable for compacted soils.

Section 1-1.3 examined three models which relate permeability to pore size distribution parameters. These are summarized in Table 1. The specific permeability K can be expressed in terms of each of these three parameters as:

$$K = C_s \cdot PSP \quad (4-2)$$

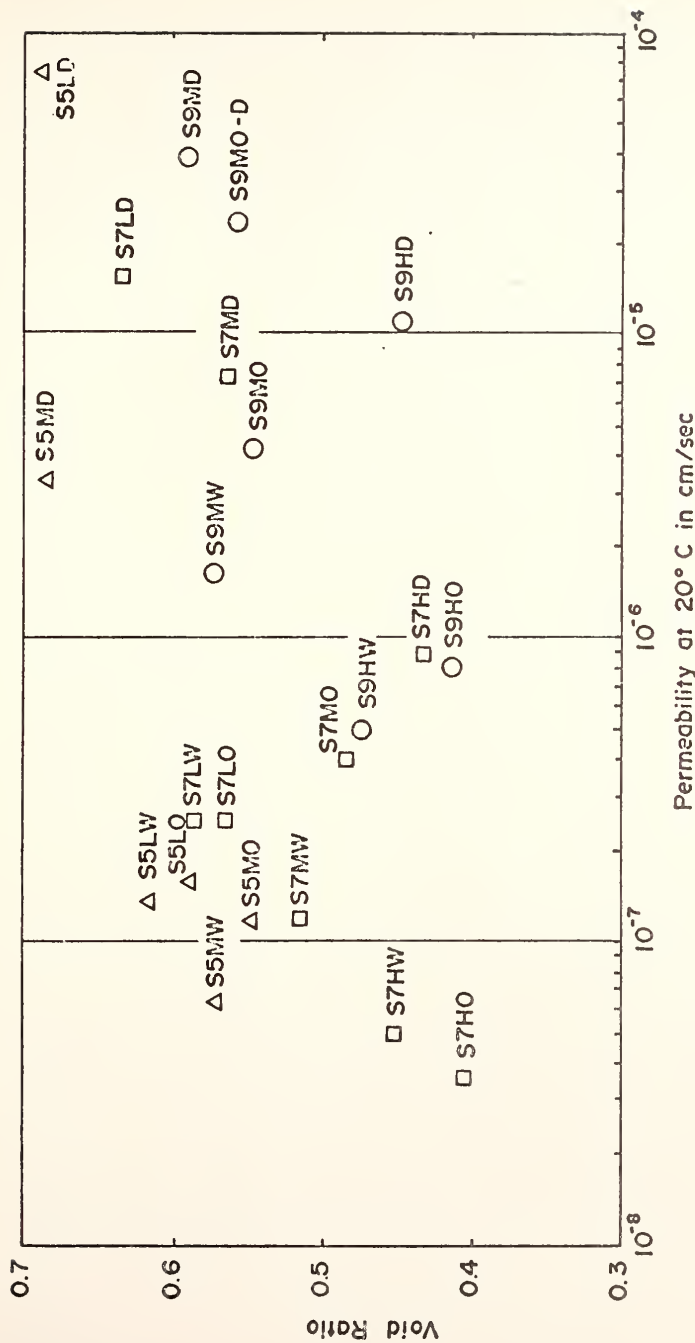


FIGURE 33 PERMEABILITY VS VOID RATIO

where PSP is one of the three pore size parameters, $E(d^2)_n$, \hat{d}^2 or $R_H^2 n$, and C_s is a shape factor which differs for each of the models.

Equation (4-2) can be written in terms of the permeability k , since $k = K \frac{Y}{\mu}$, with only a change in the value of the shape factor, as follows:

$$k = C_s \cdot PSP \quad (4-3)$$

The PSP values were calculated for each of the samples from the pore size distribution data according to the formulae shown on Table 1 and the method discussed in Section 1-2.4. These values are shown on Table 6 along with the permeability of each of the soils. An important assumption had to be made to calculate the Capillary model and Marshall model parameters. As shown on Table 1, the pore size parameters for these two models are very sensitive to the larger pore diameters. In order to obtain a relationship between permeability and the parameters it was necessary to consider only those pores less than 10 μm in size. The selection of 10 μm was arbitrary. However, as shown by the differential pore size distributions, none of the soils experienced significant or continuous intrusion for pores greater than 10 μm .

The calculation of the Hydraulic Radius pore size parameter also required an assumption. As shown on Table 1, the Hydraulic Radius parameter is most influenced by the smaller pores. The mercury intrusion equipment used, left about 1 to 5% of the pore volume unintruded. This unintruded pore volume was assigned a diameter of 0.01 μm for calculation purposes.

TABLE 6 PERMEABILITY AND EQUIVALENT PORE SIZE PARAMETERS

Sample Code	Permeability k at 20° C ($\times 10^{-6}$ cm/sec)	Hydraulic Radius Model $R_H^2 \cdot n$ ($\times 10^{-4}$ μm^2)	Capillary Model $E(d^2) \cdot n$ for $d < 10 \mu\text{m}$ (μm^2)	Marshall Model $d < 10 \mu\text{m}$ \hat{d}^2 (μm^2)
S9MO	4.3	4.3	2.8	0.51
S9MO-D	23	7.8	5.5	1.02
S9MD	39	8.1	7.5	1.39
S9MW	1.7	4.9	2.4	0.39
S9HO	0.81	3.8	1.39	0.15
S9HD	11	4.7	3.8	0.73
S9HW	0.50	2.4	2.0	0.29
S7LO	0.25	1.78	0.86	0.090
S7LD	16	3.4	2.1	0.27
S7LW	0.25	2.7	1.13	0.14
S7MO	0.40	1.03	0.85	0.084
S7MD	7.3	2.1	1.58	0.19
S7MW	0.12	0.83	0.83	0.078
S7HO	0.035	0.81	0.39	0.020
S7HD	0.89	1.23	1.00	0.11
S7HW	0.049	1.05	0.61	0.032
S5LO	0.16	1.16	0.48	0.041
S5LD	74	1.89	1.30	0.11
S5LW	0.14	1.42	0.61	0.063
S5MO	0.12	1.04	0.62	0.043
S5MD	3.3	1.74	1.23	0.12
S5MW	0.063	0.98	0.56	0.048

The values of the pore size parameters of the Capillary, Marshall and Hydraulic Radius models are plotted versus the permeability on Figures 34, 35 and 36, respectively. All axes are on a logarithmic scale. A linear trend in the data is apparent from these figures. The sample with the largest permeability, which is farthest removed from the linear trend on all these Figures, is sample S5LD. As discussed previously, the pore size distribution measurement of this sample is believed to be in error.

Simple linear regression by the method of least squares was used to estimate the relationship between the permeability and the pore size parameters. Details of this method are presented in Wapole and Myers (1972). The log of the permeability was taken as the dependent variable and the log of the pore size parameter was taken as the independent variable. The linear relation is expressed as:

$$\log k = b \log PSP + a \quad (4-4)$$

where b and a are the linear regression parameters. Equation (4-4) may be simplified by raising it to the power of 10, resulting in:

$$k = 10^a PSP^b \quad (4-5)$$

Note that equation (4-3), determined from the permeability-pore size models, is a form of equation (4-5) with $b = 1$ and $C_s = 10^a$. Thus, equation (4-5) may be expressed as:

$$k = C_s PSP^b \quad (4-6)$$

where $C_s = 10^a$.

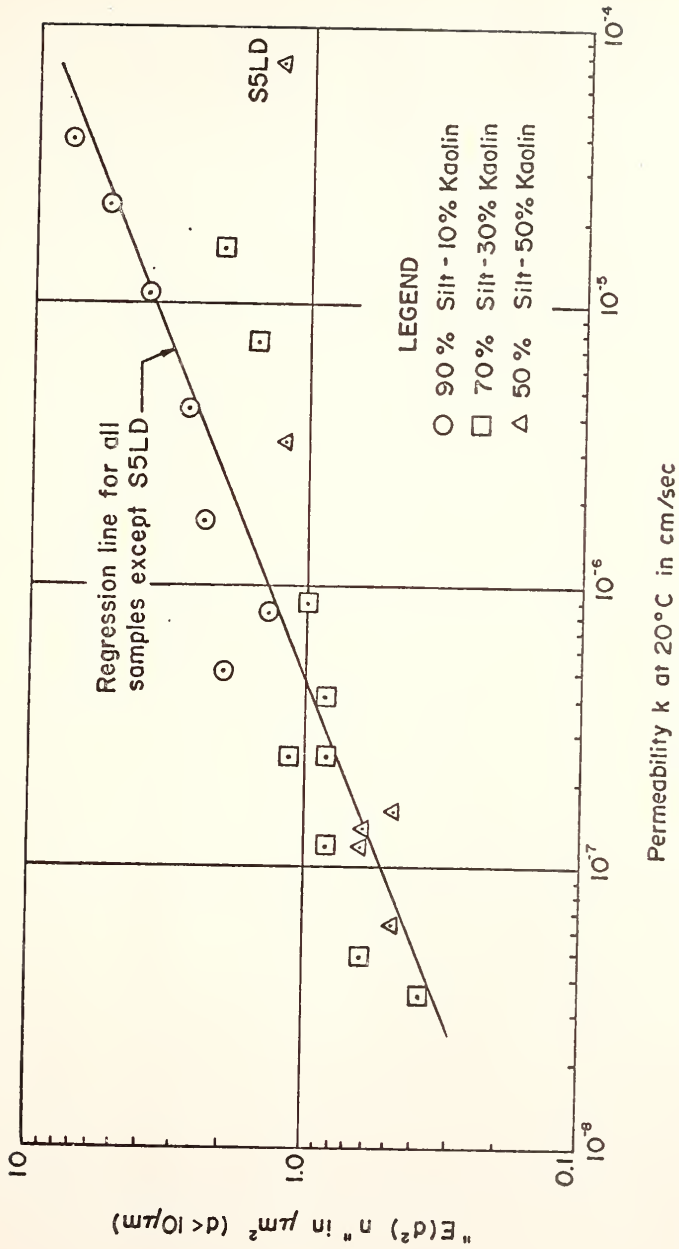
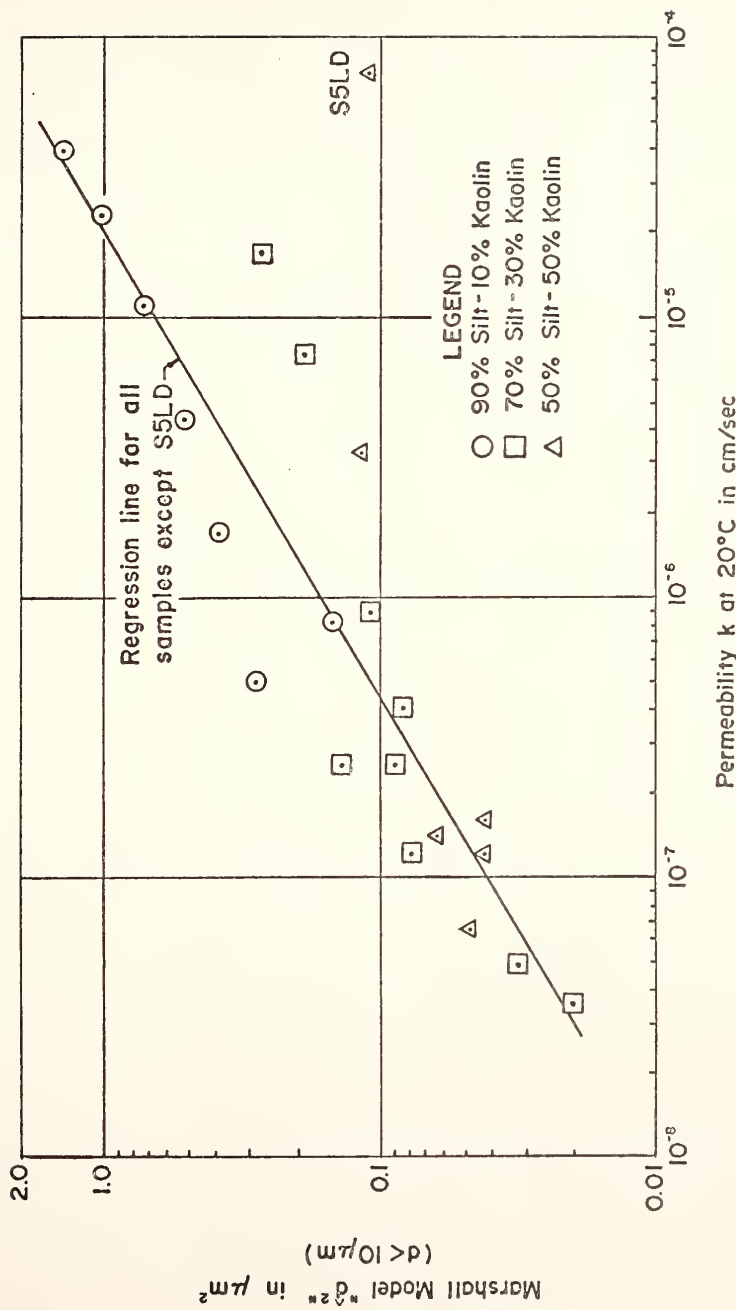


FIGURE 34 PERMEABILITY VS. CAPILLARY MODEL EQUIVALENT PORE SIZE PARAMETER, $E(d_2)n$

FIGURE 35 PERMEABILITY VS MARSHALL EQUIVALENT PORE SIZE PARAMETER, \hat{d}^2

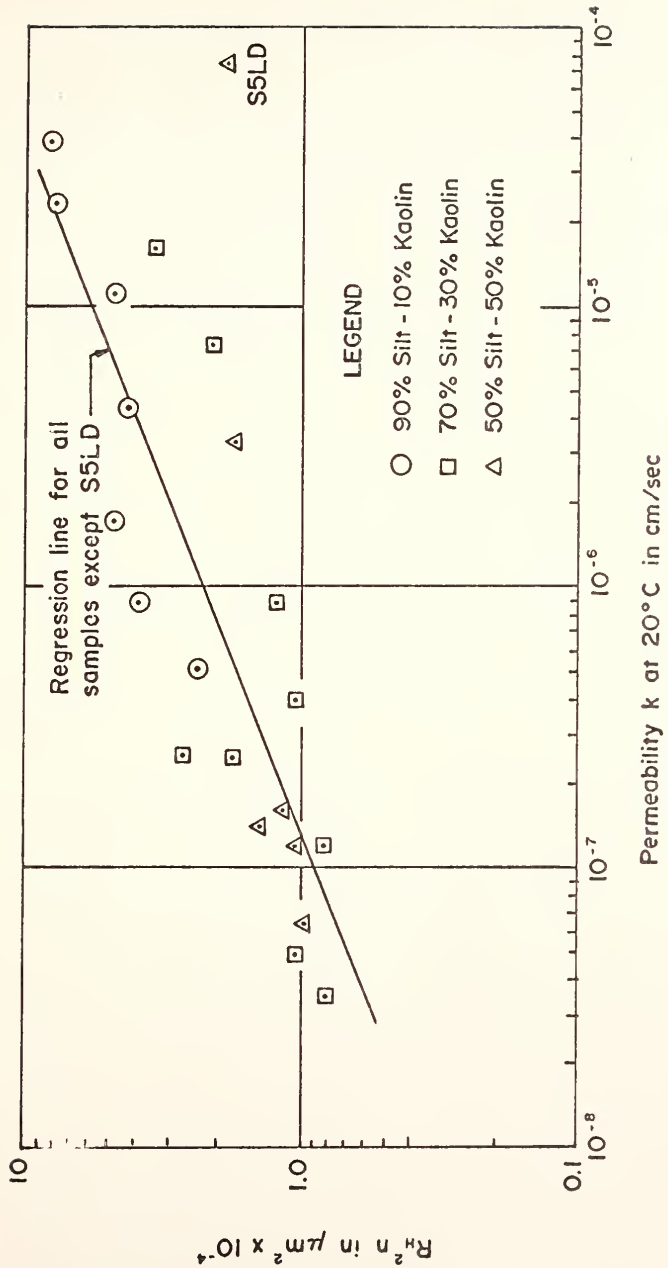


FIGURE 36 PERMEABILITY VS EQUIVALENT HYDRAULIC RADIUS PORE SIZE PARAMETER,
 $R_h^2 n$

The C_s and b parameters and the coefficient of determination " r^2 " were calculated for each and all of the soil types tested. Table 7 presents the linear regression equations and r^2 values for each of the three pore size parameters.

The accuracy of the regression equations can be judged by the b and r^2 parameters. Comparing equations (4-3) and (4-6), it is evident that the b parameter reflects the sensitivity of the permeability to the pore size parameter PSP. The closer b is to 1, the more sensitive the parameter is to the permeability. The coefficient of determination, r^2 , is a measure of the degree of association between the log of the permeability and the log of the pore size parameter for a given equation. The closer r^2 is to 1.0 the higher the degree of association between the two terms. Consequently, the closer b is to 1, and the higher the r^2 value, the closer the prediction equation fits a given theoretical model.

Table 7 indicates that for the Capillary and Marshall models, the b parameter increases and the r^2 value decreases with increasing clay content. The two pore size parameters, $E(d^2)_n$ and \hat{d}^2 , are most affected by the larger pores. It is believed that this decrease in sensitivity of the pore size parameters with increasing clay content is a result of the $d < 10 \mu\text{m}$ cut-off diameter used to calculate the parameters. The soils with the higher clay content did not have a significant intrusion for pore diameters greater than about $6 \mu\text{m}$; therefore, the pore size parameters were not as sensitive to changes in permeability. The 90% silt-10% kaolin samples display an excellent linear trend between the Capillary and Marshall parameters and the permeability as shown in Figures 34 and 35 and by the regression equations on Table 7. None of

TABLE 7 LINEAR REGRESSION EQUATIONS FOR PERMEABILITY AND PORE SIZE PARAMETERS (PSP)

<u>Capillary Model</u>	$PSP = E(d^2)n$ in μm^2 k in $\text{cm/sec} \times 10^{-6}$	<u>r^2</u>
90% silt - 10% kaolin	$k = 0.194 (PSP)^{2.73}$	0.91
70% silt - 30% kaolin	$k = 0.567 (PSP)^{3.945}$	0.87
50% silt - 50% kaolin	$k = 3.487 (PSP)^{5.88}$	0.83
all samples	$k = 0.532 (PSP)^{2.42}$	0.69
all except S5LD	$k = 0.434 (PSP)^{2.42}$	0.83
<u>Marshall Model</u>	$PSP = \hat{d}^2$ in μm^2 k in $\text{cm/sec} \times 10^{-6}$	
90% silt - 10% kaolin	$k = 17.41 (PSP)^{2.06}$	0.88
70% silt - 30% kaolin	$k = 112.4 (PSP)^{2.28}$	0.80
50% silt - 50% kaolin	$k = 4.6 \times 10^5 (PSP)^{4.95}$	0.73
all samples	$k = 23.60 (PSP)^{1.62}$	0.64
all except S5LD	$k = 20.57 (PSP)^{1.67}$	0.82
<u>Hydraulic Radius Model</u>	$PSP = R_H^2 n$ in $\mu\text{m}^2 \times 10^{-4}$ k in $\text{cm/sec} \times 10^{-6}$	
90% silt - 10% kaolin	$k = 0.015 (PSP)^{3.60}$	0.82
70% silt - 30% kaolin	$k = 0.141 (PSP)^{2.95}$	0.55
50% silt - 50% kaolin	$k = 0.046 (PSP)^{8.91}$	0.79
all samples	$k = 0.166 (PSP)^{2.43}$	0.57
all except S5LD	$k = 0.129 (PSP)^{2.47}$	0.71

the pore size parameters were as sensitive to permeability as predicted by the theoretical equations, where $b = 1$.

The regression equations calculated from all of the samples except S5LD for the Capillary and Marshall models are shown on Figures 34 and 35, respectively. The b parameter and r^2 value indicate that the equation is fairly accurate; however, several systematic errors are shown by the Figure. At the higher permeabilities the 90% silt - 10% kaolin soils generally fall along or above the regression line, and the soils with higher clay content generally fall below the regression line.

The Hydraulic Radius model is not as useful as the previous two models discussed. Each of the soil types result in a regression equation with either a very high b parameter or a low r^2 value. Figure 36 shows the regression line calculated from all the samples except S5LD. The b parameter and r^2 value of this equation (from Table 7) are completely deceiving. None of the soil types fit the regression line individually, but when considered en masse the relation appears adequate. The Hydraulic Radius model is not believed to produce an accurate pore size parameter. As mentioned previously, the parameter is mostly influenced by the small pore mode, which is not directly related to the large pore mode.

As discussed previously, the permeability is strongly influenced by the distribution of pores about the large pore mode, which occurred between 10 and 1 μm for the three soils tested. It is not a coincidence that the Marshall and Capillary pore size parameters correlated well with the permeability only when pore diameters less than 10 μm were considered. This indicates that the permeability is controlled by the

larger pores that occur in sufficient volume or frequency. The frequency is probably not given enough weight in the models considered. The Marshall model is a step in the right direction, however. As shown in Section 1-1.3, the Marshall model is based on random junctions of pores between two cross-sections of a porous medium; consequently, the frequency term appears as a squared term in the pore size parameter. By expanding this model and considering "m" cross-sections in sequence, the frequency term would be given greater weight and the permeability model may be improved. Further research would be required to confirm this.

In summary, a relationship between the pore size distribution and the permeability is clearly shown on Figures 34, 35 and 36. The Marshall or Capillary model pore size parameters may provide an excellent empirical predictive equation for a given soil type, if a proper cut-off diameter is selected for the calculations of the parameters. More sophisticated theoretical permeability models, accounting for the complexities of the pore network, are necessary to improve the prediction of permeability from pore size distribution.

5 - CONCLUSIONS AND RECOMMENDATIONS

5-1 Conclusions

1. A method is described for approximating and presenting the differential pore size distribution on a log diameter scale which is relatively free from distortions. The differential plot provides a useful complement to the cumulative pore size distribution curve by showing:
 - a. the type of distribution,
 - b. the modal or most frequent pore diameters,
 - c. any gaps or irregularities in the data,
 - d. simply, how different distributions compare.
2. Freeze drying was an effective method of drying the soils used. The maximum volume change caused by drying was 3%.
3. Critical region drying produced a chemical alteration of the soils tested. Dolomite, calcite and kaolinite in the soil reacted to form a feldspar, resulting in void ratio increases of 35 to 40%.
4. The pore size distributions of the soils tested were found to be bimodal on a log diameter scale. A large pore mode occurred between 10 and 1.0 μm , and a small pore mode occurred at 0.1 μm .
5. Changes in soil fabric caused by varying water content and compaction effort were generally at the expense of the large pore mode.

6. The shape of the differential pore size distribution about the small pore mode was not affected by the compaction variables for a given soil type.
7. The relation between the compaction variables and the permeability found in this study agree with the trends found by Lambe (1954), Bjerrum and Huder (1957), and Mitchell et al. (1965).
8. The permeability generally varied with the magnitude and frequency of the large pore mode. Decreasing the large pore mode or its frequency resulted in a decrease of the permeability.
9. Three theoretical models which relate pore size distribution to permeability were examined. Although, the models were not completely successful in predicting permeability, the pore size parameters from two of the models, with several modifications, did reflect the dependence of permeability on pore size distribution. These pore size parameters were successfully used to determine empirical permeability predicting equations for any one of the soils tested.
The general form of the predictive equations is:

$$k = C_s PSP^b$$

where k is the permeability,
 PSP is the pore size parameter calculated from the pore size distribution, and
 C_s and b are regression constants.

10. Conventional permeability predictive equations based on volumetric and grain size parameters do not accurately reflect the nature of the pore system of compacted fine-grained soils, and therefore, are unsuitable for estimating permeability. The empirical predictive equations determined in this study, (1) demonstrate the dependence

of permeability on pore size distribution and, (2) are reflective of changes in soil structure caused by altering the compaction variables.

5-2 Recommendations for Future Research

This study demonstrates: 1) the dependence of permeability on pore size distribution, and, 2) the utility of pore size distribution measurements to infer soil fabric. In light of the work reported, the following topics should be considered for further research:

- 1) Improvement of theoretical models for permeability to better account for the complex nature of the pore system and the pore size distribution.
- 2) Particle migration, piping, and filter criteria based on pore size distribution parameters. Improved pore size measurement techniques would be required for coarse soils.
- 3) Non-Darcy flow and the physio-chemical factors which affect permeability.
- 4) The influence of pore size distribution on other important engineering properties such as strength and compressibility.
- 5) The pore size distribution of field compacted versus laboratory compacted samples to assess:
 - a. the replication of the field soil structure in the laboratory,
 - b. the variability of the field compacted soil structure, and,
 - c. current field compaction specifications.
- 6) The use of pore size distribution as a routine classification test for undisturbed soils. Conventional classification tests of remolded samples are of little value in identifying structurally sensitive soils.

- 7) The relation between the small pore size range (or parameters calculated therefrom), soil mineralogy, and physio-chemical properties such as plasticity and swelling.

BIBLIOGRAPHY

BIBLIOGRAPHY

1. Ahmed, S. (1971), "Pore Size and Its Effects on the Behavior of a Compacted Clay", MSCE Thesis, Purdue University, West Lafayette, Indiana, June, 200 pp.
2. Ahmed, S., Lovell, C. W., Jr. and Diamond, S. (1974), "Pore Sizes and Strength of Compacted Clay", Journal of the Geotechnical Division, ASCE, Vol. 100, No. GT4, April, pp. 407-425.
3. American Association of State Highway Officials (1970), "Standard Method of Test for the Moisture Relations of Soils Using a 5.5 lb. Rammer and a 12 inch Drop," Standard Specifications for Highway Materials and Methods of Sampling and Testing, Part II, AASHO Designation T99-70, pp. 301-307.
4. Aughenbaugh, N. B., Johnson, R. B. and Yoder, E. J. (1963), Degradation of Base Course Aggregates During Compaction, School of Civil Engineering, Purdue University, West Lafayette, Indiana, May, 191 pp.
5. Badger, W. W. and Lohnes, R. A. (1973), "Pore Structure of Friable Loess", Soils: Loess, Suction and Frost Action, Highway Research Record No. 429, pp. 14-23.
6. Bailey, M. J. (1976), "Shale Degradation and Other Parameters Related to the Construction of Compacted Embankments", MSCE Thesis, Purdue University, West Lafayette, Indiana, August, 230 pp.
7. Barden, L. and Sides, G. R. (1970), "Engineering Behavior and Structure of Compacted Clay", Journal of the Soil Mechanics and Foundations Division, ASCE, Vol. 96, SM4, pp. 1171-1200.
8. Bear, J., (1972), Dynamics of Fluids in Porous Media, American Elsevier, New York, 764 pp.
9. Bhasin, R. N. (1975), "Pore Size Distribution of Compacted Soils After Critical Region Drying", Ph.D. Thesis, Purdue University, West Lafayette, Indiana, May, 222 pp.
10. Carman, P. C. (1956), Flow of Gas Through Porous Media, Academic Press, New York, 182 pp.
11. Cedergren, H. R. (1967), Seepage Drainage and Flow Nets, J. Wiley & Sons, New York, pp. 47-93.

12. Chemical Rubber Company (CRC), 1970-71, Handbook of Chemistry and Physics, 51st Edition, p. F-36.
13. Childs, E. C. and Collis-George, N. (1950), "The Permeability of Porous Materials", Proceedings, Royal Society of London, Vol. A201, pp. 392-405.
14. Drake, L. C. and Ritter, H. L. (1945), "Macropore-Size Distributions in Some Typical Porous Substances", Industrial and Engineering Chemistry, Analytical Edition, Vol. 17, No. 12, December, pp. 787-791.
15. Gaudette, N. G. Jr. (1960), "Application of the Kneading Compactor and Hveem Stabilometer to Bimimetic Concrete Design in Indiana", MSCE Thesis, Purdue University, West Lafayette, Indiana, December, 238 pp.
16. Gillott, J. E. (1968), Clay in Engineering Geology, Elsevier, New York, pp. 296.
17. Gupta, R. P. and Swartzendruber, D. (1962), "Flow-Associated Reduction in the Hydraulic Conductivity of Quartz Sand", Soil Science of America Proceedings, Vol. 26, No. 1, pp. 6-10.
18. Hansbo, S. (1960), "Consolidation of Clay with Special Reference to Influence of Vertical Sand Drains", Swedish Geotechnical Institute Proceedings, No. 18, Stockholm, 160 pp.
19. Harr, M. E. (1962), Groundwater and Seepage, McGraw-Hill, New York, 315 pp.
20. Harr, M. E. (1977), Mechanics of Particulate Media, McGraw-Hill Co., New York, 543 pp.
21. Hazen, A. (1911), "Discussion on 'Dams on Sand Foundations'", Transactions of American Society of Civil Engineers, Vol. 73, pp. 199.
22. Herdan, G. (1953), Small Particle Statistics, Elsevier Publishing Company, Amsterdam, 520 pp.
23. Hodek, R. J. (1972), "Mechanism for the Compaction and Response of Kaolinite", Ph.D. Thesis, Purdue University, West Lafayette, Indiana, December, 269 pp.
24. Kemball, C. (1946), "On the Surface Tension of Mercury", Transactions, Faraday Society, Vol. 42, pp. 526-537.
25. Klock, G. O., Boersma, L. and DeBarker, L. W. (1969), "Pore Size Distributions as Measured by the Mercury Intrusion Method and Their Use in Predicting Permeability", Proceedings, Soil Science, Vol. 33, No. 1, pp. 12-15.
26. Lambe, T. W. (1954), "The Permeability of Fine-Grained Soils," Permeability of Soils, ASTM STP 163, American Society of Testing Materials, pp. 56-67.

27. Lambe, T. W. (1958), "The Structure of Compacted Clay", Journal of the Soil Mechanics and Foundations Division, ASCE, Vol. 84, SM2, pp. 1654, 1-34.
28. Lambe, T. W. (1958), "The Engineering Behavior of Compacted Clay", Journal of the Soil Mechanics and Foundations Division, ASCE, Vol. 84, SM2, pp. 1655 1-35.
29. Lambe, T. W. and Whitman, R. V. (1969), Soil Mechanics, John Wiley and Sons, Inc., New York, 553 pp.
30. Langfelder, L. J., Chen, C. F. and Justice, J. A. (1968), "Air Permeability of Compacted Cohesive Soils", Journal of the Soil Mechanics and Foundations Division, ASCE, Vol. 94, SM4, pp. 981-1001.
31. Leonards, G. A. (1962), "Engineering Properties of Soils", Foundation Engineering, McGraw-Hill, New York, Chapter 2, pp. 107-139.
32. Lohnes, R. A., Tuncer, E. R. and Demirel, T. (1976), "Pore Structure of Selected Hawaiian Soils", Transportation Research Record No. G12, pp. 76-79.
33. Lowe, J. and Johnson, T. C. (1960), "Use of Back Pressure to Increase Degree of Saturation of Triaxial Test Specimens", Research Conference on Shear Strength of Cohesive Soils, ASCE, pp. 819-836.
34. Marshall, T. J. (1958), "A Relation Between Permeability and Size Distribution of Pores", Journal of Soil Science, Vol. 9, No. 1, pp. 1-8.
35. Mesri, G. and Olson, R. E. (1971), "Mechanisms Controlling the Permeability of Clays", Clays and Clay Minerals, Vol. 19, pp. 151-158.
36. Michaels, A. S. and Lin, C. S. (1954), "Permeability of Kaolinite", Industrial and Engineering Chemistry, Vol. 46, No. 6, pp. 1239-1246.
37. Miller, I. and Freund, J. E. (1977), Probability and Statistics for Engineers, 2nd Edition, Prentice-Hall, New Jersey, 529 pp.
38. Milligan, V. (1975), "Field Measurement of Permeability in Soil and Rock", In Situ Measurement of Soil Properties, ASCE, Vol. II, pp. 3-36.
39. Mishu, L. P. (1963), "Collapse in One Dimensional Compression of Compacted Clay Upon Wetting", MSCE Thesis, Purdue University, West Lafayette, Indiana, August, 105 pp.
40. Mitchell, J. K. (1956), "The Fabric of Natural Clays and Its Relation to Engineering Properties", Proceedings, Highway Research Board, Vol. 35, pp. 693-713.

41. Mitchell, J. K., Hooper, D. R., Campanella, R. G. (1965), "Permeability of Compacted Clay", Journal of the Soil Mechanics and Foundation Division, ASCE, Vol. 91, SM4, pp. 41-65.
42. Mitchell, J. K. (1976), Fundamentals of Soil Behavior, John Wiley & Sons, New York, 422 pp.
43. Olsen, H. W. (1962), "Hydraulic Flow Through Saturated Clays", Clays and Clay Minerals, 11, pp. 131-161.
44. Olsen, H. W. (1965), "Deviations from Darcy's Law in Saturated Clays", Proceedings, Soil Science of America, Vol. 29, pp. 135-140.
45. Olsen, H. W. (1966), "Darcy's Law in Saturated Kaolinite", Water Resources Res., Vol. 2, pp. 287-295.
46. Olson, R. E. (1963), "Effective Stress Theory of Soil Compaction", Journal of the Soil Mechanics and Foundations Division, ASCE, Vol. 89, SM2, pp. 27-45.
47. Orr, C., Jr. (1970), "Application of Mercury Penetration to Materials Analysis", Powder Technology, Vol. 3, No. 3, pp. 117-123.
48. Perloff, W. H. and Baron, W. (1976), Soil Mechanics: Principles and Applications, Ronald Press Co., New York, 745 pp.
49. Purcell, W. R. (1949), "Capillary Pressures-Their Measurement Using Mercury and The Calculation of Permeability Therefrom", Petroleum Transactions, AIME, Vol. 186, pp. 39-48.
50. Reed, M. A. (1977), "Frost Heaving Rate of Silty Soils as a Function of Pore Size Distribution," MSCE Thesis, Purdue University, West Lafayette, Indiana, August, 116 pp.
51. Ritter, H. L. and Drake, L. C. (1945), "Pore Size Distribution in Porous Materials", Industrial and Engineering Chemistry, Analytical Edition, American Chemical Society, Vol. 17, pp. 782-786.
52. Rootare, H. M. and Prenzlow, C. F. (1967), "Surface Areas from Mercury Porosimeter Measurements", Journal of Physical Chemistry, Vol. 71, No. 8, July, pp. 2733-2736.
53. Rootare, H. M. (1968), "A Short Literature Review of Mercury Porosimetry as a Method of Measuring Pore Size Distributions in Porous Materials, and a Discussion of Possible Sources of Errors in this Method", Aminco Lab News, Vol. 24, No. 3, pp. 4A-4H.
54. Rowe, P. W. (1972), "The Relevance of Soil Fabric to Site Investigation Practice", Gotechnique, Vol. 22, No. 2, pp. 195-300.
55. Russell, D. A. and Swartzendruber, D. (1971), "Flux-Gradient Relationships for Saturated Flow of Water Through Mixtures of Sand, Silt and Clay", Soil Science Society of America Proceedings, Vol. 35, No. 1, pp. 21-26.

56. Scheidegger, A. E. (1974), The Physics of Flow Through Porous Media, 3rd Edition, University of Toronto Press, 351 pp. (2nd Edition, 1960), (First Edition, 1957).
57. Schmid, W. E. (1957), "The Permeability of Soils and the Concept of a Stationary Boundary Layer", Proceedings, American Society for Testing Materials, Vol. 57, pp. 1195-1218.
58. Seed, H. B. and Chan, A. M. (1959), "Structure and Strength Characteristics of Compacted Clays", Journal of the Soil Mechanics and Foundations Division, ASCE, Vol. 85, SM5, pp. 87-128.
59. Sherard, J. L., Woodward, R. J., Giziensky, S. F., and Clevenger, W. A. (1963), Earth and Earth-Rock Dams, John Wiley and Sons, Inc., New York, 725 pp.
60. Silveira, A. (1965), "An Analysis of the Problem of Washing Through in Protective Filters", Proceedings of the 6th International Conference on Soil Mechanics and Foundation Engineering, Montreal, Vol. II, pp. 551-555.
61. Smart, P. (1966), "Soil Structure", Ph.D. Thesis, Cambridge.
62. Sowers, G. B. and Sowers, G. F. (1970), Introductory Soil Mechanics and Foundations, Third Ed., MacMillan Company, New York, 556 pp.
63. Sridharan, A. (1968), "Some Studies on the Strength of Partly Saturated Clays", Ph.D. Thesis, Purdue University, West Lafayette, Indiana, 179 pp.
64. Sridharan, A., Altschaeffl, A. G. and Diamond, S. (1971), "Pore Size Distribution Studies", Journal of the Soil Mechanics and Foundation Division, ASCE, Vol. 97, SM5, pp. 771-787.
65. Swartzendruber, D. (1968), "The Application of Darcy's Law", Soil Science Society of America Proceedings, Vol. 32, No. 1, pp. 11-18.
66. Taylor, D. W. (1948), Fundamentals of Soil Mechanics, John Wiley and Sons, New York, 700 pp.
67. Tovey, N. K. (1970), "Electron Microscopy of Clays", Ph.D. Thesis, Cambridge.
68. Tovey, N. K. and Yan, W. K. (1973), "The Preparation of Soils and Other Geological Materials for the SEM", Proceedings of the International Symposium on Soil Structure, Gothenburg, Sweden, pp. 59-67.
69. U. S. Department of the Army (1970), Laboratory Soils Testing, Engineering Manual EM 1110-2-1906, pp. II-8 to II-11.

70. Wahls, H. E., Fisher, C. P. and Langfelder, L. J. (1966), The Compaction of Soil and Rock Materials for Highway Purposes, U. S. Dept. of Commerce, Bureau of Public Roads, FHWA-RD-73-8, 457 pp.
71. Walpole, R. E. and Myers, R. H. (1972), Probability and Statistics for Engineers and Scientists, MacMillan Publishing Co., New York, 506 pp.
72. Washburn, E. W. (1921), "Note on a Method of Determining the Distribution of Pore Sizes in a Porous Material", Proceedings, National Academy of Sciences, Vol. 7, pp. 115-116.
73. Winslow, D. N. (1969), "The Pore Size Distribution of Portland Cement", MSCE Thesis, Purdue University, West Lafayette, Indiana, January, 102 pp.
74. Winslow, D. N. and Diamond, S. (1970), "A Mercury Porosimetry Study of the Evolution of Porosity in Portland Cement", Journal of Materials, ASTM, Vol. 5, No. 3, pp. 564-585.
75. Yong, R. N. and Sheeran, D. E. (1973), "Fabric Unit Interaction and Soil Behavior", Proceedings, International Symposium on Soil Structure, Swedish Geotechnical Society, Gothenburg, pp. 176-183.
76. Yong, R. N. and Wankentin, B. P. (1975), Soil Properties and Behavior, Elsevier, New York, 449 pp.
77. Zimmie, T. F. and Almaleh, L. J. (1976), "Shrinkage of Soil Specimens During Preparation for Porosimetry Tests", Soil Specimen Preparation for Laboratory Testing, ASTM STP 599, pp. 202-215.

APPENDICES

APPENDIX A

Replicate Pore Size Distribution Curves

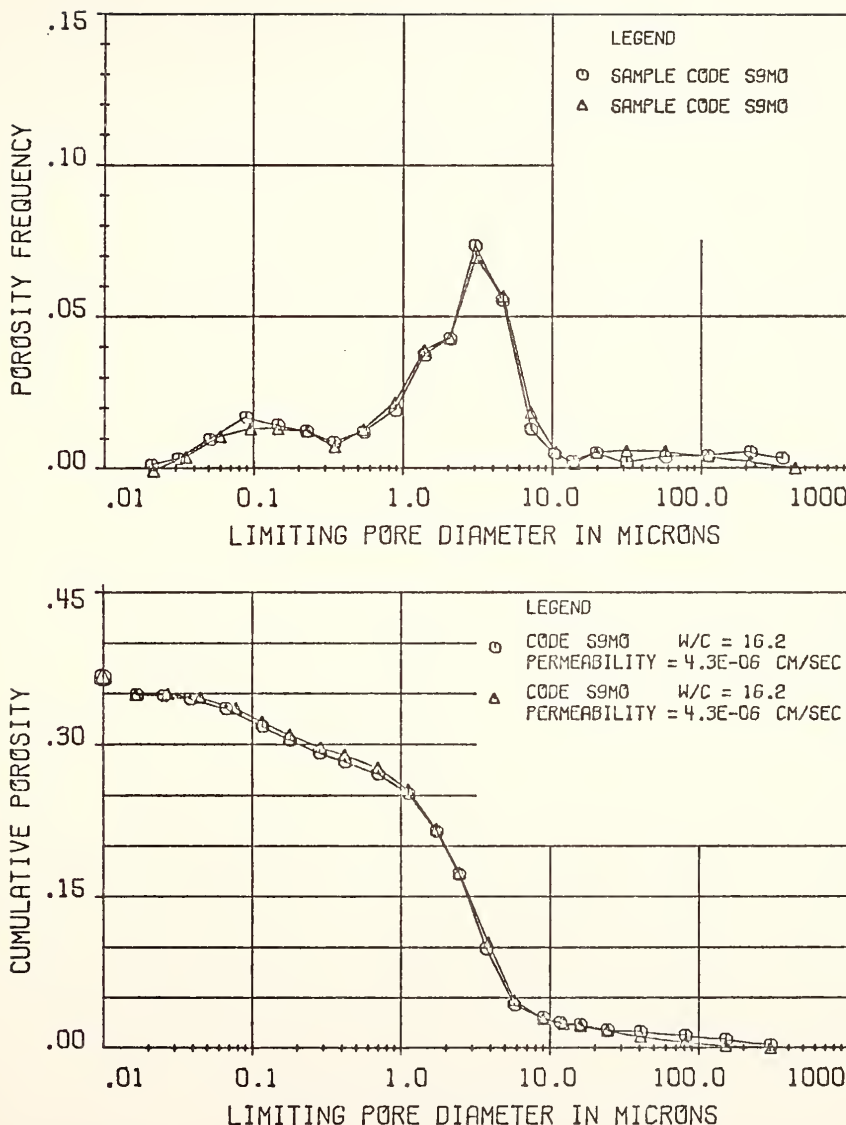


FIGURE 37 REPLICATE PORE SIZE DISTRIBUTION CURVES FOR SAMPLE S9MO

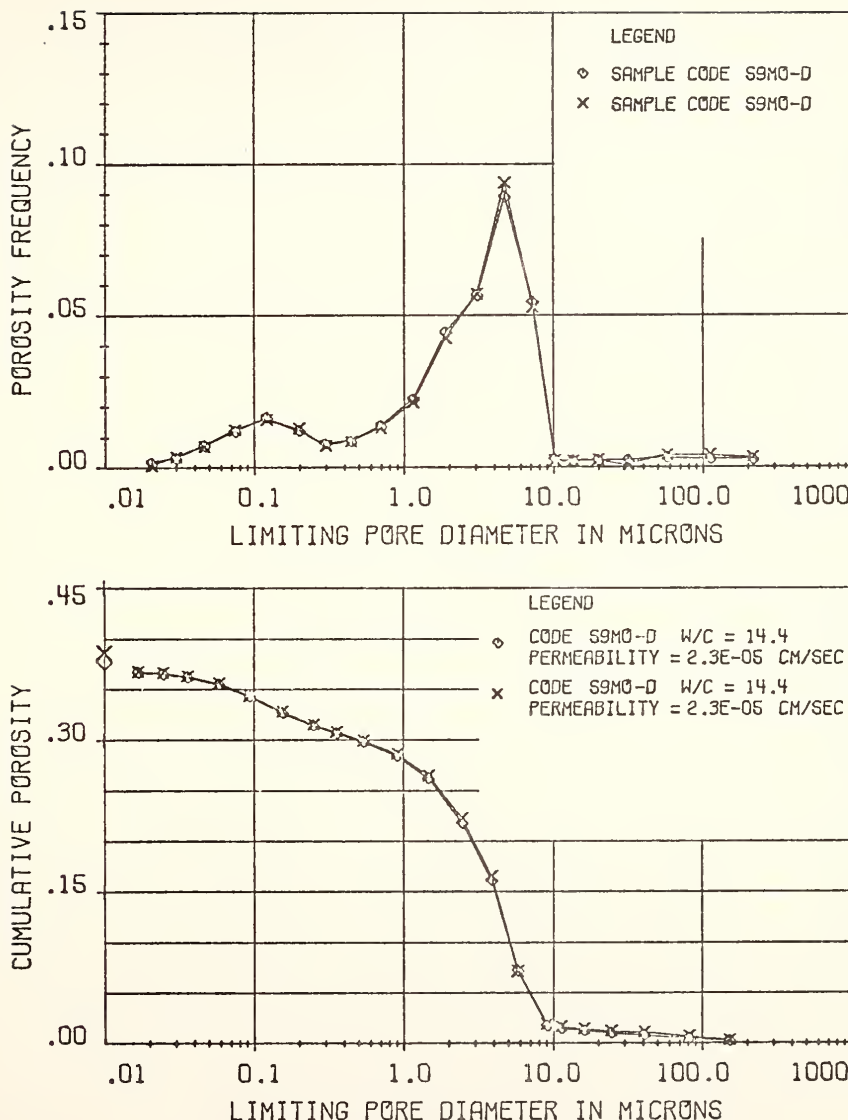


FIGURE 38 REPLICATE PORE SIZE DISTRIBUTION CURVES FOR SAMPLE S9MO-D

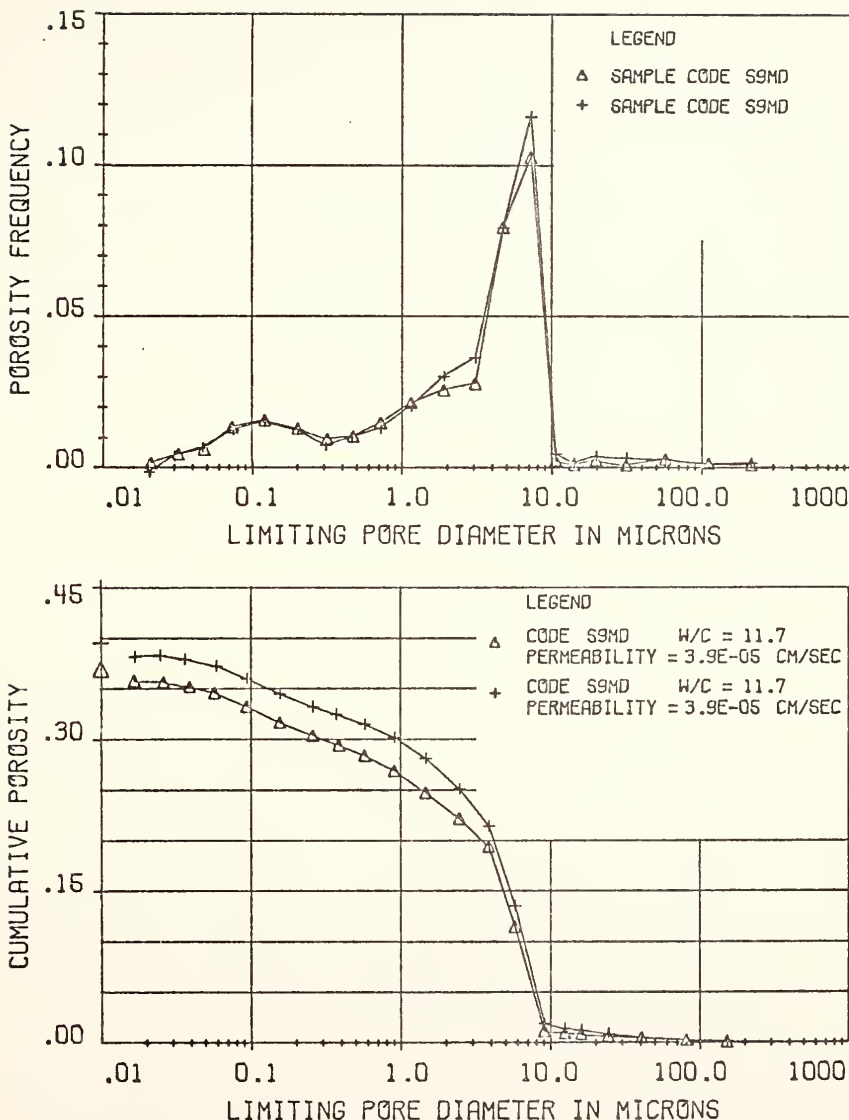


FIGURE 39 REPLICATE PORE SIZE DISTRIBUTION CURVES FOR SAMPLE S9MD

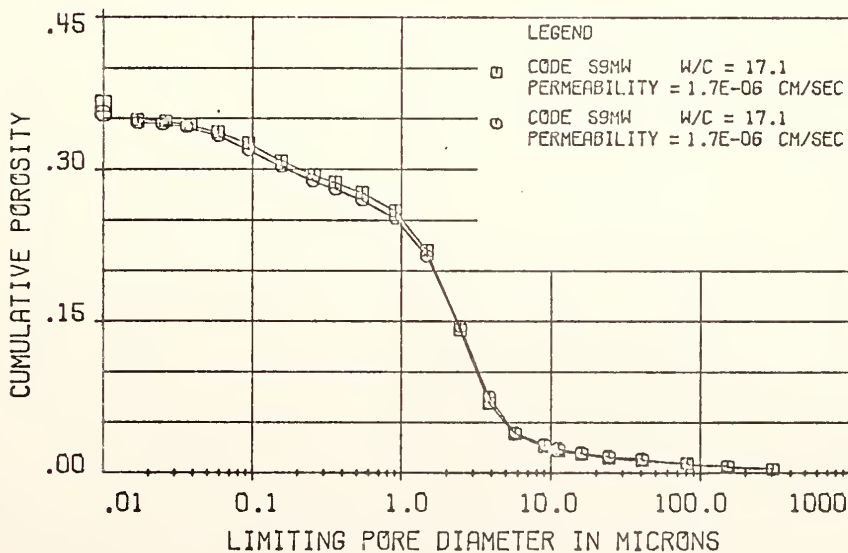
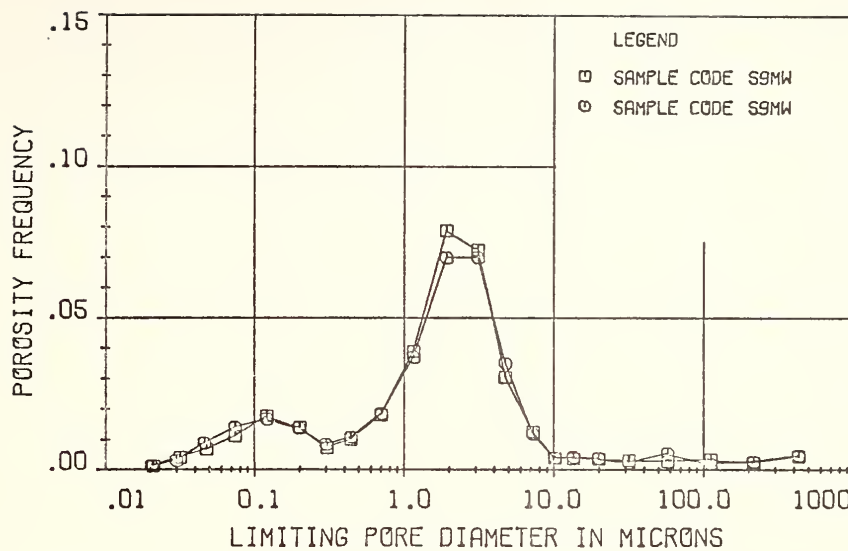


FIGURE 40 REPLICATE PORE SIZE DISTRIBUTION CURVES FOR SAMPLE S9MW

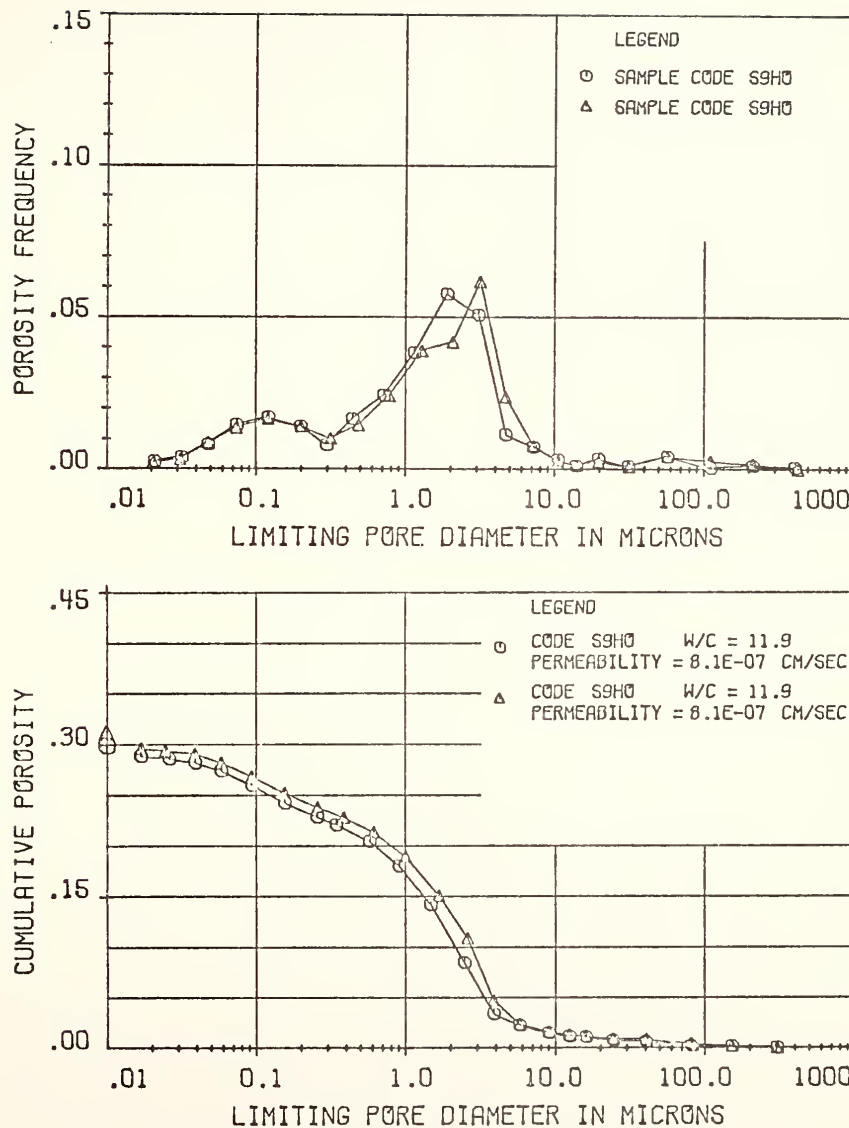


FIGURE 41 REPLICATE PORE SIZE DISTRIBUTION CURVES FOR SAMPLE S9HO

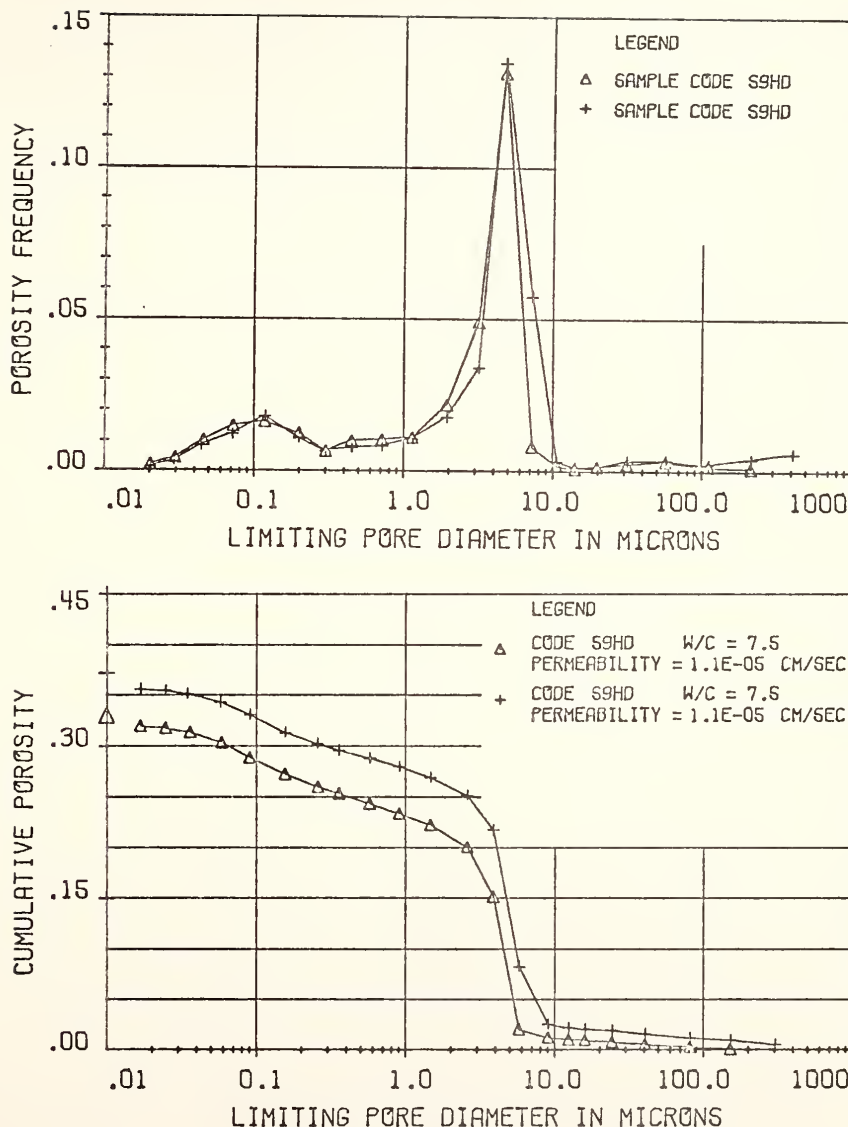


FIGURE 42 REPLICATE PORE SIZE DISTRIBUTION CURVES FOR SAMPLE S9HD

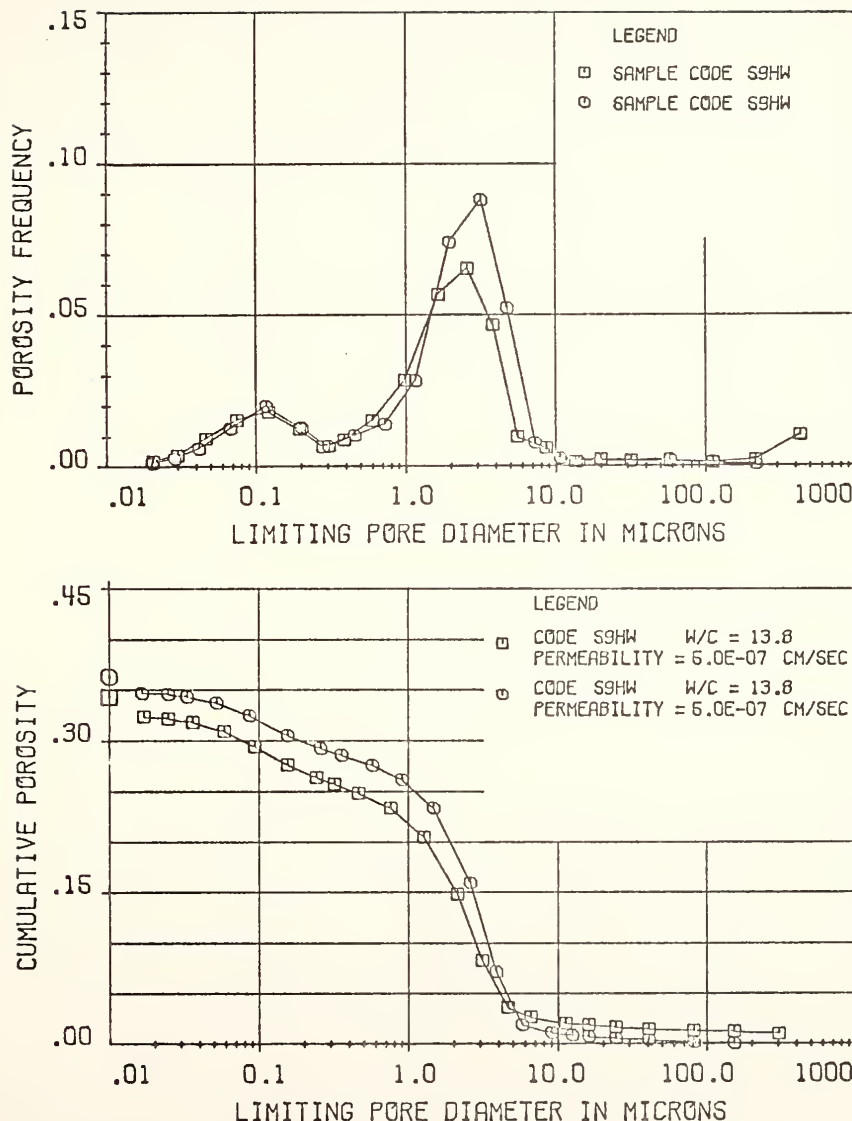


FIGURE 43 REPLICATE PORE SIZE DISTRIBUTION CURVES FOR SAMPLE S9HW

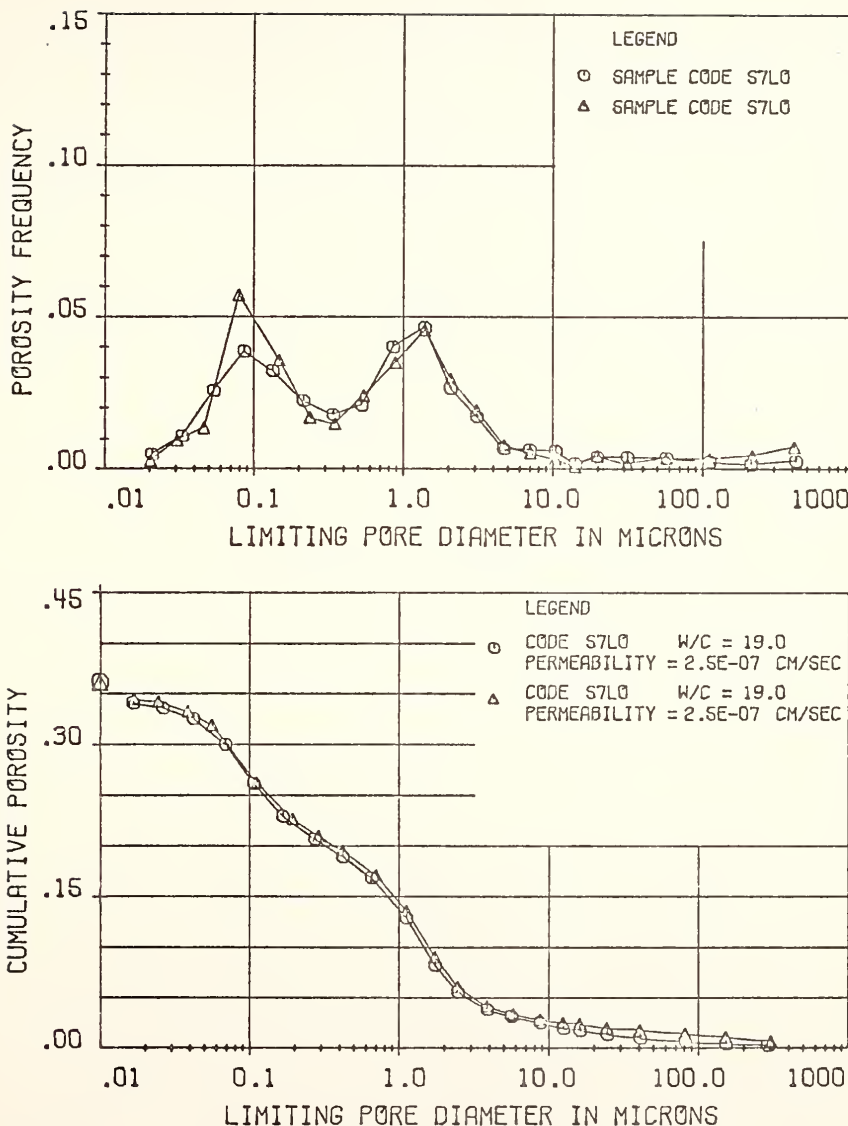


FIGURE 44 REPLICATE PORE SIZE DISTRIBUTION CURVES FOR SAMPLE S7L0

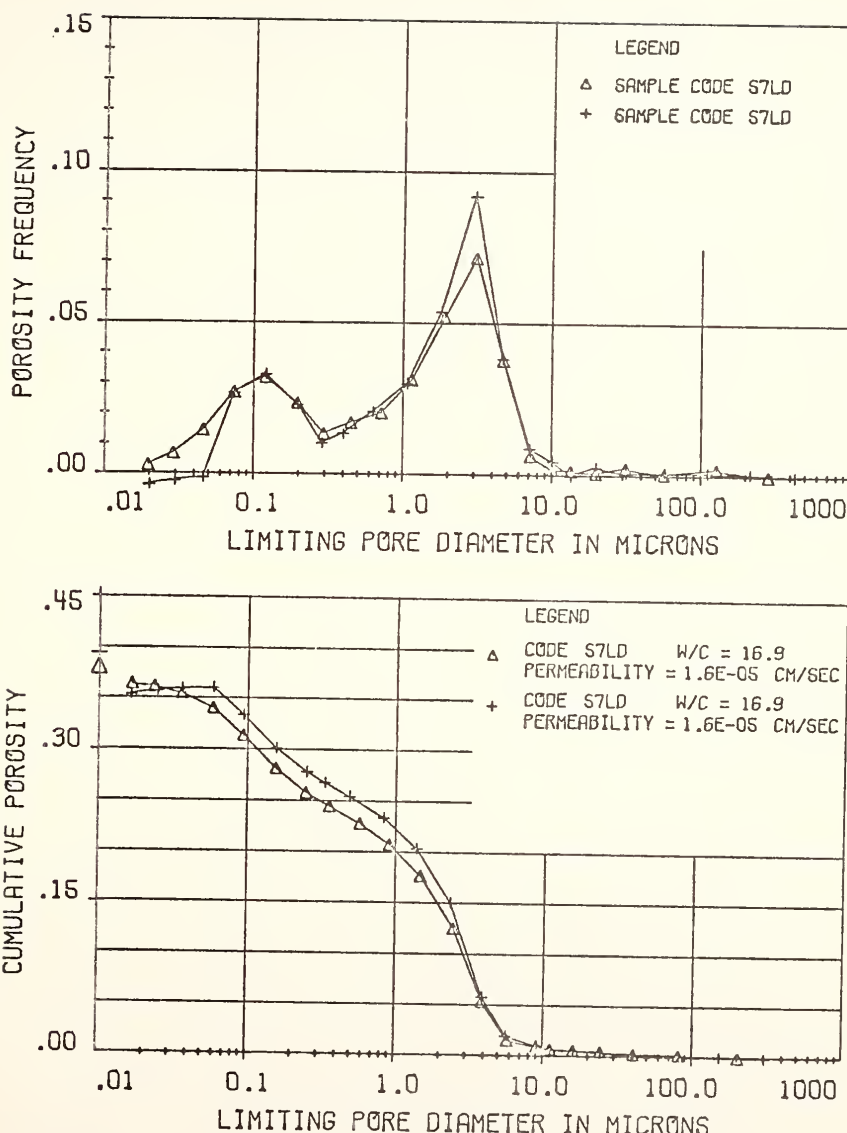


FIGURE 45. REPLICATE PORE SIZE DISTRIBUTION CURVES FOR SAMPLE S7LD

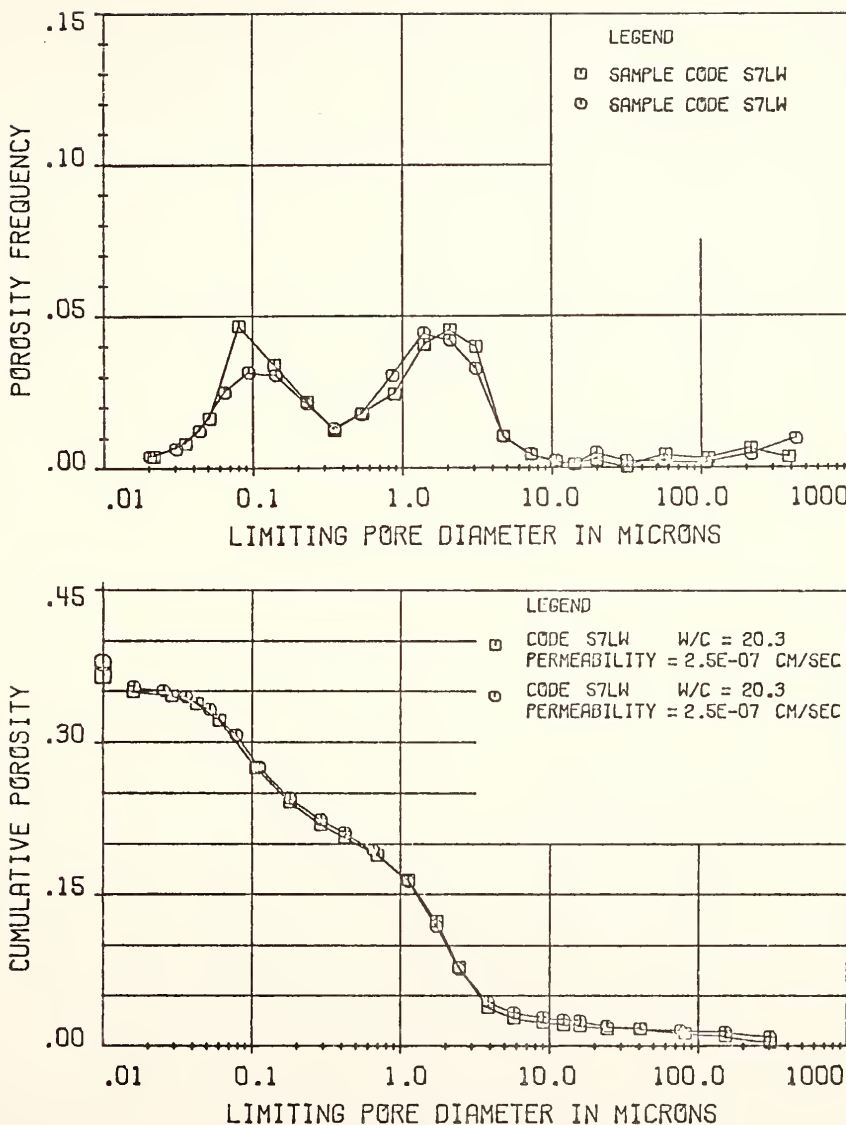


FIGURE 46 REPLICATE PORE SIZE DISTRIBUTION CURVES FOR SAMPLE S7LW

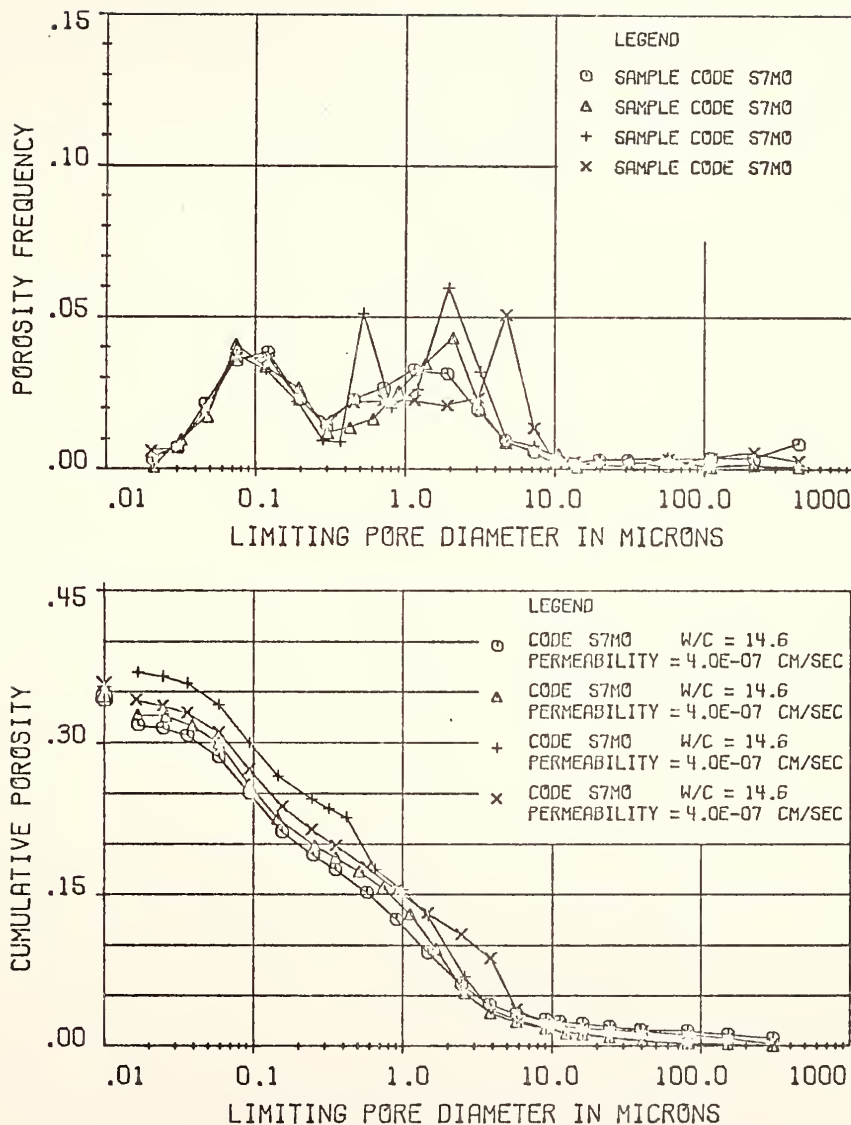


FIGURE 47 REPLICATE PORE SIZE DISTRIBUTION CURVES FOR SAMPLE S7MO

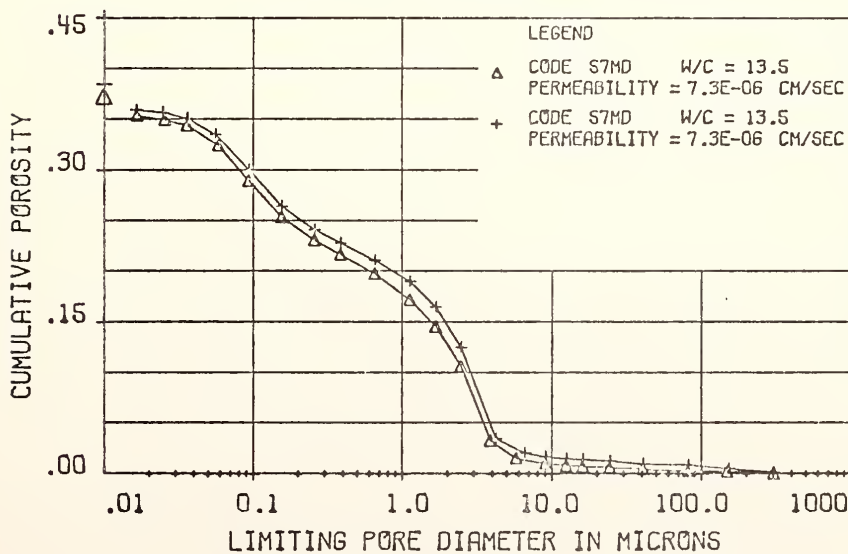
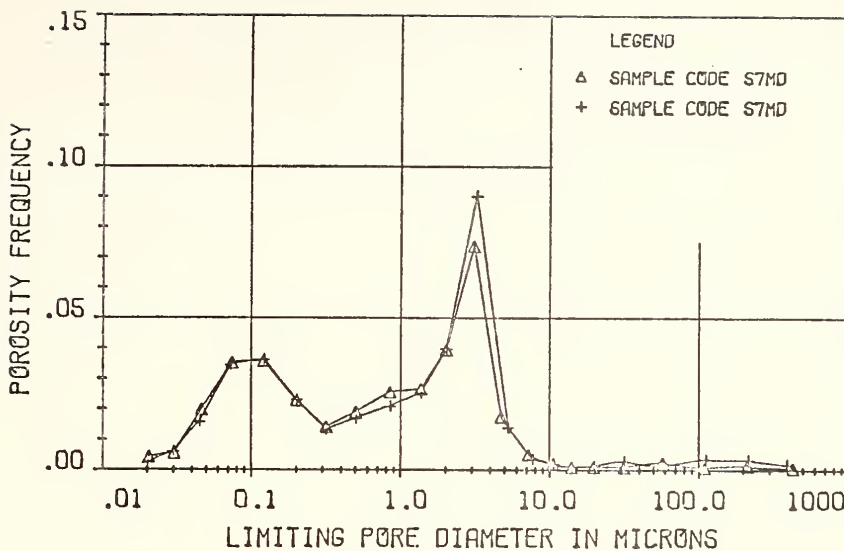


FIGURE 48 REPLICATE PORE SIZE DISTRIBUTION CURVES
FOR SAMPLE S7MD

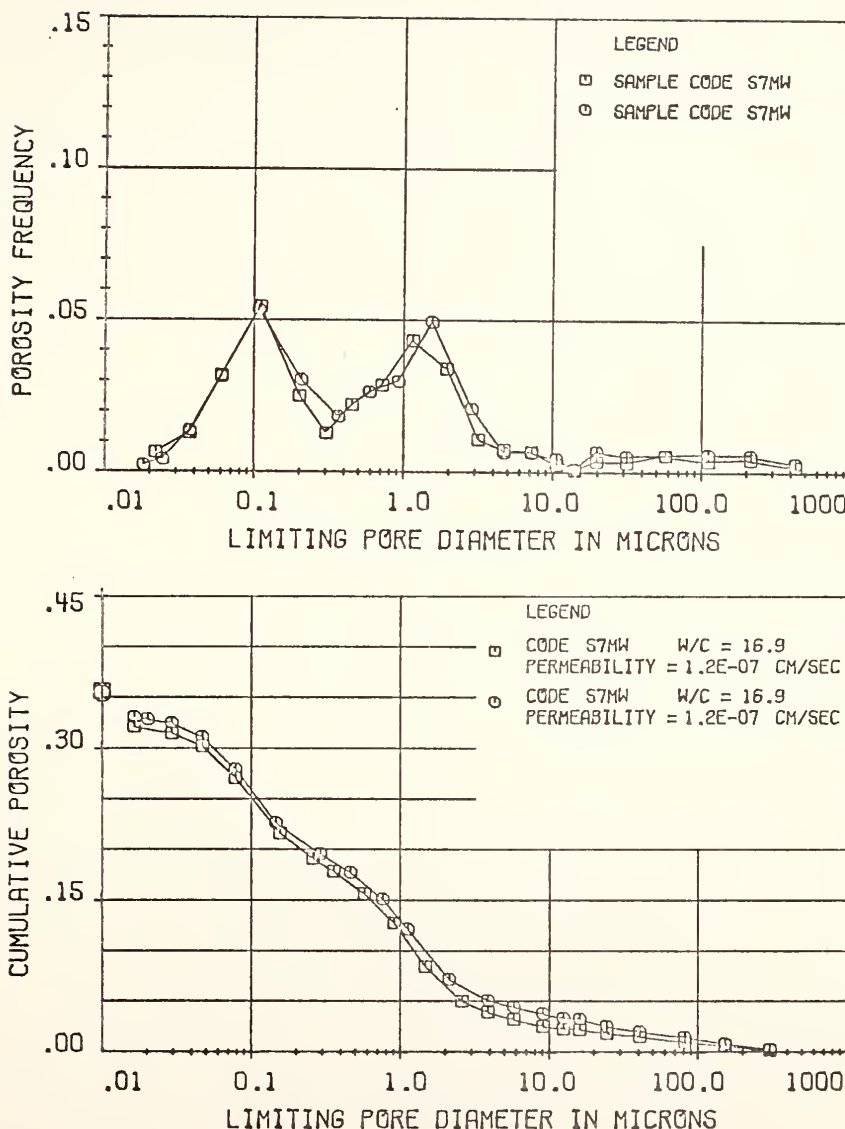


FIGURE 49 REPLICATE PORE SIZE DISTRIBUTION CURVES FOR SAMPLE S7MW

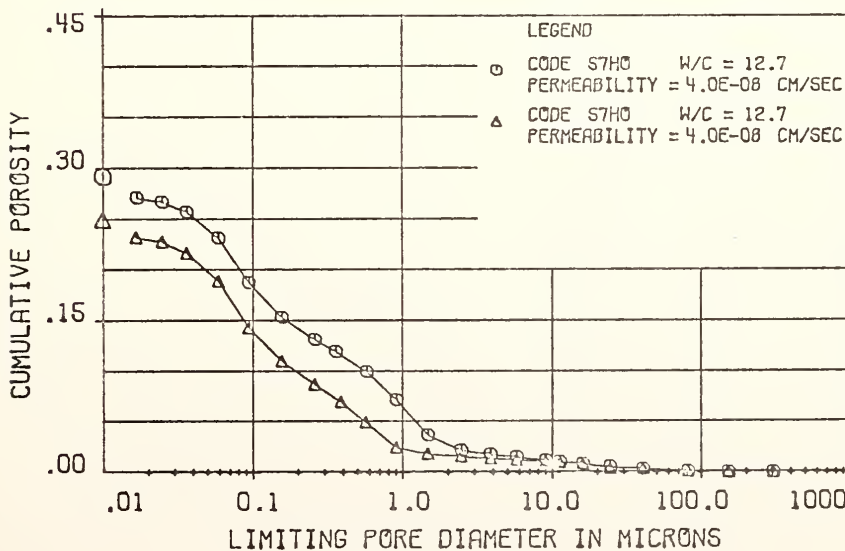
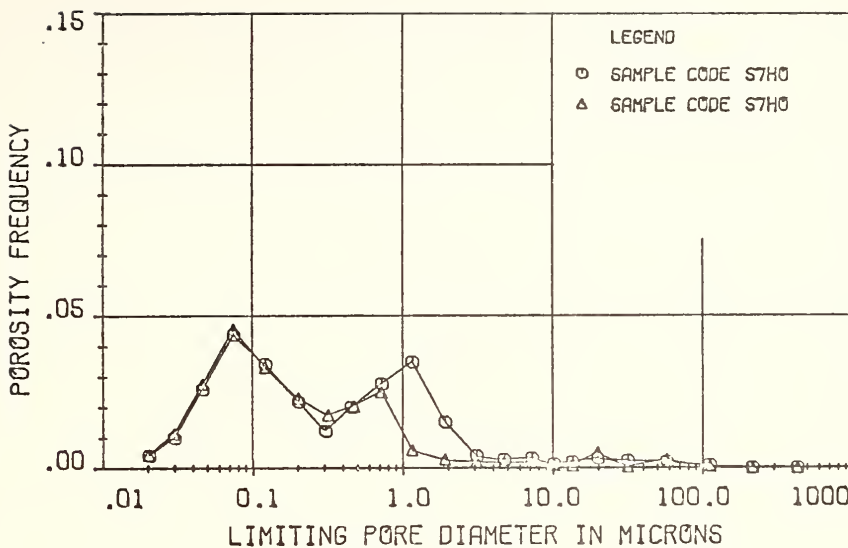


FIGURE 50 REPLICATE PORE SIZE DISTRIBUTION CURVES FOR SAMPLE S7HO

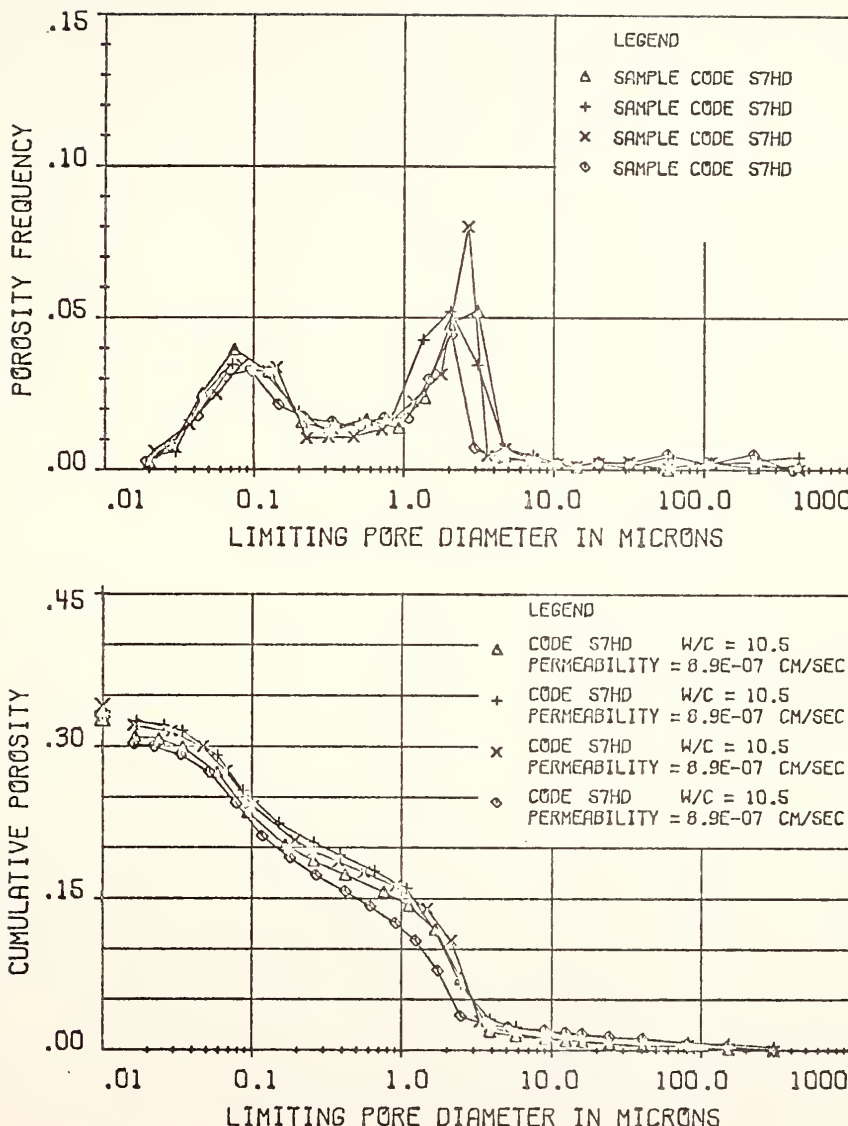


FIGURE 51 REPLICATE PORE SIZE DISTRIBUTION CURVES FOR SAMPLE S7HD

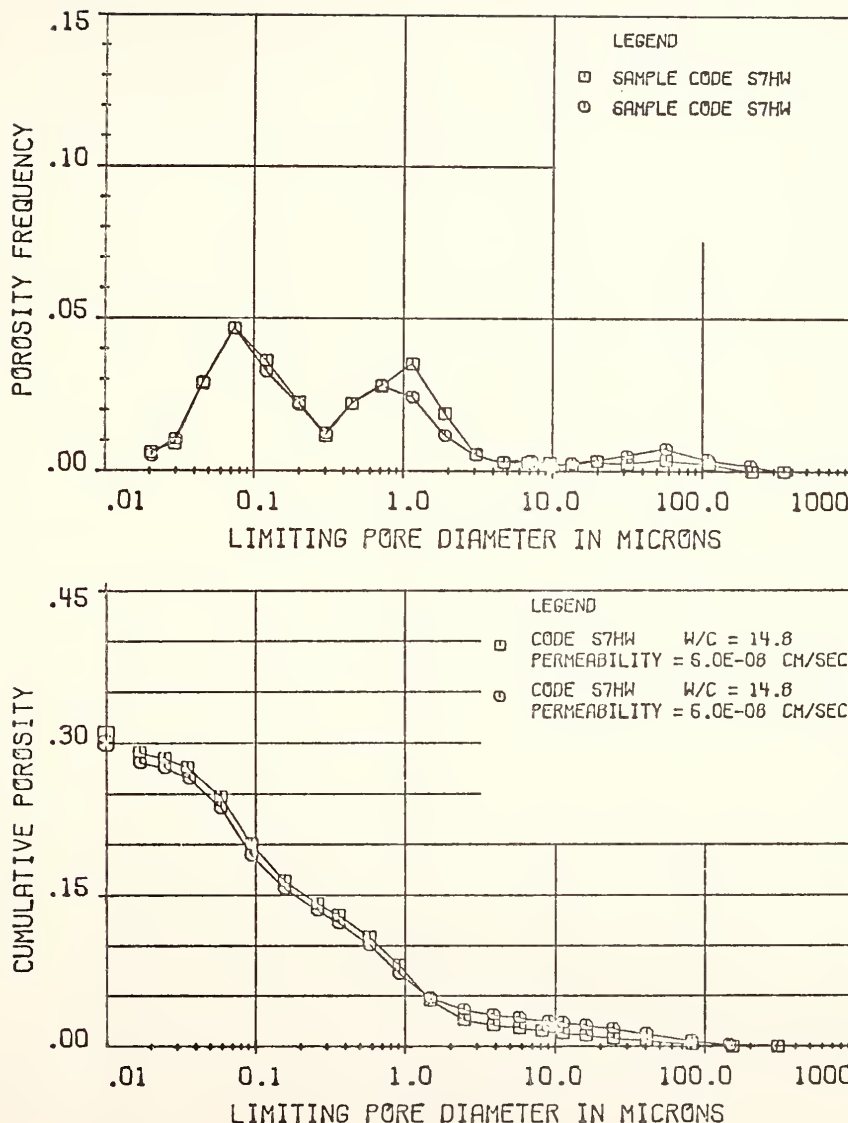


FIGURE 52 REPLICATE PORE SIZE DISTRIBUTION CURVES FOR SAMPLE S7HW

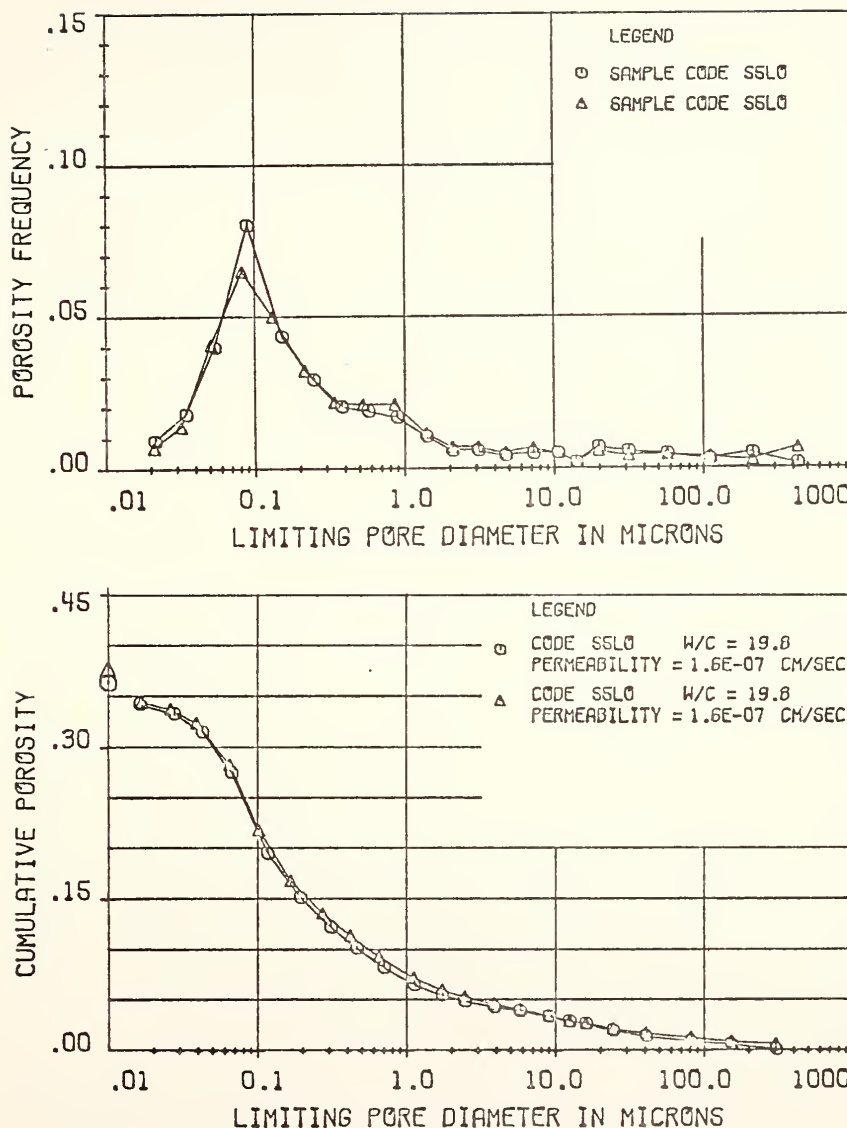


FIGURE 53 REPLICATE PORE SIZE DISTRIBUTION CURVES FOR SAMPLE S5L0

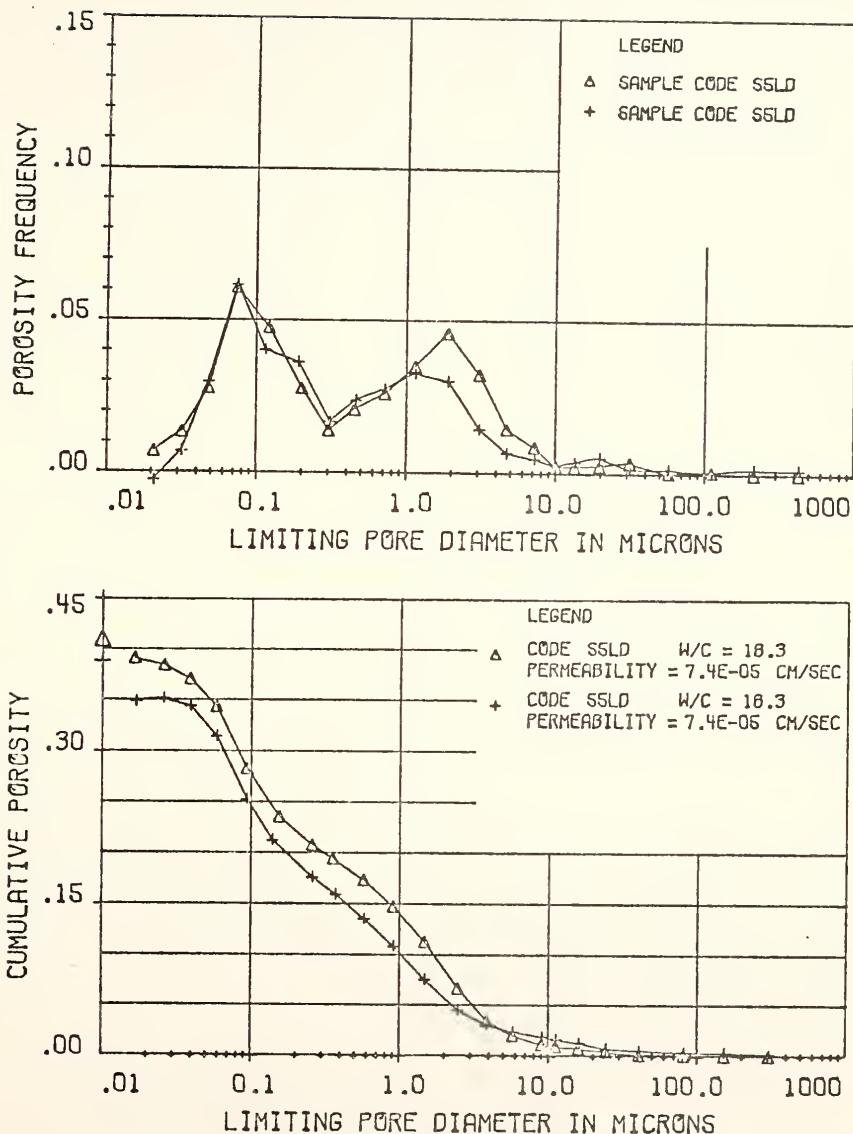


FIGURE 54 REPLICATE PORE SIZE DISTRIBUTION CURVES FOR SAMPLE S5LD

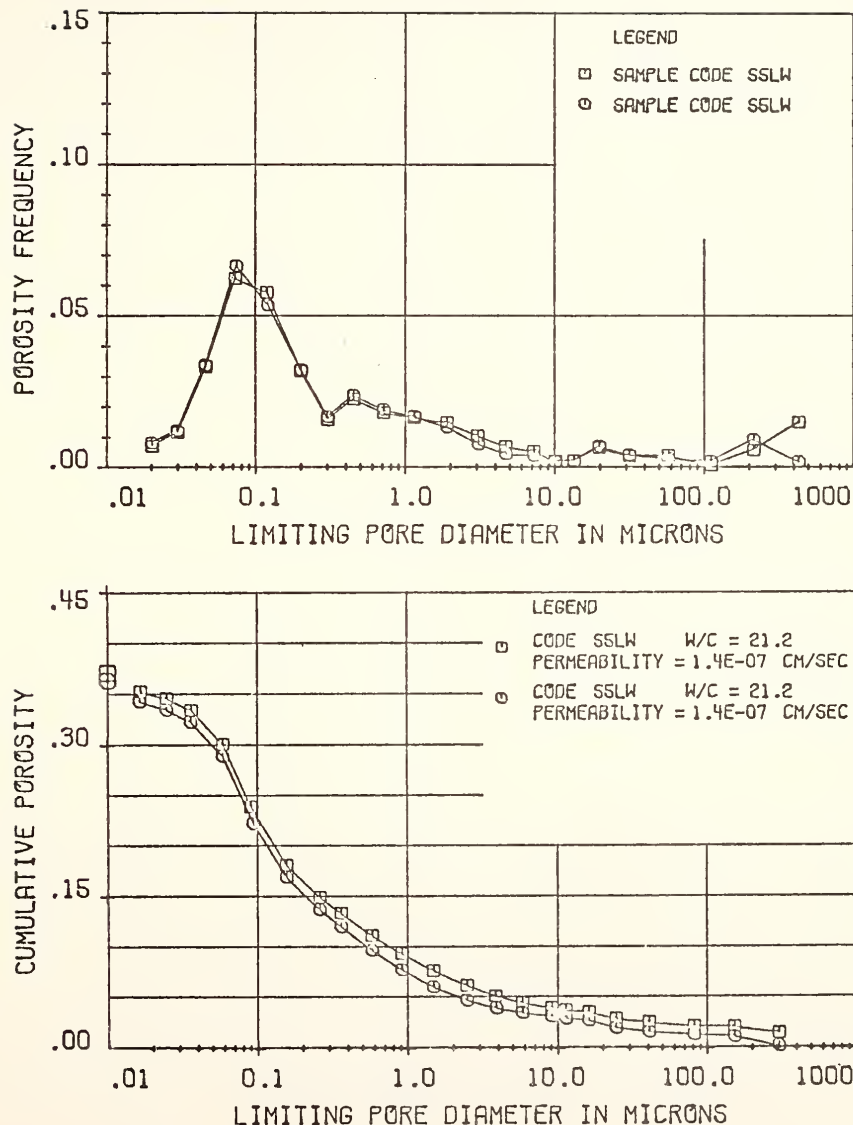


FIGURE 55 REPLICATE PORE SIZE DISTRIBUTION CURVES FOR SAMPLE S5LW

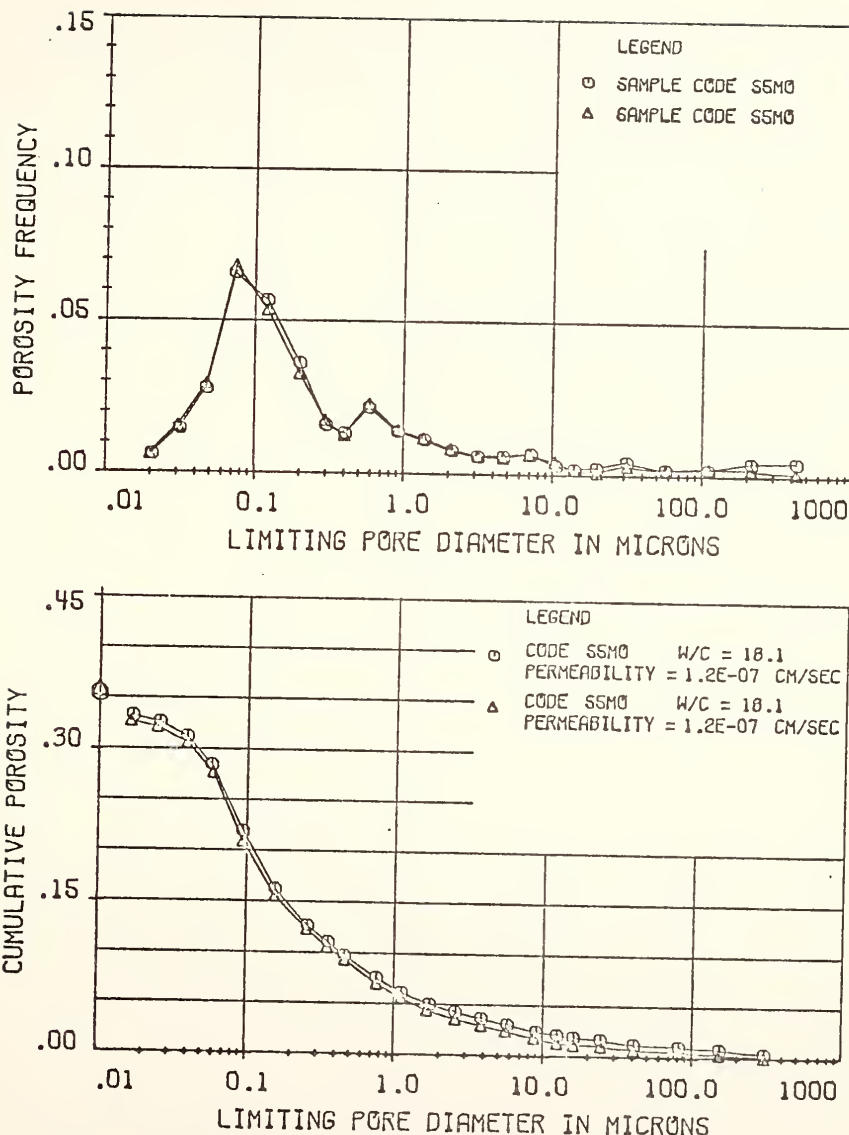


FIGURE 56. REPLICATE PORE SIZE DISTRIBUTION CURVES FOR SAMPLE S5MO

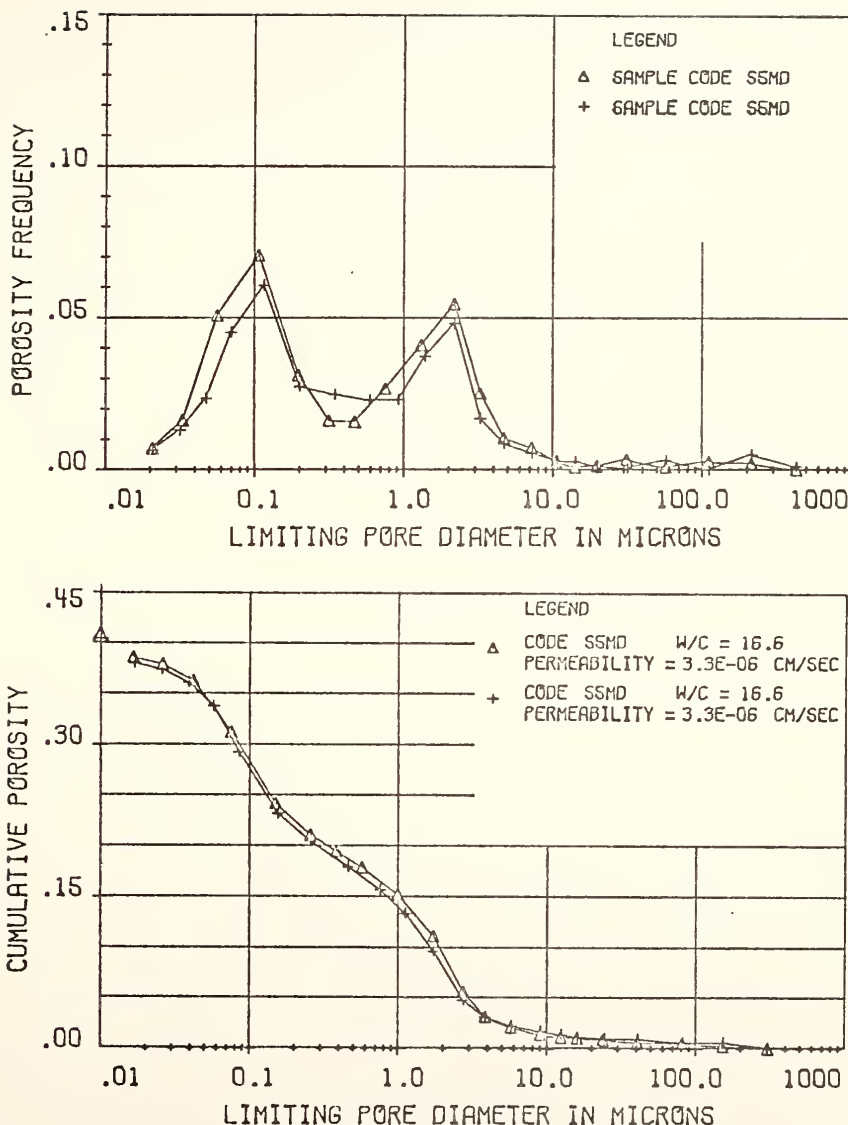


FIGURE 57 REPLICATE PORE SIZE DISTRIBUTION CURVES FOR SAMPLE S5MD

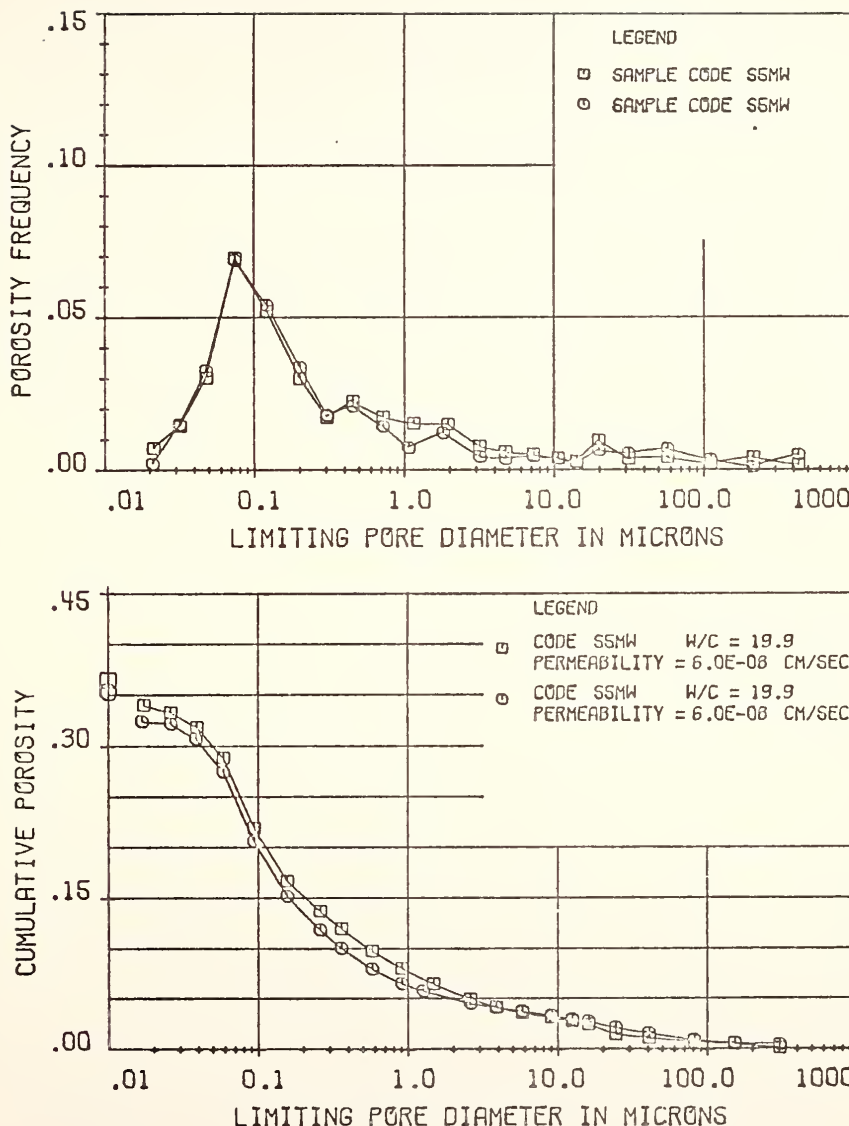


FIGURE 58 REPLICATE PORE SIZE DISTRIBUTION CURVES FOR SAMPLE S5MW

APPENDIX B

Permeability Tests

Laboratory permeability measurements of fine-grained soils may involve several sources of errors. Aside from the major difficulty of replicating field conditions in the laboratory, errors or fluctuations in permeability measurements may result from:

- 1) excess flow around the sample
- 2) leaks in the system
- 3) inadequate hydraulic capacity of the permeation equipment
- 4) evaporation
- 5) volume changes during permeation (consolidation or swelling)
- 6) changing degree of saturation
- 7) particle migration
- 8) variation in electrolyte concentration
- 9) temperature fluctuations
- 10) formation of bacteria
- 11) general measurement errors.

As mentioned previously, samples tested in this study were compacted directly in the permeation molds in order to eliminate excess flow along the boundaries. Mitchell et al. (1965) compared the permeability of two samples of compacted silty clay prepared by the same technique. One sample was compacted directly in the permeation mold and tested; the other sample was tested in a triaxial apparatus, surrounded by a

rubber membrane. Both samples were tested under identical back pressures, and showed nearly equal permeability values.

A closed system falling head permeability test was used because it was felt to have several advantages over the constant head test. The net volume of flow through the sample could be monitored with the permeability measurements, allowing for the detection of leaks, consolidation or swelling. It was necessary to assure that steady state flow conditions were achieved in the sample for accurate permeability determinations. The falling head test applied low gradients across the sample, thus minimizing seepage forces and consolidation during permeation. Back pressure could be readily applied to the samples during permeation to achieve a high degree of saturation. The only significant disadvantage of the system was the long duration of tests on samples of low permeability.

The permeability tests were usually run over a period of three to five days to check if particle migration, variations in electrolyte concentrations or other factors caused permeability fluctuations with time.

B-1 Calculations

The permeabilities were calculated from the falling head equation presented by Taylor (1948) as follows:

$$k = \frac{a L}{\Delta t A} \ln \frac{h_0}{h_1} \quad (B-1)$$

where L is the length of sample

a is the cross-sectional area of the standpipes
 A is the cross-sectional area of sample
 Δt is the time increment
 h_o is the initial total head
 h_1 is the total head at time Δt .

Figure 59 shows a sketch of the closed system falling head test. It is apparent from the figure that:

$$h_o = (h_{xo} + u_o) - (h_{yo} + u_o)$$

$$h_o = h_{xo} - h_{yo} \quad (B-2)$$

where u_o is the back pressure on the system,

and

$$h_1 = h_{xl} - h_{yl} \quad (B-3)$$

The permeability k is then calculated as:

$$k = \frac{a L}{\Delta t A} \ln \left(\frac{h_{xo} - h_{yo}}{h_{xl} - h_{yl}} \right) \quad (B-4)$$

The ratio of absolute viscosity μ at temperature T ($^{\circ}\text{C}$) to the absolute viscosity at 20°C for water was determined from the following correlation which is accurate between 20 and 100°C (CRC, Handbook of Chemistry and Physics, 1970-71, p. F-36):

$$\log \frac{\mu_T}{\mu_{20^{\circ}\text{C}}} = \frac{1.327 (20-T) - 0.001053 (T-20)^2}{T + 105}$$

therefore,

$$\frac{\mu_T}{\mu_{20^\circ C}} = 10 \quad \frac{1.327 (20-T) - 0.001053 (T-20)^2}{T + 105} \quad (B-5)$$

The normalized permeability was then calculated as follows:

$$k_{20^\circ C} = \frac{\mu_T}{\mu_{20^\circ C}} \cdot k_T \quad (B-6)$$

The net volume of inflow ΔV during permeation is:

$$\Delta V = V_{in} - V_{out} \quad (B-7)$$

$$\Delta V = \{h_{xo} - h_{x1} - (h_{y1} - h_{yo})\} a$$

$$\Delta V = a\{h_{xo} + h_{yo} - h_{x1} - h_{y1}\} \quad (B-8)$$

where a is the area of the standpipes.

Because of the lengthy duration of the permeability tests, evaporation during permeation became a concern. Assuming that the rate of evaporation in the two standpipes is equal, the evaporation in each of standpipes after time Δt may be expressed as Δh . Entering equation (B-4) with a correction for the evaporation of Δh after time Δt yields the following:

$$k = \frac{a L}{\Delta t A} \ln \frac{h_{xo} - h_{yo}}{(h_{x1} + \Delta h) - (h_{y1} + \Delta h)}$$

which is equal to:

$$k = \frac{a L}{\Delta t A} \ln \left(\frac{h_{xo} - h_{yo}}{h_{x1} - h_{y1}} \right)$$

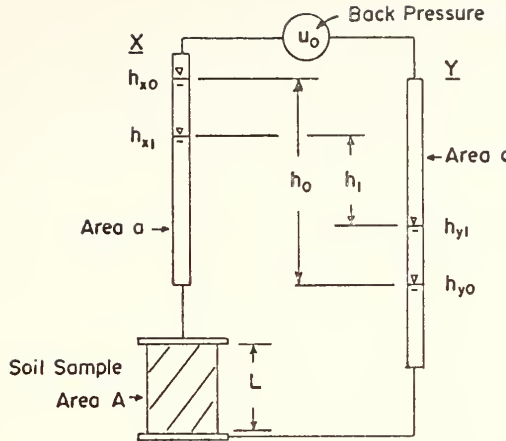


FIGURE 59 CLOSED SYSTEM FALLING HEAD PERMEABILITY TEST

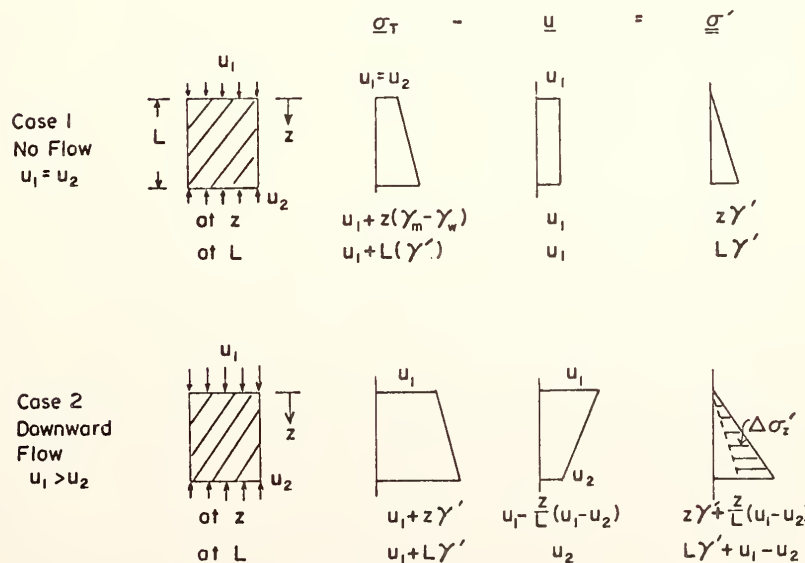


FIGURE 60 CHANGES IN EFFECTIVE STRESS CAUSED BY FLOW THROUGH SOILS

It is evident that evaporation has no influence on the calculated permeability values if the rate of evaporation is equal in both standpipes. The same is not true for the net volume of inflow, however. Applying the evaporation correction Δh to equation (B-8) yields the following:

$$\Delta V = a \{ h_{xo} + h_{yo} - (h_{y1} + \Delta h) - (h_{y1} + \Delta h) \}$$

$$\Delta V = a \{ h_{xo} + h_{yo} - h_{x1} - h_{y1} - 2 \Delta h \} \quad (B-9)$$

Therefore, the net volume of inflow does reflect evaporation losses during permeation.

B-2 Consolidation During Permeation

For several of the preliminary permeability tests performed during this investigation a 10 to 20 psi water pressure differential was placed across the samples to accelerate the saturation process. These samples consolidated up to 1/4 inch because of the high seepage forces on the soil.

Figure 60 shows an effective stress analysis of a saturated sample under a constant back pressure in a "no flow" condition, and the same sample with a constant pressure differential Δu across it to induce flow. From the figure, the change in effective stress $\Delta \sigma'_z$ with depth z between the constant pressure differential and the no flow cases is equal to:

$$\Delta \sigma'_z = \{ z \gamma' + \frac{z}{L} (u_1 - u_2) \} - \{ z \gamma' \}$$

$$\Delta \sigma'_z = \frac{z}{L} (u_1 - u_2)$$

$$\Delta\sigma_z^e = \frac{z}{L} \Delta u \quad (B-10)$$

where u_1 and u_2 are the boundary water pressures on the top and bottom of the samples, respectively
 γ' is the submerged unit weight of the soil and equal to $(\gamma_m - \gamma_w)$
 γ_m is the saturated unit weight of the soil
 γ_w is the unit weight of water and
 L is the sample length.

From equation (B-10), at the base of the sample ($z = L$), the effective stress increase is equal to the pressure differential Δu , while at the top of the sample the effective stress remains unchanged. For large pressure differentials, the sample will experience increasing consolidation and decreasing permeability with depth and time until equilibrium conditions are reached.

Constant head tests employing high pressure differentials are frequently used to accelerate permeability measurements of clays. Such tests are likely to produce doubtful results as demonstrated above. High water pressure differentials are present in some earth structures such as the core of earthen dams. In these cases it may be advantageous to account for the consolidation and for the permeability decreases which will take place with time as a result of the seepage forces.

APPENDIX C

Critical Region Drying Problems

Critical region drying was to be used to prepare samples for mercury intrusion pore size distribution measurements. However, during preliminary critical region runs, the soils used in this study underwent a 35 to 40% increase in void ratio as a result of the dehydration procedure. A mineralogic analysis of the soil revealed that the critical region process caused a chemical reaction in the soil.

The critical region drying procedure employed, was that used by Bhasin (1975) and described by Reed (1977). As mentioned in Section 1-3.3, the process involves elevating the pressure and temperature of the soil to 3800 psi and 380⁰C, respectively.

Figure 61 shows a comparison of X-ray patterns for two soil types, each air and critical region dried. The air dried soils consist primarily of quartz and dolomite, with fractions of kaolinite, calcite, and feldspar also present. Critical region drying eliminated the kaolin peaks, significantly reduced the dolomite and calcite peaks, and increased the feldspar peaks.

Detailed analysis of the changes in interplanar or d spacing of the peaks between the air dried and critical region dried specimens indicated that the mineral being formed by critical region drying was a form of plagioclase feldspar (ASTM 10-359 or 9-465)¹. The reaction

1. ASTM Inorganic Powder Diffraction File numbers.

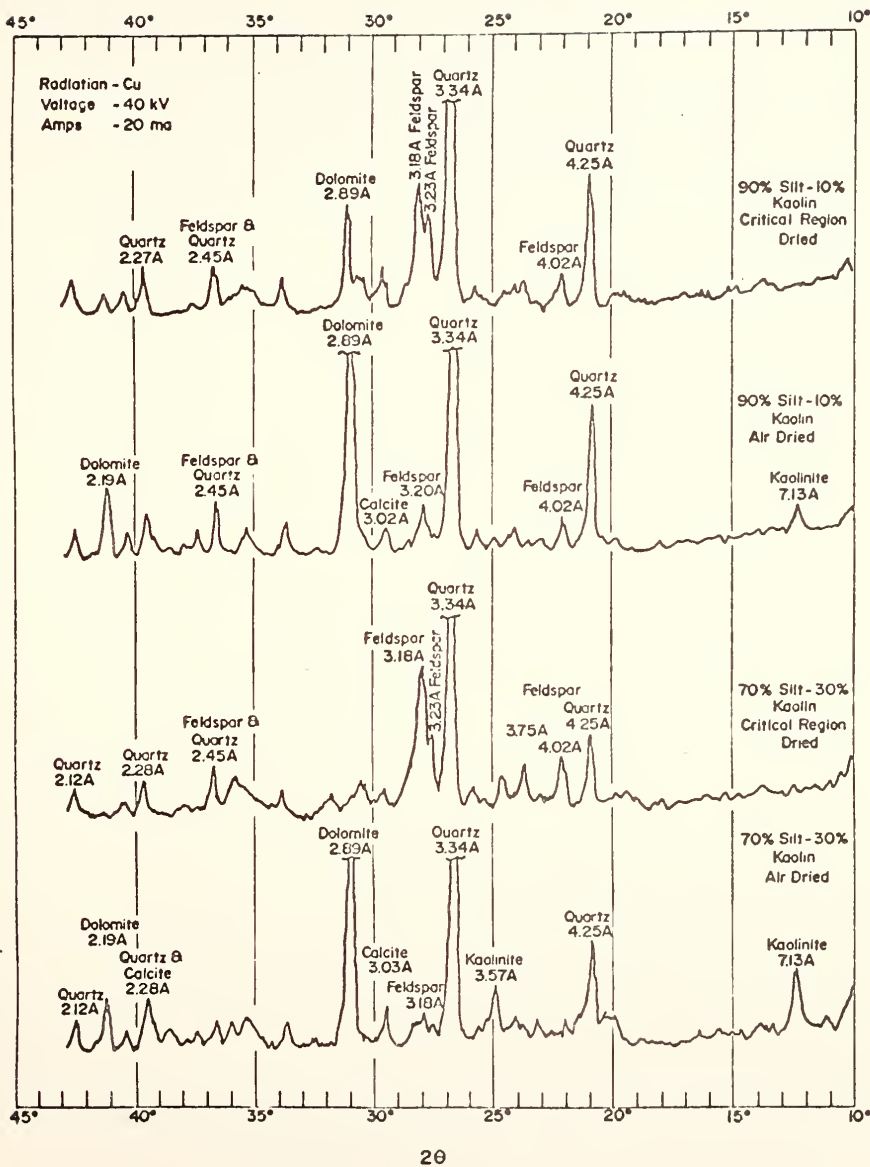


FIGURE 61 X-RAY DIFFRACTION PATTERNS OF CRITICAL REGION AND AIR DRIED SOILS

between the carbonates and kaolinite which formed this mineral was, no doubt, responsible for the structural changes undergone by the samples during critical region drying.

In light of the above findings it would be prudent to monitor critical region drying of soils with mineralogic determinations, particularly when carbonates are present.

APPENDIX D

Pore Size Distribution Computer Programs


```

C
C THIS PROGRAM CALCULATES AND TABULATES PORE SIZE DISTRIBUTION
C PARAMETERS, ALONG WITH PLOTTING PORE DIAMETER VERSUS CUMULATIVE
C INTRUSION/GRAM, CUMULATIVE INTRUSION/VOLUME AND INCREMENTAL
C INTRUSION / VOLUME. PROGRAM AFTER REED (1977).
C
C PROGRAM PORE (INPUT,OUTPUT,TAPE5=INPUT,TAPE6=OUTPUT)
C DIMENSION S(50),P(50),D(50),CU(50),SP(50),CUSP(50),GRAPH(451),
C CPORO(451),HISTO(451),C(50)
C READ, NDATA
C DO 400 J=1,NDATA
C
C THE PURPOSE OF THIS DO LOOP IS TO BE ABLE TO CALCULATE RESULTS FOR
C MORE THAN ONE SET OF DATA IN A SINGLE RUN. NDATA IS THE NUMBER
C OF SETS OF DATA TO BE CALCULATED. NDATA IS AN INTEGER VALUE, AND
C IS THE FIRST DATA CARD FOR THE SET OF DATA.
C DETERMINATION OF PORE SIZE DISTRIBUTION
C
C READ, DATE, SN
C
C DATE AND SAMPLE NUMBER (SN) ARE TYPED ON THE FIRST DATA CARD FOR
C EACH CURVE.
C
C WRITE (6,14)
14  FORMAT (1H1)
C PRINT, DATE, SN
C READ, WS, DS, DM, UP, WSP, WSPM, PE, PF, SR
C
C HS=HEIGHT OF SAMPLE, DS=SPECIFIC GRAVITY OF SOLIDS, DM=DENSITY OF
C MERCURY, UP=VOLUME OF PENETROMETER, WSP=WEIGHT OF SAMPLE AND PEN-
C ETROMETER, WSPM=WEIGHT OF SAMPLE , PENETROMETER AND MERCURY,
C PE =EVACUATING PRESSURE, PF=FILLING PRESSURE,IN MM OF MERCURY,
C SR =STEM READING AT FILLING PRESSURE. THE ABOVE VALUES ARE ALL ON
C THE SAME DATA CARD
C
C PRINT, WS, DS, DM, UP, WSP, WSPM, PE, PF, SR
C VS=WS/DS
C WM=WSPM - WSP
C UM=WM/DM
C USA=UP-UM*(1.+PE/PF)-SR
C UVO=USA-US
C VOIDR=UVO/VS
C POROS=UVO/USA
C PV=PE*UM
C VAI=PV/UM
C PRINT, #VOLUME SOLIDS IS#, US, /, #VOLUME VOIDS IS#, UVO
C PRINT, #VOID RATIO IS#, VOIDR, /, #POROSITY IS#, POROS
C READ, N, M, SI
C
C N=INTEGER VALUE FOR THE NUMBER OF LOW PRESSURE READINGS MADE, NOT
C COUNTING THE FILLING PRESSURE READING. M=INTEGER VALUE FOR THE
C NUMBER OF HIGH PRESSURE READINGS MADE, NOT COUNTING THE INITIAL
C POROSIMETER READING. SI=INTRUSION READING AT INITIATION PRESSURE
C IN ML. THE THREE VALUES ARE ALL ON ONE DATA CARD.
C
C LOW PRESSURE CALCULATIONS

```



```

      WRITE (6,5)
5      FORMAT (//,37X,#LOW PRESSURE CALCULATIONS#)
      WRITE (6,6)
6      FORMAT (//,3X,#MM OF HG PRESSURE VOL AIR STEM RDG INTRUS      I
ANTRU/GM CUMUL IN INTR/USA CU IN/VIS DIAMETER #)
      CU(1) = 0.
      CUSP(1) = 0.
      DO 100 I=2,N+1
      READ,P(I),S(I)

C
C      P(I) AND S(I) ARE THE PRESSURE AND INTRUSION VALUES FOR EACH
C      READING, P(I) IS GIVEN IN MM OF MERCURY FOR THE LOW PRESSURE
C      INTRUSION AND PSI FOR THE HIGH PRESSURE. S(I) IS IN ML. THE TWO
C      VALUES ARE TYPED ON ONE DATA CARD, WITH A CARD FOR EACH READING.
C
C      PS=P(I)*.01934
C      VA=PU*P(I)
C      CVA=VAI-VA
C      CSR=S(I)-SR
C      SN=CSR-CVA
C      IF (SN.LT.0.) GO TO 10
C      SG =SN/HS
C      GO TO 11
. 10  SG=0.
      SN =0.
11      CU(I) = CU(I-1) + SG
      SP(I) = SN/USA
      CUSP(I) = CUSP(I-1) +SP(I)
      D(I)=((-4.)*484.*COS(2.5656)*.145)/PS
      PRINT 1,P(I),PS,VA,S(I),SN,SG,CU(I),SP(I),CUSP(I),D(I)

C
C      P(I)=INTRUSION PRESSURE IN MM OF MERCURY, PS=INTRUSION PRESSURE IN
C      PSI, VA=VOLUME OF AIR IN ML, S(I)=STEM READING, SN=CORRECTED
C      INTRUSION FOR EACH INCREMENT IN ML, SG=CORRECTED INTRUSION /GRAM
C      FOR EACH INCREMENT, CU(I)=CUMULATIVE CORRECTED INTRUSION/GRAM,
C      SP(I)=INCREMENTAL POROSITY, CUSP(I)=CUMULATIVE POROSITY,
C      D(I)=LIMITING PORE SIZE DIAMETER
C
1      FORMAT(X,10F10.4)
      VAI=VA
100     SR=S(I)

C
C      HIGH PRESSURE CALCULATIONS

C
      WRITE (6,7)
7      FORMAT (//,36X,#HIGH PRESSURE CALCULATIONS#)
      WRITE (6,8)
8      FORMAT (//,3X,#PRESSURE STEM RDG HG COR      CHG HCC      INTRUS      I
BNTRU/GM CUMUL IN INTR/USA CU IN/VIS DIAMETER #)
      HCI=11.*.0011*VM/15000.
      DO 200 I=N+2,N+1
      READ,P(I),S(I)
      P(I)=P(I)+11.

C
C      HC IS CORRECTION FOR COMPRESSION OF MERCURY

C
      HC=P(I)*.0011*VM/15000.
      CHC=HC-HCI

```



```

CSR=S(I)-SI
SI=CSR-CHC
SF(I) = SN/USA
CUSP(I) = CUSP(I-1) + SP(I)
SGH=SN/HS
CU(I)=CU(I-1)+SGH

C
C D(I) PORE DIAMETER CALCULATIONS BASED ON A SURFACE TENSION VALUE
C OF 484 DYNES / CM AND A CONTACT ANGLE OF 147 DEGREES.
C
C D(I)=((-4.)*484.*COS(2.5655)*.145)/P(I)
C PRINT 2,P(I),S(I),HC,CHC,SN,SGH,CU(I),SP(I),CUSP(I),D(I)

C
C P(I)=INTRUSION PRESSURE IN PSI, S(I)=STEM READING, HC=MERCURY
C CORRECTION, CHC=CHANGE IN MERCURY CORRECTION IN ML, SN=CORRECTED
C INTRUSION IN ML, SGH=CORRECTED INTRUSION /GRAM, CU(I)=CUMULATIVE
C CORRECTED INTRUSION/GRAM, SP(I)=INCREMENTAL POROSITY, CUSP(I)=
C CUMULATIVE POROSITY
C
C 2 FORMAT (X,10F10.4)
C HCI=HC
200 SI=S(I)
DO 300 I=2,N+M+1
300 C(I)=ALOG10(D(I))
C
C THE PURPOSE OF THIS DO LOOP IS TO CONVERT THE PORE SIZE DIAMETER
C TO THE LOG OF THE DIAMETER
C
CALL PLOT1 (0,4,10,5,20)
CALL PLOT2 (GRAPH,451,3.,-2.,,4,0.)
CALL PLOT3 (1H*,C,CU,N+M)
3 FORMAT (1H1,35X,54H PLOT OF LIMITING PORE DIAMETER VS CUMULATIVE IN
INTRUSION//)
WRITE(6,3)
CALL PLOT4 (5,INTRU)
WRITE (6,20)
WRITE(6,4)
20 FORMAT (10X, #0.01#,17X, #0.1#,18X, #1.0#,17X, #10.,#17X, #100.,#16X
C#10000.#)
4 FORMAT (1H0,45X,32H LIMITING PORE DIAMETER IN MICRONS)
CALL PLOT1 (0,4,10,5,20)
CALL PLOT2 (PORO,451,3.,-2.,,4,0.)
CALL PLOT3 (1H*,C,CUSP,N+M)
12 FORMAT (1H1,26X,72H PLOT OF LIMITING PORE DIAMETER VS CUMULATIVE IN
INTRUSION/VOLUME OF SAMPLE//)
WRITE (6,12)
CALL PLOT4 (5,INTRU)
WRITE (6,20)
WRITE(6,4)
CALL PLOT1 (0,4,10,5,20)
CALL PLOT2 (HISTO,451,3.,-2.,,2,0.)
CALL PLOT3 (1H*,C,SP,N+M)
WRITE (6,13)
13 FORMAT (1H1,35X,55H PLOT OF LIMITING DIAMETER VS INTRUSION/VOLUME O
EF SAMPLE//)
CALL PLOT4 (5,INTRU)
WRITE (6,20)
WRITE(6,4)

```



```

D(1)=((-4.)*484.*COS(2.5655)*.145)/(PF*.01934)
PRINT, #PORE DIAMETER AT FILLING PRESSURE IS #,D(1)

C
C   BELOW - CALCULATION OF SPECIFIC SURFACE AREA AND HYDRAULIC RADIUS
C   DM IS MIDPOINT DIAMETER OF D(I) AND D(I-1).
C
C   SUM1 = 0.0
C   DO 500 I = 2,N+M+1
C   DM = SQRT(D(I)*D(I-1))
500 SUM1= SUM1 + SP(I)*4. /DM
I= N+M+1
SUM1= SUM1+(POROS-CUSP(I))*4./.01
PRINT, #SPECIFIC SURFACE AREA IN 1/UM IS #,SUM1
SUM2= POROS/SUM1
PRINT, #HYDRAULIC RADIUS IN UM IS #,SUM2

C
C   BELOW - CALCULATION OF MEAN PORE DIAMETER AND SECOND MOMENT ABOUT
C   THE ORIGIN FOR PORES LESS THAN 10 MICRONS.
C
C   SUM1 = 0.0
C   SUM2 = 0.0
C   DO 600 I=2,N+M+1
C   DM = SQRT(D(I)*D(I-1))
C   IF (DM. GT. 10.) DM=0.0
C   SUM1 = SUM1 + SP(I)*DM
600 SUM2 = SUM2 + SP(I)*DM**2
DMEA1= SUM1/POROS
DMEA2= SUM2/POROS
WRITE (6,21)
21 FORMAT (/,1X,#THE STATISTICAL MEASURES BELOW NEGLECT PORES#,/,1X,
#WITH A DIAMETER GREATER THAN 10. MICRONS#,/)
PRINT, #ADJUSTED MEAN PORE SIZE IS #,DMEA1,/,#ADJUSTED SECOND
BMOMENT ABOUT THE ORIGIN IS #,DMEA2

C
C   BELOW - CALCULATION OF MARSHALL MODEL PORE DIAMETER FOR PORES
C   LESS THAN 10 MICRONS.
C
C1= 0.0
C2= 0.0
DO 31 I=2,N+M+1
C3= SP(I)**2
AB= I
IF (AB. LT. 2.0) GO TO 29
DO 28 K=1,I-1
28 C1= 2.*SP(I)*SP(K)+C1
29 C1= C1+C3
DM = SQRT(D(I)*D(I-1))
IF (DM. GT. 10.) DM=0.0
C2= C2+DM**2 *C1
31 C1=0.0
SC2 = SORT(C2)
400 PRINT, #MARSHALL PORE DIAMETER SQUARED IN UM**2 IS #,C2,/,#
B#MARSHALL PORE DIAMETER IN UM IS #,SC2
STOP
END
C   DATA FOLLOWS THE 7/8/9 CARD

```



```

C
C
C THIS PROGRAM IS ESSENTIALLY THE SAME AS THE PRECEEDING PROGRAM.
C EXCEPT IT PLOTS A SET OF CUMULATIVE PORE SIZE DISTRIBUTIONS USING
C THE VERSATEC OR CALCOMP PLOTTER. FOR EXPLANATION OF THESE
C PLOTTERS, SEE PURDUE DOCUMENT JS CALCOMP. PROGRAM AFTER
C REED (1977).
C
C PROGRAM PORE (INPUT,OUTPUT,TAPES=INPUT,TAPEG=OUTPUT,PLOT)
INTEGER TITL
INTEGER TITLE
DIMENSION S(50),P(50),D(100),CU(100),SP(50),CUSP(100)
CALL PLOTS
A = 0.0
READ, NSET
C
C THE PURPOSE OF THIS DO LOOP IS TO PLOT MORE THAN ONE SET
C OF CURVES. NSET IS THE NUMBER OF SETS OF CURVES TO BE PLOTTED AND
C IS AN INTEGER VALUE THAT IS TYPED ON THE FIRST DATA CARD.
C
DO 500 K1,NSET
B = 0.0
CALL FACTOR (1.0)
CALL SYMBOL(A+1.85,.5,.7/6., 33HLIMITING PORE DIAMETER IN MICRONS,
G0.0,33)
CALL SYMBOL(A+1.,0.75,0.7/6.)
F50H.01      0.1      1.0      10.0     100.0    1000.0.0,50)
C THE ABOVE PLOTS AND LABELS THE X AXIS
CALL SYMBOL (A+2.0,1.0,0.1,3,0.0,-1)
CALL SYMBOL (A+3.0,1.0,0.1,3,0.0,-1)
CALL SYMBOL (A+4.0,1.0,0.1,3,0.0,-1)
CALL SYMBOL (A+5.0,1.0,0.1,3,0.0,-1)
C THE ABOVE PLACES TICK MARKS ALONG THE X AXIS
CALL SYMBOL (A+0.5,1.5,.7/6., 19HCUMULATIVE POROSITY,90.0,19)
CALL SYMBOL (A+0.6,1.0,.7/6.0,3H.00,0.0,3)
CALL SYMBOL (A+0.6,2.0,.7/6.0,3H.15,0.0,3)
CALL SYMBOL (A+0.6,3.0,.7/6.0,3H.30,0.0,3)
CALL SYMBOL (A+0.6,3.9,.7/6.0,3H.45,0.0,3)
C THE ABOVE PLOTS AND LABELS THE Y AXIS
CALL SYMBOL (A+1.0,2.0,0.1,3,0.0,-1)
CALL SYMBOL (A+1.0,3.0,0.1,3,0.0,-1)
CALL SYMBOL (A+1.0,4.0,0.1,3,0.0,-1)
C THE ABOVE PLACES TICK MARKS ALONG THE Y AXIS
CALL SYMBOL (A+3.85,3.86,.085,6HLEGEND,0.0,6)
C THE ABOVE WRITES LEGEND ON THE PLOT
CALL PLOT (A+1.0,4.0,3)
CALL PLOT (A+6.0,4.0,2)
CALL PLOT (A+6.0,1.0,2)
CALL PLOT (A+1.0,1.0,2)
CALL PLOT (A+1.0,4.0,2)
C THE ABOVE 5 CARDS DRAW THE OUTLINE OF THE GRAPH
C THESE CARDS FURTHER LABEL THE GRAPH AND PROVIDE THE GRID.
CALL PLOT (A+1.0,11./3.,3)
CALL PLOT (A+3.5,11./3.,2)
CALL PLOT (A+3.5,10./3.,3)
CALL PLOT (A+1.0,10./3.,2)
CALL PLOT (A+1.0,9./3.,3)
CALL PLOT (A+1.0,8./3.,3)

```



```

CALL PLOT (A+3.5,9./3.,2)
CALL PLOT (A+3.5,8./3.,3)
CALL PLOT (A+1.0,8./3.,2)
CALL PLOT (A+1.0,7./3.,3)
CALL PLOT (A+6.0,7./3.,2)
CALL PLOT (A+6.0,6./3.,3)
CALL PLOT (A+1.0,6./3.,2)
CALL PLOT (A+1.0,5./3.,3)
CALL PLOT (A+6.0,5./3.,2)
CALL PLOT (A+6.0,4./3.,3)
CALL PLOT (A+1.0,4./3.,2)
CALL PLOT (A+1.0,1.0,3)
CALL PLOT (A+2.0,1.0,3)
CALL PLOT (A+2.0,4.0,2)
CALL PLOT (A+3.0,4.0,3)
CALL PLOT (A+3.0,1.0,2)
CALL PLOT (A+4.0,1.0,3)
CALL PLOT (A+4.0,7./3.,2)
CALL PLOT (A+5.0,7./3.,3)
CALL PLOT (A+5.0,1.0,2)
CALL PLOT (A+1.0,1.0,3)
DO 6 IOU=1,5
CIOU=IOU
DO 5 IO=2,9
CIOA=IO
CIO= ALOG10(CIOA)
CALL SYMBOL (A+CIOU+CIO,1.0,.05,3.0.0,-1)
5 CONTINUE
6 CONTINUE
CALL PLOT (A+1.0,4.0,3)
READ, NDATA
C
C NDATA IS THE NUMBER OF CURVES THAT WILL BE PLOTTED FOR EACH SET OF
C CURVES. NDATA IS AN INTEGER VALUE, AND IS TYPED ON THE FIRST DATA
C CARD FOR THE SET OF CURVES.
C
C DETERMINATION OF PORE SIZE DISTRIBUTION
C
DO 400 J=1,NDATA
READ,DATE,SN
C
C DATE AND SAMPLE NUMBER (SN) ARE TYPED ON THE FIRST DATA CARD FOR
C EACH CURVE.
C
READ,WS,DS,DM,UP,WSP,WSPM,PE,PF,SR
C
C WS=WEIGHT OF SAMPLE, DS=SPECIFIC GRAVITY OF SOLIDS, DM=DENSITY OF
C MERCURY, UP=VOLUME OF PENETROMETER, WSP=WEIGHT OF SAMPLE AND PEN-
C ETROMETER, WSPM=WEIGHT OF SAMPLE , PENETROMETER AND MERCURY,
C PE =EVACUATING PRESSURE, PF=FILLING PRESSURE, IN MM OF MERCURY,
C SR =STEM READING AT FILLING PRESSURE. THE ABOVE VALUES ARE ALL ON
C THE SAME DATA CARD
C
US=WS/DS
WM=WSPM - WSP
UM=WM/DM
USA=UP-UM*(1.+PE/PF)-SR
UVO=USA-US

```



```

VOIDR=VVO/V$S
POROS=VVO/V$A
PV=PE*UM
VAI=PV/PF
READ,N,M,SI
C
C      N=INTEGER VALUE FOR THE NUMBER OF LOW PRESSURE READINGS MADE, NOT
C      COUNTING THE FILLING PRESSURE READING.  M=INTEGER VALUE FOR THE
C      NUMBER OF HIGH PRESSURE READINGS MADE, NOT COUNTING THE INITIAL
C      POROSIMETER READING.  SI=INTRUSION READING AT INITIATION PRESSURE
C      IN ML.  THE THREE VALUES ARE ALL ON ONE DATA CARD.
C
C      LOW PRESSURE CALCULATIONS
C
CU(1) = 0.
CUSP(1) = 0.
DO 100 I=2,N+1
READ,P(I),S(I)
C
C      P(I) AND S(I) ARE THE PRESSURE AND INTRUSION VALUES FOR EACH
C      READING, P(I) IS GIVEN IN MM OF MERCURY FOR THE LOW PRESSURE
C      INTRUSION AND PSI FOR THE HIGH PRESSURE.  S(I) IS IN ML.  THE TWO
C      VALUES ARE TYPED ON ONE DATA CARD, WITH A CARD FOR EACH READING.
C
PS=P(I)*.01934
VA=PV/P(I)
CVA=VAI-VA
CSR=S(I)-SR
SN=CSR-CVA
IF (SN.LT.0.) GO TO 10
SG =SN/WS
GO TO 11
10
SG=0.
SN =0.
11
CU(I) = CU(I-1) + SG
SP(I) = SN/USA
CUSP(I) = CUSP(I-1) +SP(I)
C
C      D(I) PORE DIAMETER CALCULATIONS BASED ON A SURFACE TENSION VALUE
C      OF 484 DYNES / CM AND A CONTACT ANGLE OF 147 DEGREES.
C
D(I)=((-4.)*484.*COS(2.5656)*.145)/PS
VAI=VA
100
SR=S(I)
C
C      HIGH PRESSURE CALCULATIONS
C
HCl=11.*.0011*UM/15000.
DO 200 I=N+2,M+N+1
READ,P(I),S(I)
P(I)=P(I)+11.
HC=P(I)*.0011*UM/15000.
CHC=HC-HCl
CSR=S(I)-SI
SN=CSR-CHC
SP(I) = SN/USA
CUSP(I) = CUSP(I-1) + SP(I)
SGH=SN/WS

```



```

CU(I)=CU(I-1)+SGH
D(I)=((-4.)*484.*COS(2.5656)*.145)/P(I)
HCl=HC
200  SI=S(I)
      READ(5,201) NL,A1,A2,W,H
201  FORMAT (I1,1X,A4,A2,1X,F4.1,1X,F9.8)
C
C      NL IS AN INTEGER VALUE WHICH DESIGNATES WHAT SYMBOL WILL BE
C      PLOTTED ON THE CURVE.  A1 AND A2 ARE FOR SAMPLE CODE, W IS FOR
C      WATER CONTENT AND H IS FOR PERMEABILITY IN CM/SEC.
C
C      DO 300 I=2,N+M+1
C      D(I-1) = ALOG10(D(I))
C      THE PURPOSE OF THIS DO LOOP IS TO CONVERT THE PORE SIZE DIAMETER
C      TO THE LOG OF THE DIAMETER
300  CUSP(I-1) = CUSP(I)
      D(M+N+1) =-3.0 -A
C      D(M+N+1) IS THE X AXIS VALUE RELATIVE TO THE ORDINATE OF THE PLOT
      D(M+N+2) =1.0
C      D(M+N+2) IS THE X INCREMENT FOR EACH INCH OF PLOT
      CUSP(M+N+1) =-0.15
C      CUSP(M+N+1) IS THE Y AXIS VALUE RELATIVE TO THE ORDINATE OF THE
C      PLOT.
      CUSP(M+N+2) =0.15
C      CUSP(M+N+2) IS THE Y INCREMENT FOR EACH INCH OF PLOT
      CALL SYMBOL (A+3.63,3.64-B,.07,NL,0.0,-1)
      CALL SYMBOL (A+3.85,3.64-B,.085,19HCODE           W/C =,0.0,19)
      CALL SYMBOL (A+3.85,3.50-B,.085,29HPERMEABILITY =   CM/SEC,
B0.0,29)
      CALL NUMBER (A+4.25,3.64-B,.085,A1,0.0,2HA4)
      CALL NUMBER (A+4.56,3.64-B,.085,A2,0.0,2HA2)
      CALL NUMBER (A+5.30,3.64-B,.085,W,0.0,1)
      CALL NUMBER (A+4.91,3.50-B,.085,H,0.0,4HE7.1)
C
C      THE ABOVE LISTS THE WATER CONTENT AND PERMEABILITY FOR THE PORE
C      SIZE CURVE
C
C      CALL LINE (D,CUSP,N+M,1,1,NL)
C
C      THE ABOVE PLOTS THE ACTUAL PORE SIZE CURVE
C      STEPS BELOW PLOT TOTAL POROSITY ON THE ORDINATE
C
      XN=3.0*POROS/0.45
      CALL SYMBOL (A+1.0,XN+1.0,0.0,105,NL,0.0,-1)
C      B IS FOR THE PLACEMENT OF THE PERMEABILITY AND WATER CONTENT
C      VALUES.
400  B=B+0.335
500  A = A + 7.0
C      A IS USED FOR THE LOCATION OF THE PORE SIZE PLOT
      CALL PLOT (0.0,0.0,999)
      STOP
      END

```



```

C THIS PROGRAM IS ESSENTIALLY THE SAME AS THE PRECEEDING PROGRAM,
C EXCEPT IT PLOTS A SET OF DIFFERENTIAL PORE SIZE DISTRIBUTIONS ON
C THE VERSATEC OR CALCOMP PLOTTER. FOR EXPLANATION OF THESE
C PLOTTERS, SEE PURDUE DOCUMENT JS CALCOMP.
C
C PROGRAM PORE (INPUT,OUTPUT,TAPES=INPUT,TAPES=OUTPUT,PLOT)
INTEGER TITL
INTEGER TITLE
DIMENSION S(50),P(50),D(100),CU(100),SP(50),CUSP(100),IMN(50)
CALL PLOTS
A = 0.0
READ, NSET
C
C THE PURPOSE OF THIS DO LOOP IS TO PLOT MORE THAN ONE SET
C OF CURVES. NSET IS THE NUMBER OF SETS OF CURVES TO BE PLOTTED AND
C IS AN INTEGER VALUE THAT IS TYPED ON THE FIRST DATA CARD.
C
DO 500 K=1,NSET
B = 0.0
CALL FACTOR (1.0)
CALL SYMBOL (A+1.85,.5,.7/6.,33HLIMITING PORE DIAMETER IN MICRONS,
A0.0,33)
CALL SYMBOL(A+1.,0.75,0.7/6.,
F50H.01      0.1      1.0      10.0      100.0      1000.0,0.0,50)
C THE ABOVE PLOTS AND LABELS THE X AXIS
DO 15 I=2,5
CI=I
CALL SYMBOL (A+CI,1.0,0.1,13,0.0,-1)
15 CONTINUE
C THE ABOVE PLACES TICK MARKS ALONG THE X AXIS
CALL SYMBOL (A+0.5,1.5,.7/G.,18HPOROSITY FREQUENCY,90.,19)
CALL SYMBOL (A+0.6,1.0,.7/G.,3H.00,0.0,3)
CALL SYMBOL (A+0.6,2.0,.7/G.,3H.05,0.0,3)
CALL SYMBOL (A+0.6,3.0,.7/G.,3H.10,0.0,3)
CALL SYMBOL (A+.6,3.9,.7/G.,3H.15,0.0,3)
C THE ABOVE PLOTS AND LABELS THE Y AXIS
DO 16 I=1,4
CI=I
CALL SYMBOL (A+1.0,CI,0.1,15,0.0,-1)
16 CONTINUE
C THE ABOVE PLACES TICK MARKS ALONG THE Y AXIS
CALL SYMBOL (A+4.40,3.80,.085,6HLEGEND,0.0,6)
C THE ABOVE WRITES LEGEND ON THE PLOT
CALL PLOT (A+1.0,4.0,0,3)
CALL PLOT (A+6.0,4.0,2)
CALL PLOT (A+6.0,2.5,2)
CALL PLOT (A+4.0,3.0,3)
CALL PLOT (A+1.0,3.0,2)
CALL PLOT (A+1.0,2.0,3)
CALL PLOT (A+6.0,2.0,2)
CALL PLOT (A+6.0,1.0,3)
CALL PLOT (A+1.0,1.0,2)
CALL PLOT (A+1.0,0.4,0,2)
CALL PLOT (A+2.0,4.0,3)
CALL PLOT (A+2.0,1.0,2)
CALL PLOT (A+3.0,1.0,3)
CALL PLOT (A+3.0,4.0,2)

```



```

CALL PLOT (A+4.0,4.0,3)
CALL PLOT (A+4.0,1.0,2)
CALL PLOT (A+5.0,1.0,2)
CALL PLOT (A+5.0,2.5,2)
CALL PLOT (A+6.0,2.5,3)
CALL PLOT (A+6.0,1.0,2)
CALL PLOT (A+1.0,1.0,2)
DO 18 IOU=1,5
CIOU=IOU
DO 17 IO=2,9
CIOA=IO
CIO=ALOG10(CIOA)
CALL SYMBOL (A+CIOU+CIO,1.0,.05,13,0.0,-1)
17 CONTINUE
18 CONTINUE
CALL PLOT (A+1.0,1.0,3)
DO 20 IO=1,3
CIO=IO
DO 19 IOU=1,4
CIOU=IOU
CIOU=CIOU/5.
CALL SYMBOL (A+1.0,CIO+CIOU,.05,15,0.0,-1)
19 CONTINUE
20 CONTINUE
CALL PLOT (A+1.0,4.0,3)
READ, NDATA
C
C NDATA IS THE NUMBER OF CURVES THAT WILL BE PLOTTED FOR EACH SET OF
C CURVES. NDATA IS AN INTEGER VALUE, AND IS TYPED ON THE FIRST DATA
C CARD FOR THE SET OF CURVES.
C
C
C DETERMINATION OF PORE SIZE DISTRIBUTION
C
DO 400 J=1,NDATA
READ,DATE,SN
C
C DATE AND SAMPLE NUMBER (SN) ARE TYPED ON THE FIRST DATA CARD FOR
C EACH CURVE.
C
READ,WS,DS,DM,VP,WSP,WSPM,PE,PF,SR
C
C WS=WEIGHT OF SAMPLE, DS=SPECIFIC GRAVITY OF SOLIDS, DM=DENSITY OF
C MERCURY, VP=VOLUME OF PENETROMETER, WSP=WEIGHT OF SAMPLE AND PEN-
C ETROMETER, WSPM=WEIGHT OF SAMPLE , PENETROMETER AND MERCURY,
C PE =EVACUATING PRESSURE, PF=FILLING PRESSURE,IN MM OF MERCURY,
C SR =STEM READING AT FILLING PRESSURE. THE ABOVE VALUES ARE ALL ON
C THE SAME DATA CARD
C
US=WS/DS
WM=WSPM - WSP
UM=WM/DM
USA=VP-UM*(1.+PE/PF)-SR
UVD=USA-US
VOIDR=UVD/US
POROS=UVD/USA
PU=PE*UM
UAI=PU/PF

```



```

READ,N,M,SI
C
C N=INTEGER VALUE FOR THE NUMBER OF LOW PRESSURE READINGS MADE, NOT
C COUNTING THE FILLING PRESSURE READING. M=INTEGER VALUE FOR THE
C NUMBER OF HIGH PRESSURE READINGS MADE, NOT COUNTING THE INITIAL
C POROSIMETER READING. SI=INTRUSION READING AT INITIATION PRESSURE
C IN ML. THE THREE VALUES ARE ALL ON ONE DATA CARD.
C
C LOW PRESSURE CALCULATIONS
C
CU(1) = 0.
CUSP(1) = 0.
C D(I) PORE DIAMETER CALCULATIONS BASED ON A SURFACE TENSION VALUE
C OF 484 DYNES / CM AND A CONTACT ANGLE OF 147 DEGREES.
C D(I)=(-4.*484.*COS(2.5656)*0.145)/(0.01934*PF)
DO 100 I=2,N+1
READ,P(I),S(I)
C
C P(I) AND S(I) ARE THE PRESSURE AND INTRUSION VALUES FOR EACH
C READING, P(I) IS GIVEN IN MM OF MERCURY FOR THE LOW PRESSURE
C INTRUSION AND PSI FOR THE HIGH PRESSURE. S(I) IS IN ML. THE TWO
C VALUES ARE TYPED ON ONE DATA CARD, WITH A CARD FOR EACH READING.
C
PS=P(I)*.01934
VA=PV/P(I)
CVA=VAI-VA
CSR=S(I)-SR
SM=CSR-CVA
IF (SN.LT.0.) GO TO 10
SG =SN/115
GO TO 11
10 SG=0.
SN =0.
11 CU(I) = CU(I-1) + SG
SP(I) = SM/USA
CUSP(I) = CUSP(I-1) +SP(I)
D(I)=((-4.)*484.*COS(2.5656)*.145)/PS
VAI=VA
100 SR=S(I)
C
C HIGH PRESSURE CALCULATIONS
HCl=11.*.0011*UM/15000.
DO 200 I=N+2,M+N+1
READ,P(I),SI
P(I)=P(I)+11.
HC=P(I)*.0011*UM/15000.
CHC=HC-HCl
CSR=S(I)-SI
SN=CSR-CHC
SP(I) = SM/USA
CUSP(I) = CUSP(I-1) + SP(I)
SGH=SN/115
CU(I)=CU(I-1)+SGH
D(I)=((-4.)*484.*COS(2.5656)*.145)/P(I)
HCl=HC
200 SI=S(I)
READ(5,201) NL,A1,A2,W,H
201 FORMAT (I1,1X,A4,A2,1X,F4.1,1X,F9.8)
C

```


C NL IS AN INTEGER VALUE WHICH DESIGNATES WHAT SYMBOL WILL BE
C PLOTTED ON THE CURVE. A1 AND A2 ARE FOR SAMPLE CODE, W IS FOR
C WATER CONTENT AND H IS FOR PERMEABILITY IN CM/SEC.
C
C THE PURPOSE OF THIS DO LOOP IS TO CONVERT THE PORE SIZE DIAMETER
C TO THE LOG OF THE DIAMETER
DO 300 I=2,N+M+1
DMN(I-1)=(ALOG10(D(I))+ALOG10(D(I-1)))/2.0
SP(I-1)= SP(I)
300 CUSP(I-1)= CUSP(I)
DMN(M+N+1)= -3.0-A
DMN(M+N+2)= 1.0
SP(M+N+1)= -0.05
SP(M+N+2)= 0.05
CALL SYMBOL (A+4.20,3.6-B,.07,NL,0.0,-1)
CALL SYMBOL (A+4.40,3.55-B,.085,11HSAMPLE CODE,0.0,11)
CALL NUMBER (A+5.30,3.55-B,.085,A1,0.0,2HA4)
CALL NUMBER (A+5.60,3.55-B,.085,A2,0.0,2HA2)
C
C THE ABOVE LISTS THE WATER CONTENT AND PERMEABILITY FOR THE PORE
C SIZE CURVE
C
CALL LINE (DMN,SP,N+M,1,1,NL)
C
C THE ABOVE PLOTS THE ACTUAL PORE SIZE CURVE
C
C B IS FOR THE PLACEMENT OF THE PERMEABILITY AND WATER CONTENT
C VALUES.
400 B=B+0.2
500 A=A+7.0
C A IS USED FOR THE LOCATION OF THE PORE SIZE PLOT
CALL PLOT (0.0,0.0,999)
STOP
END

APPENDIX E

Purdue University Negative Numbers for Photographs

Figure	Negative Number
1.	76449
4.	75529-24
5.	75529-34
6.	76455-2
7.	76455-10
8.	76455-26
9.	75529-25
10.	75529-28
61.	76481



COVER DESIGN BY ALDO GIORGINI